INTRINSIC INTENSITY VARIATIONS AND MODELS OF PULSARS

TIFR CENTRE, BANGALORE
3641
LIBRARY

By

S.KRISHNAMOHAN

A Thesis
Submitted for the Ph.D. degree
of the
University of Bombay

RA.354.A
KRI

NCRA LIBRARY
000501
520/525(043.2)

September 1979

INTRINSIC INTENSITY VARIATIONS AND MODELS OF PULSARS

SYNOPSIS

In contrast to the high stability of their pulse periods, pulsars show erratic variation of the intensity of their radio emission. The intensity variations are produced either by causes intrinsic to the source of emission or by the propagation effects in the interstellar medium. The intrinsic intensity variations (IIV) occur over a wide span of time scales ranging from a few microseconds to several days. In this thesis we investigate three different types of IIV : (a) the drifting subpulses, (b) the short term (minutes) and (c) the long term (days) intensity variations. Though the basic idea that pulsars are rotating neutron stars is well-accepted, there is no concurrence about the details of the mechanism by which the pulses are produced. Equally divergent are the views about the structure of the central core and the origin of neutron stars. Our investigations show that it is possible to get useful information on the models by studying the IIV of pulsars. The observational data used in this thesis have been obtained using the Ooty radio telescope.

The positions of the subpulses within the main pulse window drift with time in several pulsars. Because of the observed stability of this phenomenon at least in a few pulsars, a study of the drifting subpulses may put restrictions on possible models of pulsars. Two of the models, the polar cap (P.C.) and the relativistic beaming (R.B.) models, which have been discussed extensively in the literature, do explain the basic phenomenon of drifting subpulses. In the P.C. model the drift is caused by the uniform rotation of the subpulse producing sparks around the polar cap. In the R.B. model, it is produced by modulation of the intensity of the source with a period that is incommensurate with the rotational period of

the neutron star. In this thesis we show that the slope of the subpulse bands has a different dependence on the subpulse longitude in the two models. For the P.C. model the modulus of the slope decreases as we go from the edges to the mid region of the averaged pulse, whereas for the R.B. model it increases. From the data on PSR 0031-07 obtained with the Ooty radio telescope, we have shown that the behaviour of the measured slope agrees with the prediction of the R.B. model. We show also, that the behaviour of the drifting subpulses of a few other pulsars for which sufficient data is available in the literature is in conformity with the predictions of the R.B. model. The disagreement between the data and predictions of the P.C. model can be removed if the sparks rotate faster as they move away from the great circle passing through the rotational and the magnetic poles of the neutron star. However, such an assumption seems contrived and may not be justified.

Study of the short term IIV, i.e. those with time scales of a few minutes to roughly an hour, is very important. If neutron stars possess central solid cores they may wobble or precess freely and thus produce modulation of the intensity with periods in a range similar to that of the short term IIV. Such a study is difficult due to the presence of interstellar scintillations (ISS) which also have similar time scales at metre wavelengths. In order to overcome this difficulty, we have developed a method to separate analytically the autocorrelation function (ACF) due to IIV and that due to ISS, by using multichannel data. The method utilises the difference in the decorrelation frequencies of the IIV and the ISS. The IIV are likely to be practically completely correlated across the bandwidths that are generally used in observations whereas the ISS are correlated only over narrow bandwidths. Hence, the relative power in the two types of fluctuations change with the bandwidth used. The method has been applied successfully to the intensity data from 24 pulsars which were observed with the Ooty radio telescope.

The results show that occurrence of IIV with time scales similar to those due to ISS is very common in pulsars. Moreover, both the time scales and the modulation index for the same pulsar vary with time. This may partially account for the inconsistency of pattern velocities of ISS that are deduced from multistation observations by various workers. Our results regarding short term IIV are discussed below.

Nine out of the 24 pulsars showed significant quasi-periodic modulations in their IIV. Four of them were observed on more than one occasion and it was found that the behaviour of IIV was different on different days. Notably, PSR 1919+21 showed different behaviour of IIV even on two consecutive days. If the quasiperiodicities in the IIV are produced by the wobble of neutron stars, significant periodic residuals in the times of arrival as well as variations of the pulse shape are expected. Moreover, the residuals and the variations should be correlated with the phase of the wobble periodicity. For example, based on a crude approximation that the radiating beam of a pulsar could be represented by a circular gaussian, residuals exceeding 10 ms are expected in the times of arrival of pulses from PSR 1919+21. For the other pulsars, the residuals are expected to be less than or equal to 3 ms. Admittedly, the results of such calculations are uncertain since the nature of the polar diagram of the radiating beam is uncertain. Even then, measurable periodic residuals should have been found at least for PSR 1919+21. But, we have not found any residuals exceeding a fraction of a ms. In addition, for this and two other pulsars which showed quasiperiodicities in their IIV, there is no significant seismic activity on their neutron stars as inferred from the published data on the times of arrival for those pulsars. Hence, excitation of wobble in the presence of dissipation in the solid part of the neutron star would be difficult. From these results we conclude that wobble has not been detected in any of the pulsars which were studied by

us and that one has to examine the possibility of oscillations in the emission mechanism itself to explain the observed quasiperiodicities in the IIV.

We have shown that the observed probability density distributions of the long term IIV, i.e. those with time scales greater than a few days can be described satisfactorily by χ^2-distributions. Such distributions are expected if the intensity fluctuations are due to the fluctuation of the number of particles radiating coherently in a given region. In deriving the χ^2-distributions, the radiation from many such regions is assumed to add up incoherently to produce the observed emission. Based on these distributions we have given, as a function of the search number, the cumulative number of new pulsars expected to be found on repeatedly searching the same region of the sky with the same sensitivity. Nearly 20 % more new pulsars are expected to be found on the first repeat search. We show also that the luminosity function deduced from either a single survey or surveys with very different sensitivities, is not affected by the omission of flux variability in the calculation of selection effects. However, if surveys over the same region of the sky with similar sensitivities are combined without taking into account the flux variability, then the deduced birth rate of pulsars could be overestimated by more than 20 %. Also, we have outlined a probabilistic approach for the estimation of selection effects so that surveys could be combined with due regard to the flux variability.

At the end of the thesis the results are summarised and the limitations of the present work are indicated.

STATEMENTS REQUIRED BY THE UNIVERSITY OF BOMBAY

Statement required under O.770

No part of the work presented in this thesis has been submitted previously to this or any other university or body for a degree, diploma or any other academic award.

Statements required under O.771

1) The work described in this thesis is based on new observations of the intensity variations of pulsars made by me using the Ooty radio telescope, as well as on existing observations of the long term intensity variations made by others. A new method to separate the autocorrelation function of the intensity fluctuations intrinsic to the source and that of the interstellar scintillations has been reported. The work presented in the thesis has lead to several important conclusions regarding the models of pulsars.

2) The work reported in this thesis is original. References have been given at appropriate places in the text, whenever the work done by others has been used.

3) The observations were made in collaboration with Shri V.Balasubramanian. However, most of the analysis and interpretation described in this thesis have been done by me.

LIST OF PUBLICATIONS

1) 'Parameters of Twelve Weak Pulsars at 327 MHz'
Krishnamohan,S., Balasubramanian,V., and Swarup,G., 1971. Nature Physical Science, 234, 151.

2) 'Accurate Position of PSR 1749-28 from Lunar Occultations'
Pramesh Rao,A., and Krishnamohan,S., 1972.
Nature Physical Science, 238, 69.

3) 'Simultaneous Observations of Pulsar Intensity Variations at Parkes and Ootacamund'
Slee,O.B., Ables,J.G., Batchelor,R.A., Krishnamohan,S., Venugopal,V.R., and Swarup,G., 1974.
Mon. Not. R. astr. Soc., 167, 31.

4) 'Mode change in PSR 1700-32 and PSR 1237+25'
Krishnamohan,S., and Balasubramanian,V., 1976.
Bull. Astr. Soc. India, 4, 84,(Abstract)

5) 'Interstellar Scintillation of Pulsars'
Balasubramanian,V., and Krishnamohan,S., 1978.
Bull. Astr. Soc. India, 6, 53,(Abstract).

6) 'Discovery of Two Pulsars'
Mohanty,D.K., and Krishnamohan,S., 1978.
Bull. Astr. Soc. India., 6, 54,(Abstract).

7) 'Observations of Drifting Subpulses and their Implications on Models of Pulsars'
Krishnamohan,S., 1979,(to appear in Mon. Not. R. astr. Soc.).

ACKNOWLEDGEMENTS

It is a great pleasure to express my gratitude to Professor Govind Swarup for his guidance and constant encouragement. Many thanks are due to him for introducing me to the ways and means of radio astronomy.

The smooth running of the Ooty radio telescope would not have been possible, but for the willing cooperation of the engineering, the observing and the technical staff. I take this opportunity to thank them all.

I had the benefit of useful discussions with several of my colleagues. In particular I should like to thank V. Balasubramanian and D.K. Mohanty.

I should also like to thank Mathews, Srinivasan, Premkumar and Siva for the neat jobs of typing, tracing and reprography. I thank G. Sankarasubramanian for helping me in proof-reading.

It is a pleasure to thank my wife Bhagyam for providing me a never dying source of encouragement and my sons Raghu and Ravi for keeping me in good humour with their little pranks.

TABLE OF CONTENTS

Page No.

TIFR CENTRE, BANGALORE 3641 LIBRARY

List of Figures

List of Tables

Chapter 1

INTRODUCTION

1.1 Pulsars

The accidental discovery of pulsars a decade ago by the Cambridge radio astronomers (Hewish et al. 1968) was received with much enthusiasm by not only astronomers but also physicists. The discovery was immediately followed by hectic activity by observers and theoreticians. These studies, especially those of periods and the period derivatives of pulsars led to the identification of pulsars as neutron stars - the highly condensed remains of dead stars whose formation in supernova explosions was postulated as far back as 1934 (Baade and Zwicky 1934), but which had eluded the detection untill the discovery of pulsars. Barring the black holes whose existence is not yet well established, the neutron stars have the highest matter density reaching all the way up to $\sim 10^{15}$ gm cm^{-3} and magnetic field strength reaching up to $\sim 10^{12}$ gauss. The nonavailability of such an exotic state of matter in the terrestrial laboratories has attracted many investigators from varied disciplines to the study of pulsars as exemplified by the study of the structure of the neutron stars. Stable neutron stars have mass in the range of 0.1 to 2.5 times the solar mass squeezed into a radius of $\sim$ 10 km. 'Glitches' - the sudden changes in the periods of pulsars - gave indications that the protons and

the neutrons inside a neutron star exist in the superfluid state (Baym et al. 1969). Their observations also indicate that in some neutron stars there could be a solid core (Pines, Shaham and Ruderman 1972).

Neutron stars are presumed to be born in supernova events. Only in the case of the Crab and the Vela pulsars, a satisfactory physical association between the pulsars and the supernova remnants has been established. In the case of a few other pulsars, associations were suggested mostly based on the positional coincidence only. As pulsars are high velocity objects (Manchester, Taylor and Van 1974; Anderson, Lyne and Peckham 1975; Backer and Sramek 1976) it is difficult to establish associations based on positional coincidence alone. One way to overcome this difficulty may be to establish the association between the two populations on a statistical basis. Several investigators (Large 1971; Roberts 1976; Davies, Lyne and Seiradakis 1977, Taylor and Manchester 1977; Manchester 1979) have tried to check the hypothesis that all pulsars are born in supernova events by tallying their birth rates. These investigations were inconclusive since the calculations of the birth rate of both the populations are subject to many uncertainties.

The periods of the known radio pulsars range from 0.03 to 4 secs. The high stability of the periods had initially given a considerable hope that one would be able to use them as standard clocks in testing the predictions of the general theory of relativity. But once elaborate measurements

of the times of arrival of pulsar signals were done, it became clear that the periods were not stable enough to perform the tests. But the recent possible detection of gravitational radiation (Taylor, Fowler and McCulloch 1979) in the binary pulsar PSR 1913+16 has shown that the initial optimism was not completely unjustified.

1.2 Models of Pulsars

Though the basic identification of pulsars as rotating magnetised neutron stars (Gold 1968) is well-accepted, there is no agreement regarding the mechanisms for emission and beaming of pulsar signals. The observed high brightness temperatures $\sim 10^{30}\ ^{o}K$ imply that a coherent emission mechanism is operative in pulsars. Basically three types of mechanisms were proposed:

(i) Direction-dependent masing (Ginzburg and Zaitzev 1969),

(ii) Curvature radiation on open field lines above magnetic polar caps (Radhakrishnan and Cooke 1969; Goldreich and Julian 1969; Sturrock 1971; Ruderman and Sutherland 1975) and

(iii) Relativistic compression of radiation which may be quasiisotropic in the frame of reference in which the source is at rest (Smith 1969, 1970; Zheleznyakov 1971; Zheleznyakov and Shaposhnikov 1975)

The last two models i.e. the polar cap (P.C.) and the relativistic beaming (R.B.) models are dealt with extensively in the literature. Whereas the P.C. models try to explain both

the generation and the pulsation of the radiation, the R.B. models attempt to explain only the pulsation. Both the models are able to explain some, but not all, of the wealth of the observed properties of pulsars(see, for example, Ginzburg and Zheleznyakov 1975; Manchester and Taylor 1977 for excellent reviews).

1.3 Intensity Variations of Pulsars

The erratic variability of the intensity of pulsars in contrast to the high stability of their periods is very striking. The time scales of the intensity variations range from a few microseconds (Hankins 1971) to more than an year (Helfand, Fowler and Kuhlman 1977). However, both the upper and the lower bounds are limited by the observations and they may in fact span a much wider range. It is not clear how the multitude of the types of the intensity variations are interrelated. Fig.1.1 shows a scheme to classify the intensity variations on a phenomenalogical basis. They are arranged such that the time scales increase from the left to the right of the diagram. However, there is considerable uncertainty in the diagram since phenomena like mode changing do not have a well-defined time scale.

The variations of the intensity of pulsars can be classified into two categories: (a) the interstellar scintillations (ISS) and (b) the intrinsic intensity variations(IIV). They can be distinguished by their decorrelation frequencies. The decorrelation frequency (Δf) is a frequency interval over which the correlation coefficient of the intensity fluctuations

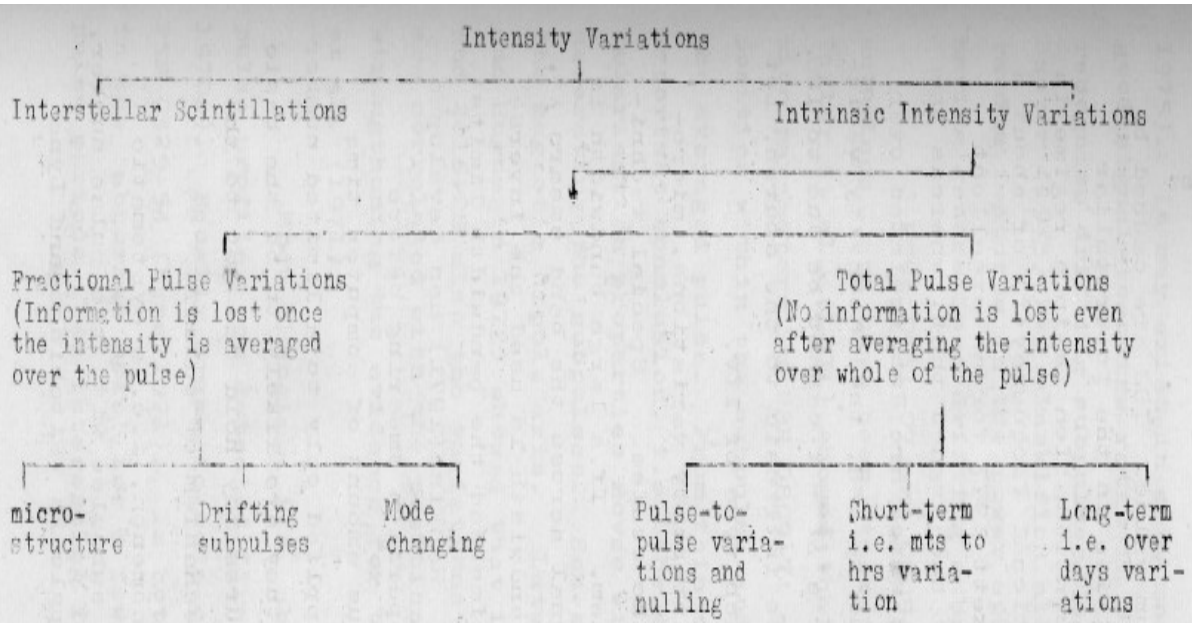

Fig.1.1. A scheme to classify the various types of intensity variations of pulsars.

falls to half of its maximum value. ISS are caused by the electron density irregularities in the interstellar medium. For all pulsars the scintillation is in a regime in which $\Delta f/f \ll 1$ for an observational frequency(f) of about a few hundred megahertz (see Rickett 1977 for an excellent review of ISS). Scheuer (1968) had argued that, whereas the fluctuations over a few minutes which are decorrelated over a Δf such that $\Delta f/f \ll 1$ are due to ISS, the intensity variations which are correlated over a $\Delta f \sim f$ cannot be due to ISS. Such variations are likely to be intrinsic to the source. Let us now review, very briefly, each type of IIV.

Among the intrinsic intensity variations, microstructures have the shortest time scales. Special techniques are required to observe them. If a large bandwidth is used, the dispersion of the signal across the band smears it. On the other hand, if a small bandwidth is used the inverse relationship between the rise time and the bandwidth limits the attainable time resolution. Hankins(1971) has developed a method to correct for the dispersion smearing before detection. Due to the tremendous amount of computer time required, the method had been applied only to a limited number of low dispersion pulsars. As they are likely to be the basic blocks of emission, microstructures may hold the key to the understanding of the emission mechanism of pulsars.

Drifting subpulse phenomenon, i.e. a systematic variation of the longitude of a subpulse with the pulse number, had been detected so far in 18 pulsars (Ritchings and Lyne

1975). It may exist in many more pulsars. But, unless a good signal-to-noise ratio is obtained, it is difficult to recognise drifting subpulses, especially the unstable ones. Backer (1973) had classified all pulsars which produce non-random features in the power spectra of their intensity as having generalised drifting subpulses.

PSRs 0031-07 and 0809+74 have very stable drifting subpulses and have been, therefore, studied very extensively. Taylor et al. (1971) showed that variations of the polarisation parameters in PSR 0809+74 are well correlated with the position within the subpulse and not with the position within the averaged pulse. From this observation they come to an important conclusion, i.e. the symmetry axis determining the polarisation properties moves with the region responsible for generating the subpulses. Hence, the symmetry axis cannot be the magnetic dipole axis. Later studies (Manchester, Taylor and Huguenin 1975) showed that in the case of PSRs 0031-07 and 2016+28 also the variations of the polarisation parameters are correlated with the position within the subpulse, and thus strengthening the evidence for the conclusion drawn by Taylor et al. (1971).

Mode changing, i.e. abrupt changes in the integrated pulse profile, was detected first in PSR 1237+25 (Backer 1970c). Equally dramatic mode changing was detected later in PSR 0329+54 (Lyne 1971). In both the cases the pulsar stays in the 'abnormal mode' for a few tens to more than a thousand pulse periods. An interesting feature that was noticed in the

case of PSR 1237+25 (Backer 1970c) was that the switching from one mode to another is quite abrupt, taking less than a pulse period. In other pulsars like PSRs 1133+16, 2045-16 (Helfand, Manchester and Taylor 1975) and 1700-32 (Krishnamohan and Balasubramanian 1976) mode changing is not so dramatic. Lyne (1971) has shown that though the pulse shape changes drastically, the polarisation characteristics do not change appreciably during mode changing in PSRs 0329+54 and 1237+25. This, along with the observation of Hesse, Sieber and Wielebinski (1973) that the nature of mode changing in PSR 0329+54 depends on the radio frequency of observations suggests that it is the radiating particles and their coherence that are responsible for mode changing and not the magnetic field configuration.

Total pulse intensity variations do not lend themselves to an objective sub-classification, unlike in the case of the fractional pulse intensity variations. Probably, only the pulse nulling phenomenon during which practically no radio emission is detectable (Ritchings 1976) is an exception. Other sub-classifications are based purely on the time scales involved in and as such may not have much physical significance. The physical cause underlying all of them may be the same. As the maintenance of coherence in radioemission requires special conditions like particle bunching, masing or other similar mechanisms requiring unstable states, it is difficult to maintain the same degree of coherence, rotation after rotation. Any disturbance in

the degree of coherence would lead to intensity variations. Whereas the intensity of the Crab pulsar varies at radio frequencies by a factor of nearly thousand (Heiles, Campbell and Rankin 1970; Argyle and Gower 1972), it is practically constant at optical frequencies (Hegyi, Novick and Thaddeus 1971). If the emission is caused by the same particles in both the frequency ranges, the observations suggest that the intensity variations at radio frequencies are caused by variation in the degree of coherence in the radio emitting region and not by the variation in the total number of the radiating particles.

Most of the pulsars show pulse to pulse intensity variations with a typical time scale of a few to a few tens of pulse periods. Pulse nulling phenomenon which was detected first by Backer (1970b), had been studied very extensively by Ritchings (1976). From a study of 32 pulsars, Ritchings (1976) had shown that pulse nulling is a characteristic of the pulsar's old age.

Short-term intensity variations which have typical time scales ranging from a few minutes to a few hours are difficult to study since the time scales overlap with those for ISS. Since intrinsic intensity variations (IIV) have been reported in literature for time scales both higher and lower than those for ISS, they may exist with time scales similar to those for ISS also. From the variation of modulation index with bandwidth, Balasubramanian (1979) has recently inferred that intrinsic variations with short time

scales do exist in several pulsars. But the method used by him has limitations since it does not allow quantitative measurements of the parameters of these variations.

Long-term intensity variations with time scales greater than a few days have been studied extensively by several investigators (Hesse 1972; Huguenin, Taylor and Helfand 1973; McLean 1973; Helfand, Fowler and Kuhlman 1977). Recent studies (Helfand et al. 1977) have shown that these variations are fairly well-correlated over a few hundred MHz. A periodicity may be expected in the long-term intensity variations if they are caused by a long-term wobble of the neutron star, but none was detected (Helfand et al. 1977).

1.4 The Present Work

In this thesis we study three different types of intrinsic intensity variations, namely the drifting subpulses, the short-term variations and the long-term variations. New observations are reported for the first two types of variations. Implications of the observed behaviour of subpulses on models of pulsars are presented. The short-term variations are investigated to detect short-term wobble of neutron stars which may be present. The effect of long-term variations on the determination of the luminosity function of pulsars is examined in the light of the existing observational data.

The procedures adopted for the data acquisition and the preliminary analysis are described briefly in Chapter 2.

The predictions of the polar cap and the relativistic beaming models, regarding the longitudinal dependence of the slope of the drifting subpulse bands are worked out in Chapter 3. The expected behaviour from the two models differ markedly, making the slope a powerful observable to distinguish between the two models. Because of the finite width of the subpulses, it is difficult to determine the slope directly from the longitude vs pulse-number diagrams. The longitude-resolved Fourier transform method of Backer (1970a) is ideally suited for such a purpose. The slope was measured for the subpulse bands of PSR 0031-07 by using this method on the data obtained with the Ooty radio telescope. The modulus of the slope increases as we go from the leading edge to the centre of the pulse and then decreases as we approach the trailing edge. This behaviour is opposite to what is expected from the polar cap models, at least in the form as developed by Ruderman and Sutherland (1975). But, it is readily in agreement with the predictions of the relativistic beaming models. Also, we discuss the compatibility of the known behaviour of subpulses belonging to a few other pulsars with the predictions of both the models, and show that they also support our conclusions.

In Chapter 4, we review various arguements which show that it is not implausible that some neutron stars, especially the heavy ones, have central solid cores. If solid cores do exist, then one would expect the period of wobble of neutron stars to be in the range of a few minutes

to roughly an hour. Intrinsic variations with this range of time scales were not studied earlier due to the difficulty in distinguishing them from interstellar scintillations. We developed a method to separate the autocorrelation function (ACF) due to the intrinsic variations and that due to scintillations, by exploiting the difference in their correlation bandwidths. As a byproduct the method gives the ACF of ISS which is not contaminated by the presence of IIV, and thus enables a comparison with the predictions of the scintillation theories. The method had been applied on the intensity data of 24 pulsars which were observed using the Ooty radio telescope. Some of the pulsars were observed on more than one occasion. The results show that wobble of neutron stars is a very unlikely explanation for the quasi-periodic modulations which were observed for some of the pulsars.

In Chapter 5, we examine the effect of long-term intensity variations on pulsar searches and the derived luminosity function. The intensity data on 5 pulsars published by Huguenin et al. (1973) have been used to obtain the probability distribution of intensities. We show that x^2-distributions describe them well. It may be noted that x^2-distributions are expected from the coherent nature of pulsar radiation. We show that though the number of new pulsars discovered on repeatedly searching the same region of the sky depends appreciably on the nature of intensity variations, the luminosity function derived from a single

search is unaffected by the variations. Also, we describe a method to combine different searches done over a given region of the sky so as to derive the luminosity function by adopting a probabilistic approach to the evaluation of selection effects.

The conclusions are summarised in Chapter 6.

Chapter 2

DATA ACQUISITION AND PRELIMINARY REDUCTION

2.1 The Ooty Radio Telescope

Most of the observational data on pulsars that have been utilised in this thesis were acquired using the Ooty radio telescope (Swarup et al. 1971). The receiver of the telescope has a total bandwidth of 4 MHz centred at a frequency of 326.5 MHz. A given source can be observed continuously for nearly 9.5 hrs by following it in the east-west direction by the mechanical rotation of the telescope. The declination coverage of the telescope is $\pm 35^{\circ}$. The telescope provides twelve simultaneous beams, each of size $2^{\circ} \times 5'.5 \sec \delta$, where δ is the declination. The spacing between adjacent beams in declination is $3' \sec \delta$. Only one of the beams is used for studying the known pulsars. The output from the beam is connected to a 12 channel filter bank. The bandwidth of each channel could be either 300 kHz or 50 kHz. The actual bandwidth that is used is selectable by a toggle switch. Nominally, the central frequency of the adjacent filters differ by an amount equal to the bandwidth of the filters, except for the last two channels of the 50 kHz system. For these channels, the central frequencies differ from those of the previous channels by 0.5 MHz. A post-detection RC time constant of 3 ms was used on each channel. For each channel there are two parallel outputs available, one going to a multiplexer connected to an analog to digital

converter (ADC) and the other to a chart recorder. The chart recorder is used for monitoring purposes only. The ADC is interfaced to an on-line minicomputer, Varian 620/i. The computer is also interfaced with a rubidium time and frequency standard and a six channel digital to analog converter (DAC) apart from many other standard I/O equipment.

2.2 Data Acquisition

To study a host of pulsar phenomena, it is desirable to have a time resolution which is less than the pulse width, say of about a few milliseconds. Further, pulsars should be observed with narrow enough bandwidth, so that the dispersion smearing of the signal in the individual channels does not obliterate the details that one is looking for. For example, at the operating frequency of the telescope the dispersion smearing, Δt , is given by

$$\Delta t \simeq 0.23 \times \Delta f \times DM \text{ ms}$$

where Δf is the bandwidth in MHz and DM is the dispersion measure expressed in pc cm^{-3}. So, even for a DM $\sim$ 30 pc cm^{-3}, one is forced to use filters of bandwidth $\sim$ 300 kHz to get a resolution $\sim$ 2 ms. In order to improve the signal-to-noise ratio as well as to study many phenomena, it is desirable to acquire data using simultaneously many narrow band receivers. To reduce the volume of the data to be handled we utilised the fact that the typical duty-cycle of pulsars is less than 10 %. Therefore we have sampled with full resolution during a time window in which the pulse is expected to be present

and used the receiver output during the rest of the pulse period to define a general background level.

The data used in this thesis were acquired using a general purpose pulsar data acquisition program. A block diagram of the set up used for controlling the data acquisition is shown in Fig.2.1. The preset timer generates two pulse trains (a) PT1, with a variable period that can be set to one microsecond accuracy, and (b) PT2, with a period equal to 2 ms. The pulses are produced by counting down the 1 MHz signal that is generated by the rubidium time and frequency standard. When the pre-computed apparent period of a pulsar is set on the preset timer, the period of PT1 would correspond to the apparent period of the pulsar. The width of the last pulse of PT2 is adjusted, once per pulsar period, such that there are always integral number of PT2 pulses per every PT1 pulse period. This ensures that both the pulse trains are synchronous. One could have achieved the same by leaving the period of PT2 flexible. But as the earlier scheme was simpler, it was adopted. PT1 and PT2 were connected to a high level and a low level of a priority interrupt module (PIM) of the computer. PT1 was also used to trigger an oscilloscope which was used as a high time resolution monitoring device.

To put a data window one should know the expected epoch of a pulse for a given pulsar. The first phase of the data acquisition program determines the epoch by performing an on-line software de-dispersed folding of the data from the 300 kHz filter bank. As the folding progresses, the folded

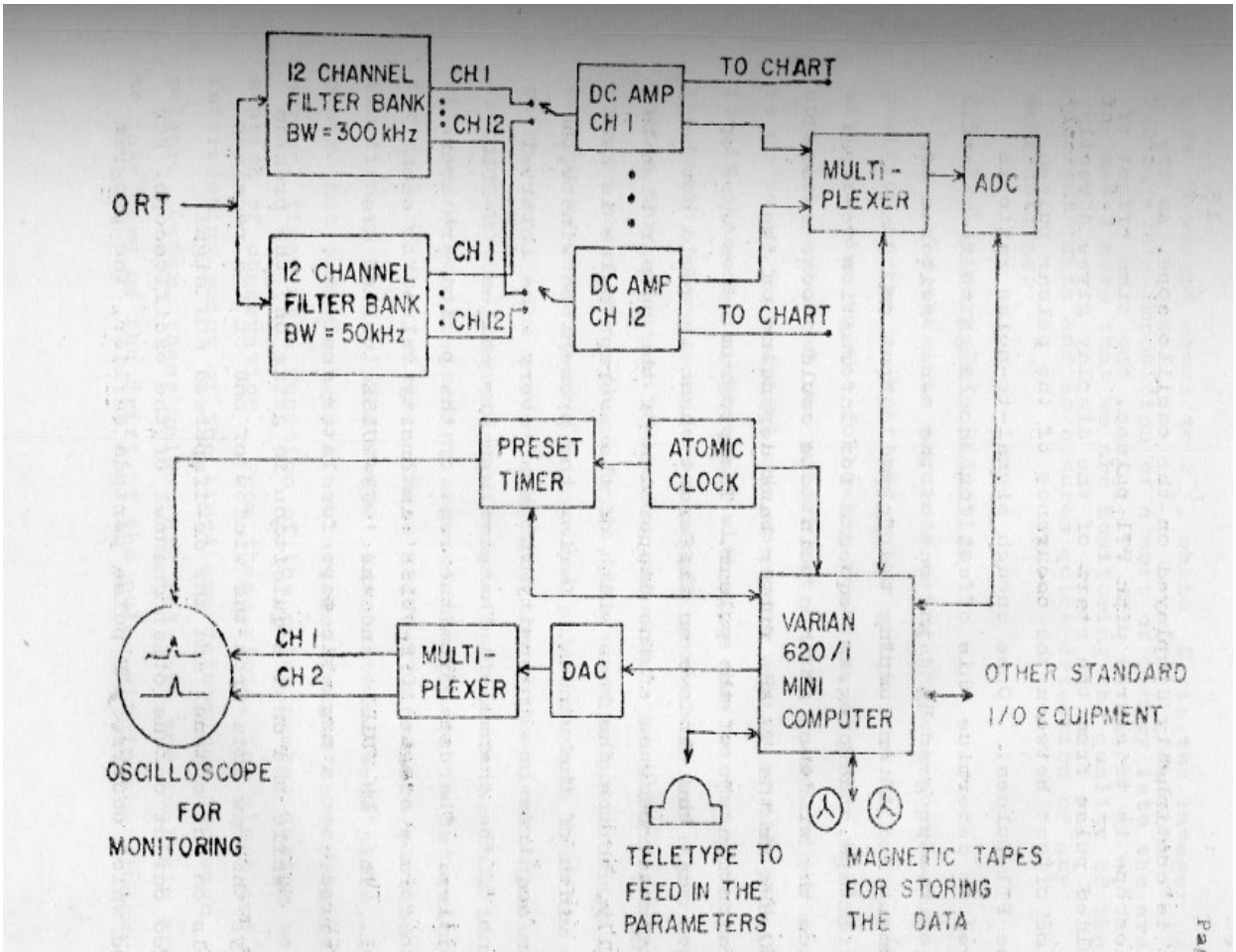

Fig.2.1. A block diagram of the set up used for observing pulsars with the Ooty radio telescope.

output is continually displayed on the oscilloscope. As the oscilloscope is triggered with PT1 pulses, the time offset of the folded pulse from the start of the display gives directly the time offset between the occurence of the pulsar pulses and the PT1 pulses. Once enough signal-to-noise ratio is achieved to determine this offset, one could go to the next phase of the program by using one of the sense switches of the computer. After dumping the folded output on to a magnetic tape, the program requests for information required to place the window. At this point one could choose either the 300 kHz or the 50 kHz filter bank depending on the dispersion measure of the pulsar. The program takes care of the fact that the windows on different channels would not be simultaneous, because of the dispersion of the pulsar signals. Typically, thrice the base width of the average pulse is used as the width of the window. During the prescribed window, the program acquires one intensity value at every 2 ms interval for each of the channels. These values are called 'ON-PULSE' intensities. The data from the rest of the period are averaged to form a single 'OFF-PULSE' intensity value for each channel. The 'ON-PULSE' and the 'OFF-PULSE' values are transferred onto a magnetic tape for later analysis.

While the data acquisition is going on, the program displays the raw data from the window of one of the receiver channels on one channel and the de-dispersed and signal averaged output on the other channel of the oscilloscope. For a pulse which occurred, N pulse periods earlier, the program

gives a weight equal to 2^{-I}, where I is the integer part of N/256. This imposition of a sort of memory into the averaging makes sure that we are monitoring the quality of the 'current' data and so ensures quick detection of any malfunctions.

2.3 Preliminary Data Reduction

In the data acquired using the above procedure, the position of the peak of the pulse within the window may drift with time due to the following reasons: a) error in the apparent period of the pulsar set by the preset timer could be up to ± 0.5 μs and b) the apparent period of the pulsar itself changes continuously with time due to the rotation of the Earth, whereas we use a single period as the apparent period throughout an observing session. As a first step towards correcting these drift, the average pulse shape is determined once every few hundred pulse periods from the data on the tape. The arrival time of the pulse within the window, defined as the interpolated sample number of the half intensity point on the leading edge of the pulse, is determined for each of the trials. These arrival times are plotted as a function of the pulse number. From several such plots, it was clear that two straight lines are sufficient to represent the arrival times as a function of the pulse number during each session of observation. From these plots, the slope and the intersecting point of the lines are determined for each pulsar. Later, these values are fed into the analysis program to take care of the drift of the pulse within the window.

Chapter 3

DRIFTING SUBPULSES

3.1 Introduction

Of the various types of intensity variations taking place within a pulse window, the drifting subpulse phenomenon as observed in PSRs 0031-07 and 0809+74 is the most systematic one. The phenomenon was first observed by Drake and Craft (1968) as a second periodic pulsation in sequences of pulses from PSRs 1919+21 and 2016+28. Later on it was shown to produce well-defined features in the power spectra of the intensity fluctuations of pulsars (Lovelace and Craft 1968; Taylor, Jura and Huguenin 1969; Backer 1970a; Taylor and Huguenin 1971). The two pulsars, PSRs 0031-07 and 0809+74, which have stable subpulse behaviour have been studied extensively giving a wealth of details. The drifting subpulse behaviour of PSR 0031-07 generally assumes one of the three distinct modes with different interband spacings P_3 in the longitude vs pulse-number diagrams; but the drift rate adjusts itself such that P_2, the spacing between two subpulses in the same pulse remains approximately constant irrespective of the value of P_3 (Huguenin, Taylor and Troland 1970). In the case of PSR 0809+74, the drift rate has sudden discontinuities (Cole 1970) at the null pulses, but once these jumps are taken care of, the interband spacing, P_3, is very stable (Page 1973; Unwin et al. 1978). Because of the stability of the phenomenon, a study of the drifting subpulses is likely to help in the selection of a possible model for the pulsed emission.

In the longitude vs pulse-number diagrams, the drifting subpulses occupy sloping bands. We investigate in the next section the longitudinal dependence of the slope of the subpulse bands, from geometric considerations alone, as given by the polar cap and the relativistic beaming models. To verify the predictions we had observed PSR 0031-07 which shows strong drifting-subpulse behaviour. The observed longitudinal dependence of the slope agrees better with the predictions of the relativistic beaming model than with the polar cap model.

3.2 Expected Dependence of the Slope of Subpulse Bands on Longitude

The scale of the longitude is defined such that one pulse period equals to 360° of longitude. It should be borne in mind that equal intervals of longitude during a pulse period as observed from the earth need not necessarily mean equal intervals of longitude in a frame co-rotating with the neutron star.

3.2.1 Polar cap models

In the oblique rotator polar cap models (Radhakrishnan and Cooke 1969; Sturrock 1971; Ruderman and Sutherland 1975) the radiation is generated on the open magnetic field lines around the magnetic poles. For our discussion we consider the model by Ruderman and Sutherland (1975), since as far as subpulse drift is concerned, their conclusions are unaltered by the modifications by Cheng and Ruderman (1977). According to this model a polar

magnetospheric gap is formed above the magnetic poles of a neutron star, since ions cannot be pulled out of the stellar surface except in case of the young Crab pulsar. Potential difference across the gap could be $\sim 10^{12}$ Volts. The gap continually breaks down, by the formation of electron positron pairs in localised sparks. The electrons flow back to the stellar surface and the ultra relativistic positrons escape into the magnetosphere, where they cause coherent microwave radiation. It is assumed that the location of the spark on the polar cap determines the subpulse's position within the pulse window. Ruderman and Sutherland (1975) show that the sparks drift around the magnetic pole with an average speed Δv, given by

$$\Delta v = \frac{\Delta V}{B_S r_P} c$$

where, ΔV is the potential drop over the length of a spark, B_S is the strength of the magnetic field on the surface of the neutron star, r_P is the radius of the polar cap and c is the velocity of the light.

To apply the model let us define the geometry as in Fig.3.1, so that the subpulses march form the trailing to the leading edge as in the case of PSRs 0031-07. Let the great circle passing through the rotational and the magnetic poles define the reference longitude $\lambda=0^{\circ}$. In polar cap models, the observed longitude of a subpulse and the longitude λ of the subpulse-producing spark on the unit sphere shown in

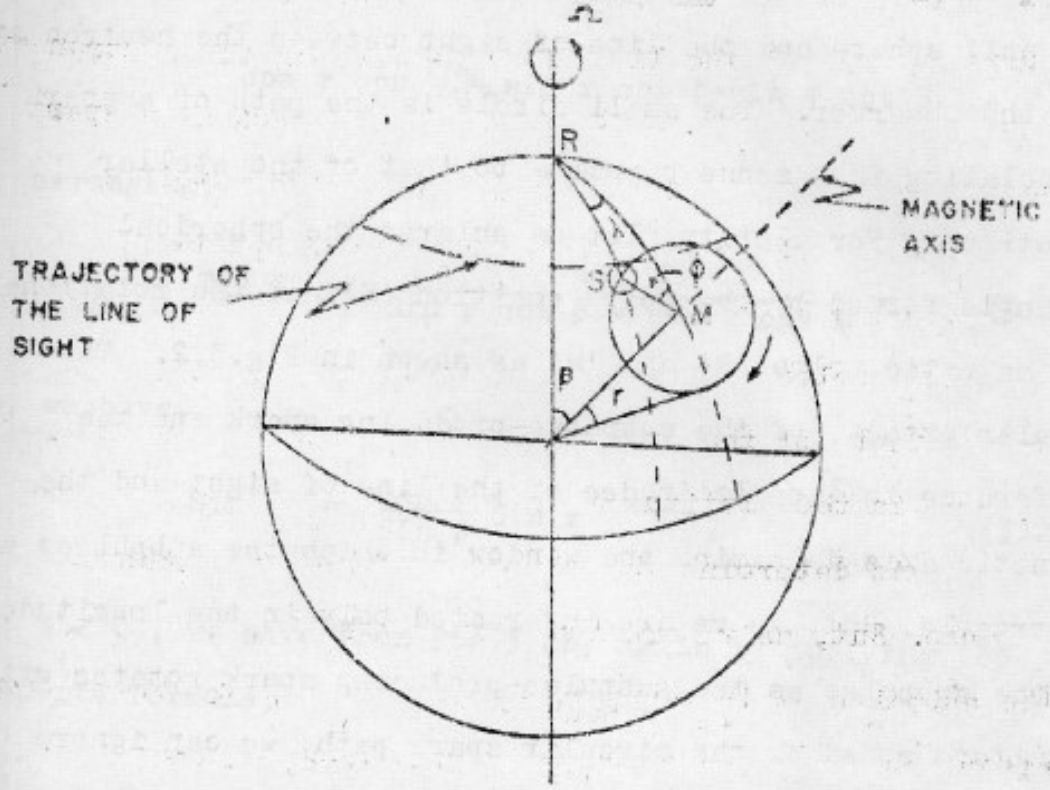

FIG. 3·1 GEOMETRY OF THE OBLIQUE ROTATOR POLAR CAP MODEL

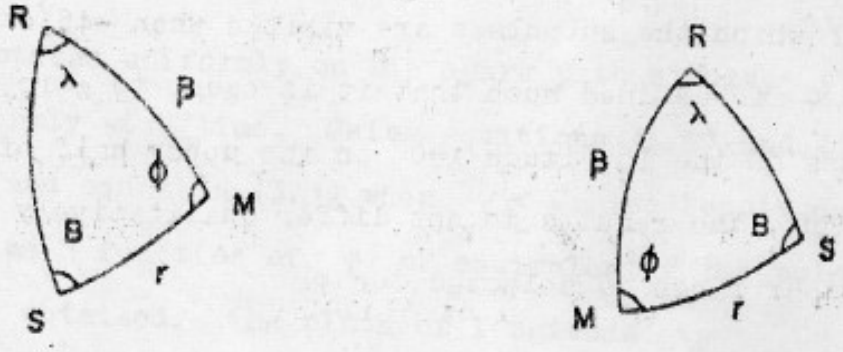

a) FOR $\phi > 0$ b) FOR $\phi < 0$

FIG. 3·2 ENLARGED SPHERICAL TRIANGLES

Fig.3.1 are directly proportional to each other. The dashed small semi-circle is the path of the point of intersection of the unit sphere and the line of sight between the neutron star and the observer. The small circle is the path of a spark circulating in a sense opposite to that of the stellar rotation. For clarity, let us enlarge the spherical triangle formed by the spark position 'S' and the rotational and magnetic poles 'R' and 'M' as shown in Fig.3.2. The angular extent of the subpulse-producing spark and the difference in the latitudes of the line of sight and the magnetic axis determine the window in which the subpulses are observable. But, as we are interested only in the longitude of the subpulse as the subpulse-producing spark rotates with a uniform speed on the circular spark path, we can ignore the angular extent of the spark and represent it by a point. We work out below the predictions of the polar cap model for the case in which the subpulses are visible when $-45^{\circ} < \varphi < +45^{\circ}$, where φ is defined such that it is equal to zero when a spark is on the longitude $\lambda=0^{\circ}$ on the upper half of the spark path. But, the results do not differ qualitatively even if some other range is selected for φ.

Applying the four-parts formula (Smart 1965) to the spherical triangle in Fig.3.2a, we obtain

$$\cos r \cos \varphi = \sin r \cot \beta - \sin \varphi \cot B$$

On rearranging,

$$\text{Tan } B = \frac{\text{Sin } \varphi}{\text{Sin } r \cot \beta - \cos r \cos \varphi} \qquad (3.1)$$

Also, we have,

$$\text{Sin } \lambda = \frac{\text{Sin } B}{\text{Sin } \beta} \text{ Sin } r \qquad (3.2)$$

when $\varphi < 0$, we have from Fig.3.2b, again by applying the four-parts formula,

$$\text{Tan } \lambda = \frac{\text{Sin } \varphi}{\text{Sin } \beta \cot r - \cos \beta \cos \varphi} \qquad (3.3)$$

As a spark rotates uniformly on the spark path circle, φ changes uniformly with time. Using equations (3.1) and (3.2) when $\varphi > 0$ and equation (3.3) when $\varphi < 0$, the longitude of the subpulse as a function of φ or equivalently the pulse number can be obtained. The plots of longitude vs pulse-number for a few representative values of r and β are shown in Fig.3.3. These plots represent the theoretically expected path of the subpulses on the basis of the polar cap models. The longitude dependence of the modulus of the slope of the bands is also shown on the plots. Compared to the central region of the window i.e. $\lambda = 0^{\circ}$, the subpulses

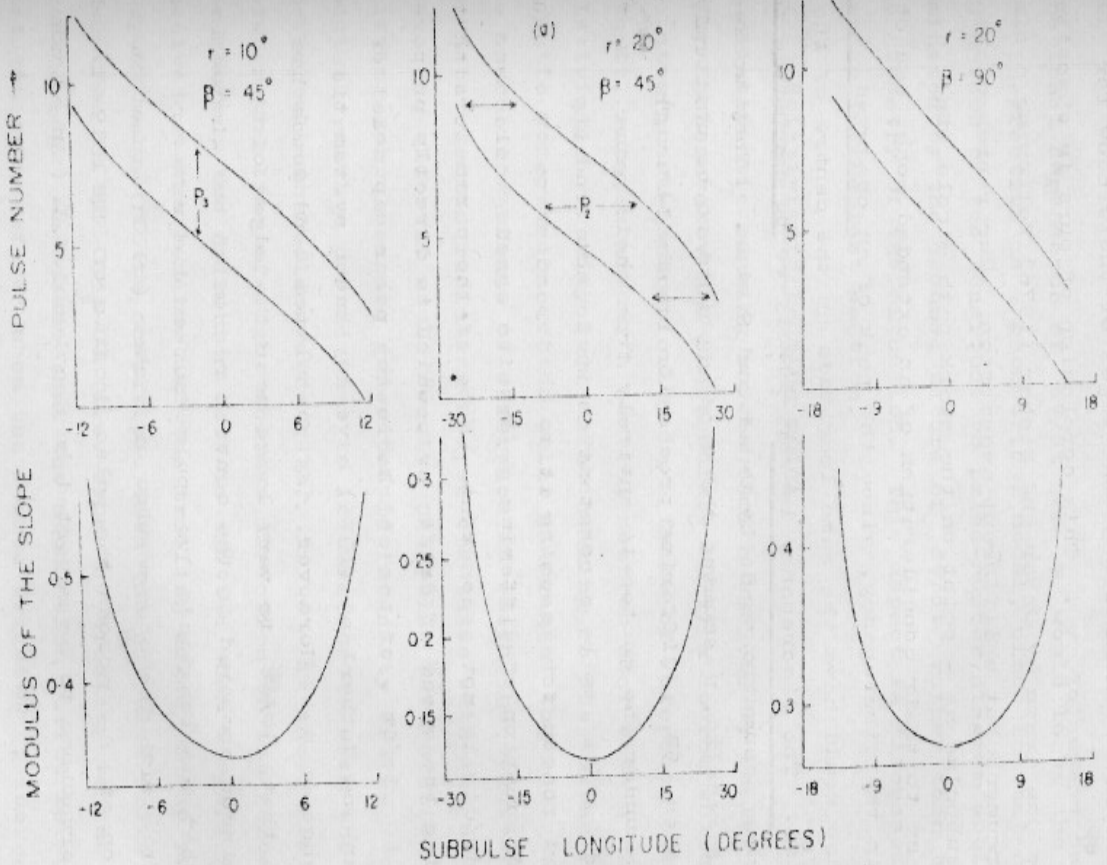

Fig.3.3. Subpulse paths and their slopes as predicted by the polar cap model. See Fig.3.1 for an explanation of r and β.

move slowly in longitude at the edges of the window for all assumed ranges of φ. This conclusion of ours is opposite to the one drawn by Oster and Sieber (1976) following a similar argument but a different assumption. Our representation of a subpulse as a point on the spark path circle, in contrast to their consideration of an extended zone, cannot explain the discrepancy, since the peak of an observed subpulse would have the same longitude as the centre of the subpulse. The discrepancy is very likely to be caused by the following assumption made by Oster and Sieber. They worked out the results, "assuming the window points to be uniformly reached in $5P_1$ (differing precession speeds !)". The wording under the quotes is entirely from their paper. We assumed $d\varphi/dt$ to be a constant as we do not find any a priori reason for assuming it to be dependent on φ. But their assumption of differing precession speeds would mean that $d\varphi/dt$ is not a constant. None of the parameters that determine the speed of drift Δv, which is directly proportional to $d\varphi/dt$, of the sparks in the polar cap model of Ruderman and Sutherland (1975) have any known systematic dependence on φ. Moreover, any postulated dependence has to be such that $d\varphi/dt$ is very large near the edges of the pulse window compared to the central region of the window in order that the longitude vs pulse-number diagrams are compatible with the observation of Backer (1970a) about the variation of P_2 across the pulse profile of PSR 1919+21 and our observations to be reported in Section 3.3.3. An ad hoc

functional dependence of $d\varphi/dt$ on φ would leave the model very ineffective as a geometrical model, since in that case the nature of the longitude vs pulse-number diagram would be dominated by the assumed nature of $d\varphi/dt$ rather than by the geometry of the situation. This aspect is discussed further in the last section.

3.2.2 Relativistic beaming model

In relativistic beaming models (Smith 1969,1970; Zheleznyakov 1971; Zheleznyakov and Shaposhnikov 1975) a source which radiates quasi-isotropically in a frame of reference comoving with it, rotates around a central neutron star with a highly relativistic velocity (v). The beaming is due to the relativistic compression of the polar diagram of the radiation of the source in a frame of reference in which the observer is at rest. As the radiating source corotates with the neutron star, the observer would receive one pulse per rotation period. Drifting subpulses are generated if intensity of the source is modulated with a period that is incommensurate with the period of the pulsar (Zheleznyakov 1971). If Θ' is the angle between the line of sight and the direction of the velocity of the source, the radiation that is emitted when $\Theta'=\pm\pi/2$ is received at the leading and the trailing edges of the pulse respectively. To be compatible with the subpulse drift direction in PSR 0031-07 (i.e. from the trailing to the leading edge) we assume that the modulation period is such that the value of Θ' when the source brightens , increases

every pulse period by $\Delta\Theta'$. In the comoving frame the source brightens once per $P+\Delta t'$ secs, where $\Delta t'$ is the time required for the source to move by $\Delta\Theta'$ in angular position. In a longitude vs pulse-number diagram, we are interested in the fractional part of the time interval in units of the period of the pulsar. Using the relativistic Doppler shift formula, the relation between $\Delta t'$ and the corresponding time interval Δt in the observer's frame of reference can be written as

$$\Delta t = \frac{1-\beta \cos \Theta}{(1-\beta^2)^{\frac{1}{2}}} \Delta t'$$

where $\beta = v/c$

and Θ is an angle in the observer's frame of reference corresponding to Θ' . Their relation is given by the aberration formula,

$$\text{Sin } \Theta = \frac{(1-\beta^2)^{\frac{1}{2}}}{1+\beta\cos\Theta'} \text{ Sin } \Theta'$$

This gives

$$\text{Cos } \Theta = \frac{\beta+\cos \Theta'}{1+\beta\cos\Theta'}$$

So,

$$\Delta t = \frac{1- \{ \frac{\beta^2+\beta \cos \Theta'}{1 + \beta \cos \Theta'} \}}{(1-\beta^2)^{\frac{1}{2}}} \Delta t'$$

Using the above formula along with the information that θ' increases uniformly with pulse number, plots of longitude vs pulse-number as shown in Fig.3.4 can be constructed. The figure also shows, the longitude dependence of the modulus of the slope of the subpulse bands.

3.3 Observations of Drifting Subpulses

There are three different methods by which drifting subpulses have been studied. The simplest of them is the phase-time diagram (Drake and Craft 1968; Taylor and Huguenin 1971). We would like to call such diagrams as longitude vs pulse-number diagrams since we use the word 'phase' for the phase of Fourier components. As subpulses have finite width and limited signal-to-noise ratios the quantitative information one can get from such diagrams is restricted. Problems due to low signal-to-noise ratios could be partially overcome using the two-dimensional correlation method (Taylor, Manchester and Huguenin 1975). However, this method has limitations since it gives the subpulse properties which are averaged over all possible longitudinal positions for the subpulses. The third method, called the longitude-resolved Fourier analysis method (Backer 1970a; Backer, Rankin and Campbell 1975) is free from such a limitation. Although we also use the two-dimensional correlation analysis for monitoring purposes as described below, the results obtained by us are based on the last method applied to the data on PSR 0031-07. The other pulsar with stable drifting subpulses,

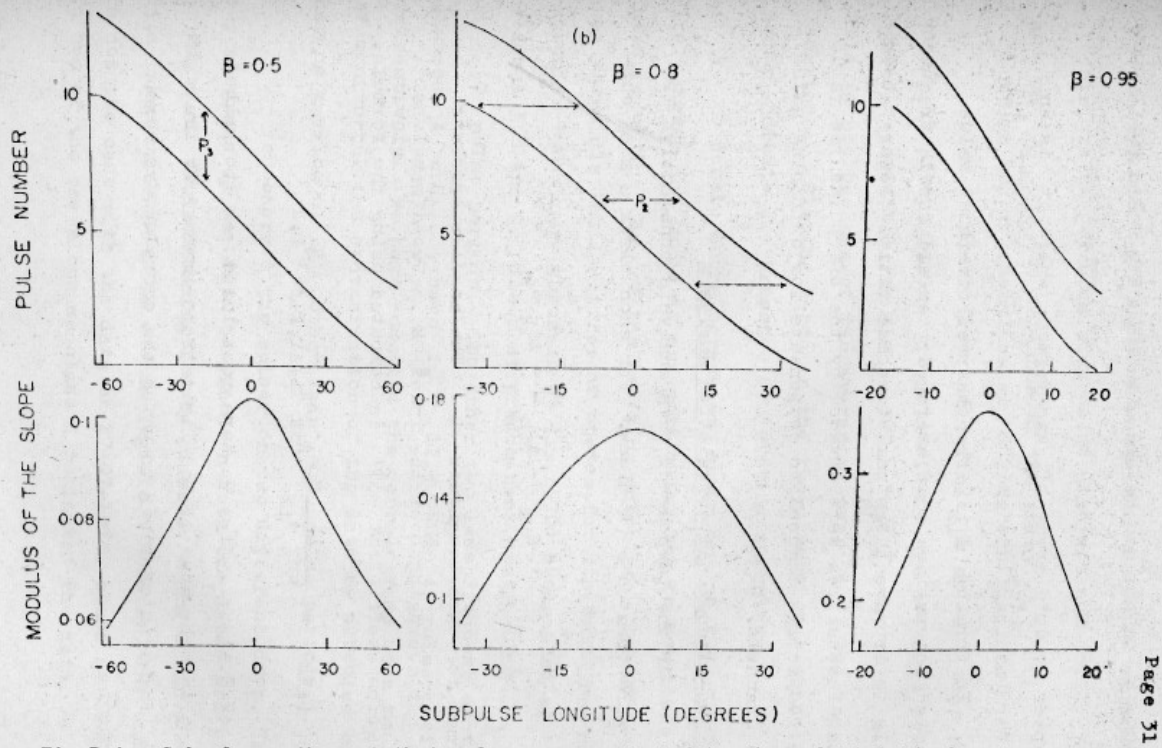

Fig.3.4. Subpulse paths and their slopes as predicted by the relativistic beaming model. $\beta = v/c$, where v is the velocity of rotation of the source and c is the velocity of light.

PSR 0809+74, is not accessible with the Ooty radio telescope.

From the raw data which were acquired as explained in Chapter 2, data array A'_{ik} was formed, where i is an index for the longitude and k is an index for the pulse number. In forming A'_{ik}, the observed off-pulse value subtracted intensities were averaged over all the 12 frequency channels to improve the signal-to-noise ratio. Before averaging, the intensities were divided by the off-pulse rms value of the respective channel to compensate for differing gains of the channels.

3.3.1 Two-dimensional correlation analysis

For the purpose of this analysis consecutive 128 pulses were treated as a block. For each block a mean subtracted array

$$A_{ik} = A'_{ik} - \langle A'_{ik} \rangle_k$$

is formed for each longitude i. The angular brackets stands for averaging over the index k. Two-dimensional correlation coefficient 'T' is computed using the formula,

$$T(\Delta i, \Delta k) = \frac{1}{\text{var } A_{ik}} \langle A_{ik} A_{i+\Delta i, k+\Delta k} \rangle_{i,k}$$

where $\Delta k = 0, \pm 1 \ldots, \pm 11$. We have restricted Δk to ± 11 pulse periods because of the limitations imposed by the width of the line printer paper on which the correlograms were displayed.

$\Delta i = 0, \pm 1, \ldots, \pm 25$ samples (= one third of the maximum longitude that is available)

and var A_{ik} is the variance of the array A_{ik}.

As is clear from the definition of T, this method would give the subpulse properties that are averaged over all possible positions for the subpulses within the pulse window. This is so, because of the averaging over i, the index for longitudes. Sloping bands in the two-dimensional correlograms indicate the presence of drifting subpulses.

Sample correlograms are shown in Fig.3.5. The spacing between the bands at any particular lag in longitude is a measure of the P_3 of the drifting subpulses. PSR 0031-07 has three distinctly different states for its drifting subpulse behaviour (Huguenin et al. 1970) designated as classes A,B and C. The most predominent state, Class B, has $P_3 \sim 7$ pulse periods. The other two less frequent states, classes A and C, have $P_3 \sim 12.5$ and 4 pulse periods respectively. We have computed the correlograms as a means of monitoring the contamination of the data by subpulse bands having a value of P_3 other than ~ 7 pulse periods.

We observed the pulsar on two different days. Sample correlograms of the data obtained on both the dates are given in Fig.3.5. The contamination by classes A and C in the data taken on 29-06-1976 was negligible. However, the same is not the case with the data on 27-07-1978, since at least in one of the correlograms class A dominated the data.

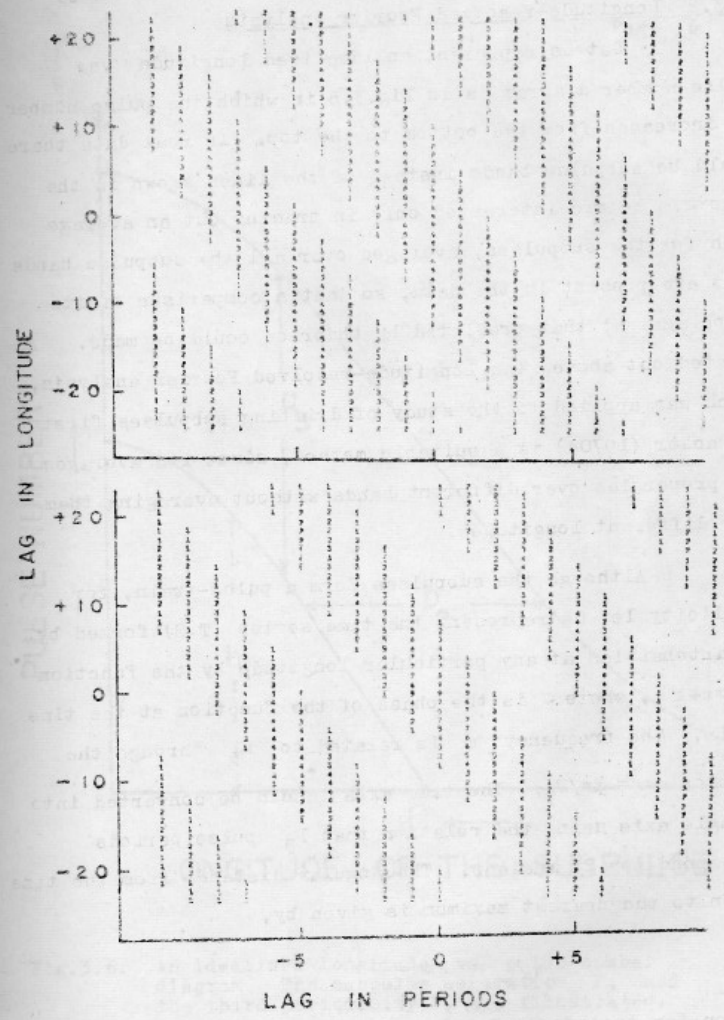

Fig.3.5. Two-dimensional correlograms of data on PSR 0031-07. Top plot is from data obtained on 29/06/1976 and bottom plot is from data obtained on 27/07/1978.

3.3.2 Longitude-resolved Fourier analysis

Let us represent an idealised longitude vs pulse-number diagram as in Fig.3.6 in which the pulse number k increases from the bottom to the top. In real data there would be subpulse bands instead of the lines shown in the figure. We are interested only in tracing out an average path for the subpulses, averaged over all the subpulse bands that are present in the data, so that a comparison of its slope against that predicted by theories could be made. As pointed out above, the longitude-resolved Fourier analysis, which was applied to the study of drifting subpulses first by Backer (1970a) is a suitable method, since its averages the properties over different bands without averaging them over different longitudes.

Although the subpulses form a pulse-train, for simplicity let us represent the time series (T.S) formed by the intensities at any particular longitude by the function $\cos(\omega t+\zeta)$, where ζ is the phase of the function at the time origin. The frequency ω is related to P_3 through the equation $\omega = 2\pi/P_3$. The time axis could be converted into an angle axis using the relation that P_3 pulse periods correspond to 2π radians. The angular distance from the time origin to the nearest maximum is given by,

$$\psi' = 2\pi - \zeta$$

The Fourier transform $\widetilde{T.S.}$ of the time series (T.S.) extending over a duration $\pm T$ is given by

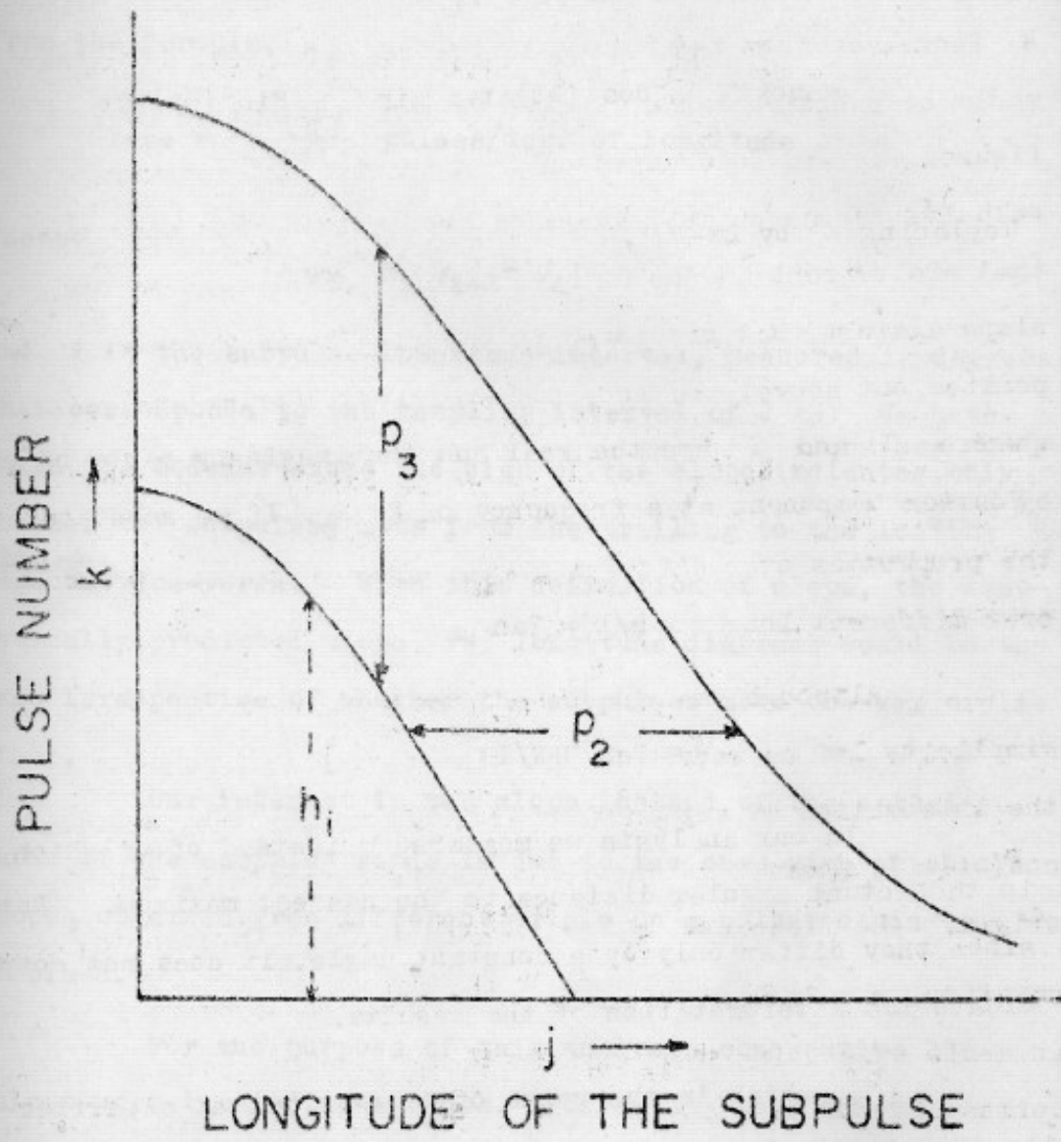

Fig.3.6. An idealised longitude vs pulse-number diagram. The subpulse separation P_2 and the third periodicity P_3 are illustrated.

$$\widetilde{T.S.} = \int_{-T}^{+T} \cos(\omega t + \zeta)\, e^{-i\omega t}\, dt$$

$$= \cos\zeta \int_{-T}^{+T} \cos^2(\omega t)\,dt + i \sin\zeta \int_{-T}^{+T} \sin^2(\omega t)\, dt$$

Replacing ζ by $2\pi - \psi'$,

$$-I/R = \tan\psi'$$

where R and I are the real and the imaginary parts of the Fourier component at a frequency of $2\pi/P_3$. If we substitute $\psi = \psi' + \pi/2$

$$R/I = \tan\psi$$

i.e.

$$\psi = \tan^{-1}\{R/I\}$$

In our analysis we measured ψ instead of ψ' which is the actual angular distance to the nearest maximum. But since they differ only by a constant angle, it does not complicate the interpretation of the results.

ψ_i which is the value of ψ measured at a particular longitude i and the h_i shown in the Fig.3.6 are related through

$$\psi_i - \pi/2 = 2\pi\, h_i/P_3$$

A plot of ψ_i against the longitude i represents the path of an average subpulse band across the pulse window. The slope of subpulse bands at a longitude i can be computed from the formula,

$$\text{Slope} = \frac{\Delta \psi_i \cdot P_3}{2\pi \cdot \Delta \ell} \quad \text{pulses/deg. of longitude}$$

where,

$$\Delta \psi_i \equiv | \psi_{i+1} - \psi_i |$$

and $\Delta \ell$ is the subpulse-longitude interval, measured in degrees, that corresponds to the sampling interval of 2 ms. We have taken the modulus since the sign of the slope indicates only whether the subpulses move from the trailing to the leading edge or vice-versa. With this definition of slope, the theoretically predicted slope vs longitude diagrams would be the same irrespective of whether the subpulses move one way or the other.

Our interest in the slope instead of the actual paths of the subpulse bands is due to the ease with which slopes obtained from different trials on a pulsar could be combined.

For the purpose of this analysis consecutive 256 pulses were treated as a block. For each block a mean subtracted array was formed for each longitude i , giving

$$A_{ik} = A'_{ik} - \langle A'_{ik} \rangle_k$$

To limit the leakage of power from a frequency to the adjacent frequencies in the Fourier transform, a cosine taper data

window was applied (Otnes and Enochson 1972). The data window uses the following weights.

$$\cos^2 \frac{5\pi t}{2T} \quad \text{for} \quad -T \leq t \leq -8T/10$$

$$1 \quad \text{for} \quad -8T/10 < t \leq 8T/10$$

$$\cos^2 \frac{5\pi t}{2T} \quad \text{for} \quad 8T/10 < t \leq +T$$

$$0 \quad \text{otherwise.}$$

A fast Fourier analysis was performed on the data from which the power spectrum

$$P_i(f) = R_f^2 + I_f^2$$

was derived. R_f and I_f denote real and imaginary parts of the Fourier component at a frequency f . The existence of a non-random feature in the power spectrum indicates the presence of a quasiperiodic intensity modulation in the data. Narrower the feature, more stable is the underlying phenomenon.

The existence of a feature, either narrow or broad, in the power spectrum does not by itself indicate the presence of drifting subpulses. From the observed behaviour of subpulses in PSRs 1919+21 and 2016+28, Backer (1973) had made a case for classifying all pulsars which have non-random features in their power spectra as having generalised drifting subpulses. If it is due to drifting subpulses, a feature

in the power spectrum at a frequency f_3 would imply a period $P_3 = 1/f_3$.

After identifying a peak at f_3 in the power spectrum, the angle ψ_i is calculated using the relation,

$$\psi_i = \mathrm{Tan}^{-1} \{R_f/I_f\}$$

where R_f and I_f correspond to the frequency f_3 in the data at a constant longitude i . Sloping lines in phase (ψ_i) vs longitude diagrams establish the presence of drifting subpulses.

3.3.3 Results and discussions

PSR 0031-07 was observed on two different days to study the dependence of the modulus of the slope on the longitude of the subpulse. The pulsar was strong for considerable duration on both the days. The plot of the slope vs longitude which was obtained from the observations on 29-06-1976 is shown in Fig.3.7. The value of $\Delta\psi_i$ that was used in obtaining the slope at each longitude was the arithmetic mean of the values obtained from 10 different blocks of data on the same day. For most of the longitudes one or two values of $\Delta\psi_i$ differred markedly from the rest of the values. To maintain uniformity, we ignored two values of $\Delta\psi_i$ which differred the most from the rest of the values in arriving at the mean value at each longitude. The error bars shown in the diagram are the rms errors in estimating the mean value

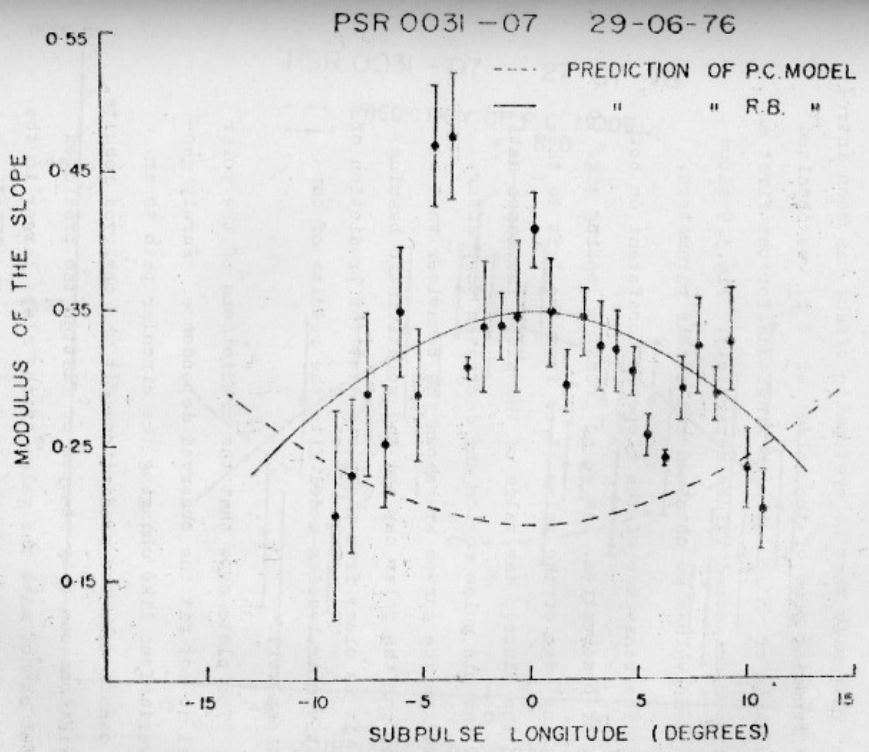

Fig.3.7. A comparison of the observed modulus of the slope with the predictions of the polar cap (P.C.) and the relativistic beaming (R.B.) models. The slope is measured in units of pulses/degree of longitude.

from eight measurements. A similar plot obtained from the observation on 27-07-1978 is shown in Fig.3.8.

To verify that no systematic effect has been introduced by ignoring some of the values of $\Delta\psi_i$ we obtained the mean value of $\Delta\psi_i$ at each longitude for the first and the last four unignored values separately. Fig.3.9 shows that the mean values so obtained are stable parameters.

The behaviour of the slope is consistent on both the days of observation. As we go from the leading edge to the trailing edge of the pulse (i.e. from the left to the right of the plots), the value of the slope increases until we reach the mid pulse region and decreases thereafter. Superposed on the curves are shown the behaviour that is expected from the polar cap and the relativistic beaming models. It is clear from the plots that the prediction of the relativistic beaming model fits the results of our observations well.

The plots show that the predictions of the polar cap model do not fit the observed dependence. Purely geometric variations like changing the circular path to an ellipse cannot make the predictions fit the observed results. Such variations can only steepen or flatten the predicted curve, but cannot make the value of the slope larger in the middle of the pulse compared to those at the edges. As had been discussed previously the trend of the slope on longitude can be reversed if the sparks move slower at $\lambda = 0^{o}$ and

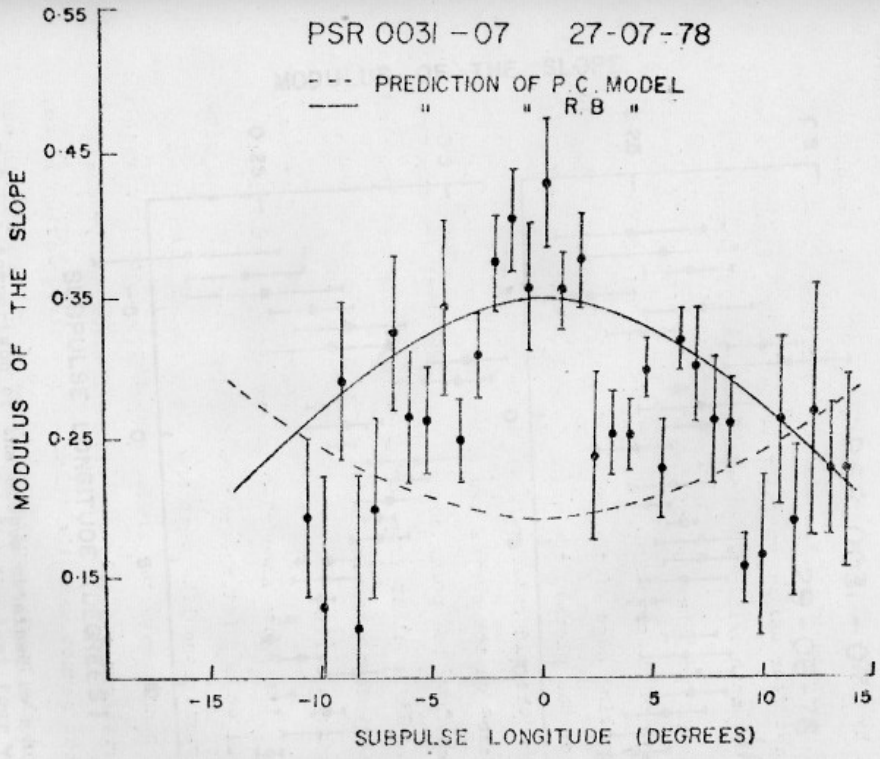

Fig.3.8. A comparison of the observed modulus of the slope with model predictions.

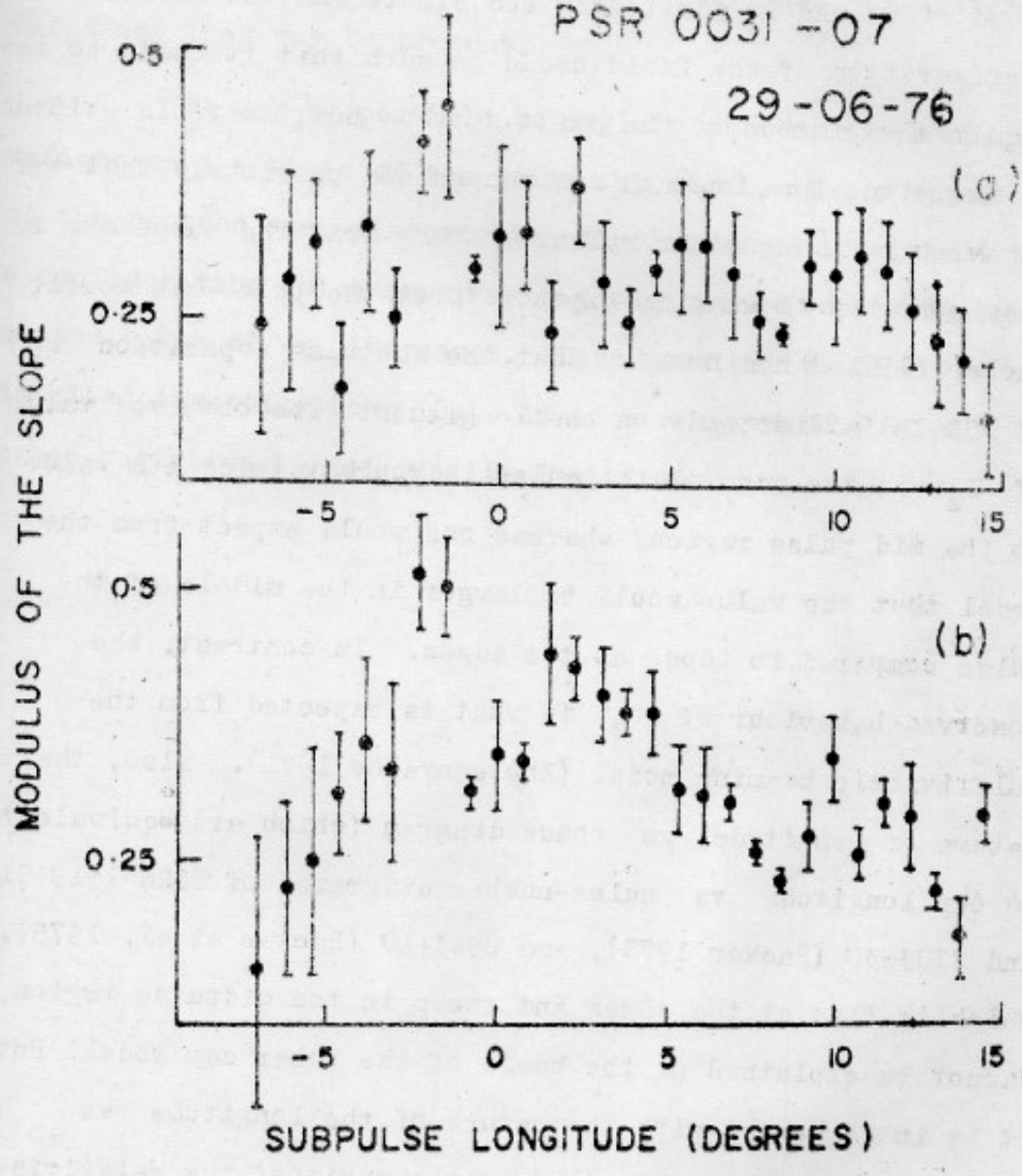

Fig.3.9. A comparison of the slopes obtained by averaging (a) the first four and (b) the last four values of $\Delta\Psi_1$ at each longitude.

faster as the value of λ increases. One may argue that the above may be the case for PSR 0031-07 since the dipolar nature of the magnetic field which is assumed in deriving the drift speed of sparks is admittedly too simple and the actual configuration of the field could be such that it leads to the required variation of the drift speed. But, there is evidence in the literature, though not recognised previously that the behaviour of many other pulsars having drifting subpulses is also contrary to what is expected from the polar cap model. Backer (1970a) had noticed that the subpulse separation P_2 of PSR 1919+21 depends on the longitude. The observed value of P_2 at the edge of the pulse is roughly twice its value at the mid pulse region, whereas one would expect from the model that the value would be larger in the middle of the pulse compared to those at the edges. In contrast, the observed behaviour of P_2 is what is expected from the relativistic beaming model (Zheleznyakov 1971). Also, the nature of longitude vs phase diagram (which are equivalent to our longitude vs pulse-number diagrams) of PSRs 1919+21 and 2303+30 (Backer 1973), and 0943+10 (Backer et al. 1975), which is flat at the edges and steep in the midpulse region, cannot be explained on the basis of the polar cap model. But, it is in agreement with the nature of the longitude vs pulse-number diagrams derived on the basis of the relativistic beaming model. Though, some of the above measurements in the literature may not be statistically very significant, put together they do add support to our conclusions. In the

case of PSR 0809+74 no systematic variation of the drift rate with longitude was noticed (Page 1973). But, the presence of the drift rate discontinuities which are known to exist for this pulsar (Cole 1970; Page 1973) may mask any systematic trend that may be present.

It may be possible to explain all the above observations on the basis of the polar cap model, if the spinning of the neutron star distorts the dipolar magnetic field into a configuration which ensures that the sparks rotate faster as the value of $|\lambda|$ increases. This possibility deserves a detailed investigation. But, an ad hoc assumption of such a speed variation is not readily justified.

Chapter 4

NEUTRON STAR WOBBLE AND SHORT-TERM INTENSITY VARIATIONS OF PULSARS

4.1 Introduction

Within the pulse window, pulsars show a variety of intensity variations spread over a large range in time scales. The microstructure phenomenon, which is the fastest of the variations has time scales as low as a few microseconds (Hankins 1971). On the other extreme, mode changing which is the slowest, has time scales in excess of several minutes (Backer 1970c; Lyne 1971).

Even after the intensity is first averaged over the whole pulse and then, over many pulses, variations with time are still seen. Such variations are unlikely to be caused by the intensity variations taking place within the window for the following reasons:

a) Since microstructure is a very fast phenomenon, it is unlikely to cause appreciable variations after the intensity is averaged over many pulses.

b) Though the drifting subpulse phenomenon causes considerable amount of variations of the total pulse intensity at frequencies lower than about 200 MHz, it does not cause noticeable variations at higher frequencies for many pulsars (Taylor, Jura and Huguenin 1969; Backer 1970a).

c) The mode change is an infrequent phenomenon occurring at irregular intervals. Moreover, observationally there is no obvious dependence of the pulse shape on the intensity of the pulsar.

The intensity variations of the total pulse could be caused either by some memory mechanism in the emission process or by geometric effects. In the former case, the energy output in the form of radio pulses changes with time. In the latter case, the output could be a constant as the observed intensity variations are caused by changes in the orientation of the emission beam with respect to the line of sight joining the Earth and the pulsar. It is difficult to discuss memory mechanism in pulsars as the emission process itself is not well-understood. In this chapter we examine one of the geometric means that could produce intensity variations with time scales of several minutes - wobble of a neutron star having a solid core. In the next section we show that it may be possible to detect wobble through intensity variations which are broad band in nature. In practice, identifying variations with a period of several minutes in the intensity of pulsars is difficult at metre wavelengths due to the presence of interstellar scintillations which also have similar time scales. In the later part of the chapter we develop a method to separate the autocorrelation function (ACF) of the intrinsic intensity variations from that of the interstellar scintillations by exploiting the difference in their decorrelation bandwidths. This procedure, called

'HAMSA' after a fictious bird in Hindu mythology which is believed to be capable of separating milk from a mixture of milk and water, was applied to the intensity variations of 24 pulsars that were observed at Ooty. The results are discussed in the last section of the chapter.

4.2 Free Precession or Wobble of Neutron Stars

The view that pulsars are rotating neutron stars (Gold 1968) is generally accepted, though the details of the mechanism through which the radiation of pulsars is produced is not well established. Spinning bodies with finite rigidity deform under the combined action of gravitational and centrifugal forces. The shape of an invicid body adjusts itself so that the spin axis is aligned with one of the principal axes of moment of inertia. But, in the case of a solid body the axes need not be aligned and such a body can undergo free precession or wobble even in the absence of an external torque. Such a wobble has been well-studied in the case of the Earth and is called the Chandler wobble, after its discoverer. Since neutron stars have solid crusts and may have solid cores also, pulsars may also sustain such a wobble. Though its detection is still elusive, wobble of neutron stars was postulated to explain many different phenomena, such as:

a) The drifting subpulse phenomenon of pulsar (Vila 1969).

b) The supposed periodicity in the time of arrival residuals of the Crab pulsar (Ruderman 1970; Chiuderi and Occhionero 1970; Burns 1970).

c) The X-ray emission from Cen XR-3 (Henriksen, Feldman and Chau 1971).

d) The high-low states of X-ray emission from Her X-1 with a periodicity of 35 days (Brecher 1972).

e) The intensity modulation of γ-rays from CG 195+4 with a period of 59s (Maraschi and Treves 1977), and

f) The quasiperiodic variation of the period P_3 of PSR 1919+21 with a time scale of 30 min (Wolszczan 1978).

As we shall see later on, if wobble of pulsars is detected, the frequency of the wobble is likely to indicate whether solid cores exist in neutron stars or not. Because of its relevance to the nature of the nuclear forces at very high matter densities, any attempt to detect neutron star wobble is worthwhile.

4.2.1 Structure of neutron stars

The possibility of existence of wobble and its likely frequency are intimately related to the structure of neutron stars. Specifically, the shear modulus and the volume of the solid portion of the neutron star influence the possible frequency of wobble. Below, we review briefly the relevant aspects of the structure of a neutron star. Detailed reviews of the structure including the question of the existence of a solid core were given by Cameron and Canuto (1974); Baym and Pethic (1975); and Pandharipande, Pines and Smith (1976).

Neutron stars are highly compact objects with their mass in the range of 0.1 $M_\odot$ to $\sim$ 1.5 to 2.5 $M_\odot$ and radii

$\sim$ 10 km, where $M_\odot$ denotes a solar mass. The central densities may reach more than 10^{15} g cm^{-3}, i.e. the densities are supranuclear. The uncertainty in the upper limit on the mass reflects our ignorance of the equation of state at very high densities (Baym and Pethic 1975; Pandharipande et al. 1976). For the purpose of our discussion a neutron star may be schematically represented as in Fig.4.1. The inner parts of a neutron star cool to temperatures below a few times 10^8 ^oK during their early life. Neutron stars can be considered as zero temperature stars from the point of view of melting of the crystelline crust as melting requires temperature in excess of 10^{10} ^oK. The superfluidity of the neutron and the proton gas is also stable since the transition temperatures greatly exceed 10^9 ^oK. Now we briefly look at each of the three parts of a neutron star.

a) The solid crust: The matter density in the solid crust ranges from 10^6 g cm^{-3} on the surface to $\sim 2.4 \times 10^{14}$ g cm^{-3} at the base of the inner crust. The matter is composed of relativistic electron gas, superfluid neutron gas and nuclei. The nuclei are in a stable Coulomb lattice. The shear modulus μ of the lattice is given by,

$$\mu = \frac{0.37}{2^{1/3}} (ze)^2 n_z^{4/3}$$

where ze is the charge per nucleus and n_z is the number density of nuclei (Baym and Pines 1971). $\mu \sim 10^{29}$ dyne cm^{-2} for the outer crust and $\sim 10^{31}$ dyne cm^{-2} at the base of the inner crust.

TIFR CENTRE, BANGALORE 3641 LIBRARY

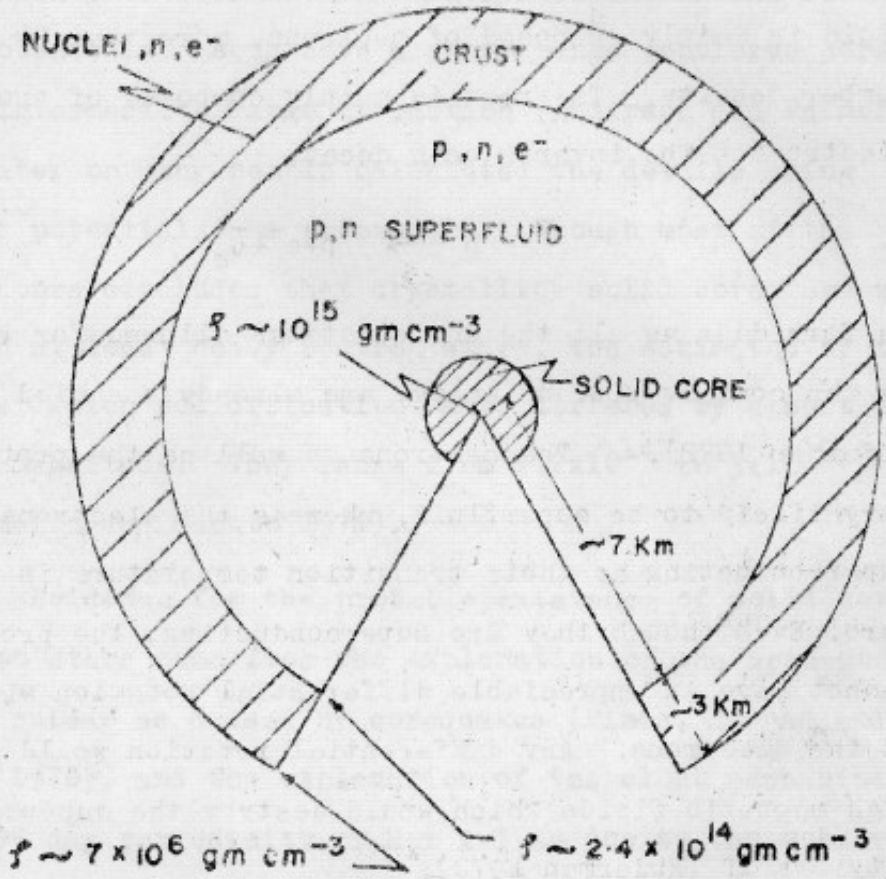

Fig.4.1. A schematic diagram of the structure of neutron stars.

b) The superfluid part: In this region the density of matter ranges from $\sim 2.4 \times 10^{14}$ g cm^{-3} to ρ_c, where ρ_c is the density at which solidification may take place. The fluid is mainly composed of neutrons, more than 90 % by number density. The rest is mainly composed of protons and electrons. The inverse beta decay,

$$n \longrightarrow p + e^- + \bar{\nu}_e$$

is forbidden as all the energy states allowed for electrons by the conservation of energy are already occupied (e.g. Ruderman 1972). The neutrons as well as the protons are very likely to be superfluid, whereas the electrons are not superconducting as their transition temperature is close to zero. Even though they are superconducting, the protons cannot have an appreciable differential rotation with respect to the electrons. Any differential rotation would produce high magnetic fields which would destroy the superconductivity itself (Ruderman 1972).

The success of the two component theory of post-glitch healing of pulsars (Baym et al. 1969), in interpreting the Crab and the Vela pulsar timing data provides evidence for the presence of superfluid in neutron stars.

c) The solid core ?: Our knowledge of core of the neutron star is the most uncertain, since phenomenological nucleon-nucleon potentials that were successful at subnuclear densities may not be valid on extrapolation at supranuclear densities which one encounters in neutron stars.

Solidification of neutron fluid at very high pressure similar to the one undergone by He^3 was originally suggested based on the similarity between neutron-neutron potential and He^3 atomic potentials. Both have a short range repulsive core with an intermediate range attraction (Anderson and Palmer 1971). Later on many people calculated the details using different potentials and procedures. Though most of the investigators concluded that crystalline solid cores are very likely in at least heavy neutron stars, the estimates of the density at which solidification starts differed by almost an order of magnitude. They range from 4.2×10^{14} to 3×10^{15} g cm^{-3} (Cameron and Canuto 1974).

Evidence for the probable existence of solid cores in neutron stars came from the explanation of the spin-ups of the Vela pulsar as caused by corequakes (Pines, Shaham and Ruderman 1972), and the explanation of the clock mechanism for the 35 day periodicity of Her X-1 as due to the wobble of the neutron star (Pines, Pethic and Lamb 1973). However, in the second case the evidence is not very convincing (Pandharipande et al. 1976).

4.2.2 Frequency of wobble

For a perfectly rigid body which is axially symmetric, the wobble frequency Ω_w is given by (e.g. Goldstein 1950),

$$\Omega_w = \frac{\Delta I}{I} \Omega \cos \alpha$$

where ΔI is the excess of the perpendicular moment of inertia over the paraxial moment of inertia I, Ω is the angular frequency with which the body is rotating and α is the angle between the spin axis and the axis of the principal moment of inertia.

A neutron star is not a perfectly rigid body for two reasons: i) Though the solid portion of the neutron star is very tough by terrestrial standards, it is not rigid in the presence of the immense gravitational force present in the neutron stars. ii) All stable neutron stars have proton and neutron superfluid regions below their solid crust. For a non-rigid body the wobble frequency (Pines and Shaham 1972a),

$$\Omega_w = \frac{3}{2} \frac{B}{A+B} \varepsilon_o \Omega \quad ,$$

where A and B depend on the gravitational and the elastic energy stored in the star and ε_o is a reference oblateness which corresponds to the oblateness at which the crust or the core of the star would be strain-free. For a neutron star ε_o would depend on the oblateness at the time of solidification and the subsequent seismic history. For a self-gravitating incompressible sphere of radius R and crystal volume V_c,

$$A = \frac{3}{25} \frac{GM^2}{R}$$

and

$$B = \frac{57}{50} \mu V_c$$

The numerical values of A and B depend on the assumed structure. The most recent estimation of the values for these parameters were given by Pandharipande et al. (1976) for four different interaction models for the neutron matter and a range of masses for the neutron star. For those stars which do not have a solid core B << A and so,

$$\Omega_w/\Omega = \frac{3}{2} \frac{B}{A} \varepsilon_o \qquad (4.1)$$

and for those stars which have a solid core B ~ A and so,

$$\Omega_w/\Omega = \frac{3}{4} \varepsilon_o \qquad (4.2)$$

For liquid core stars B/A ranges from 6×10^{-3} to 2×10^{-4} for stars with mass in the range of 0.29 $M_\odot$ to $M_\odot$. As one can place limits on the value of ε_o from the interpretation of glitches, in principle, one could say whether a neutron star contains a solid core or not from the wobble frequency since equations (4.1) and (4.2) predict frequencies differing by atleast two orders of magnitude.

4.2.3 Amplitude, excitation and damping of wobble

The amplitude of wobble is equal to the angle α between the principal axis of maximum moment of inertia and the spin axis of the body. For a neutron star, the wobble amplitude is probably limited by the maximum possible storage of the elastic energy. If the amplitude of the wobble exceeds a critical value, 'Θ' type quakes are likely to occur (Pines and Shaham 1972b). For a neutron star with a solid core the critical angle is ~ 6° and for a star with a liquid core it could be ~ 15° (Pines and Shaham 1974).

Given the large possible wobble amplitudes, the observability of neutron star wobble depends on the mechanisms for both exciting and damping the stellar wobble. There are many different mechanisms for both of them (Goldreich 1970; Chau, Henriksen and Rayburn 1971; Heintzmann, Kundt and Schrüfer 1973; Pines and Shaham 1974; Macy 1974; Baym, Lamb and Lamb 1976 and the references contained therein). Apart from these mechanisms most of which specifically depend on the presence of high magnetic fields associated with neutron stars, excitation of wobble may be produced by star quakes similar to the excitation of Chandler wobble by the earth quakes (Mansinha and Smylie 1968). Electro-magnetic torque mechanisms have characteristic times comparable to slowing down times. Crust-liquid coupling would produce wobble dissipation times $\sim 3 \times 10^4$ yrs for the Crab pulsar and ~ 500 yrs for the Vela pulsar (Pines and Shaham 1974). But if dissipation by internal friction in crust or core is important, then damping time comparable to wobble periods may be realized (Macay 1974).

4.2.4 Intensity variations produced by wobble

The nature of intensity variations caused by wobble is intimately linked with the pulsar beaming models. As discussed in section 1.2, there are broadly three different types of models: 1) direction dependent masing models, 2) polar cap models and 3) relativistic beaming models. In polar cap models, the diagram of emission is likely to be defined by the configuration of the open field lines close to

the neutron star and hence is rigidly tied to the crust of the neutron star. One can understand the qualitative features of the intensity variations caused by the wobble by referring to Fig.4.2. Because of the wobble, the centre of the radiating source would describe a circular path, when its position is projected on to an unit sphere. This path, represented by the circle C is in addition to the circular path the source would follow due to the rotation of the neutron star. The dashed circle r is the extent of the radiating source, assumed to be circular for simplicity. If the path L of the line of sight does not pass through the circle C , but is such that its closest distance h from the circle C is less than the radius r of the radiating source, then there would be one intensity maximum per wobble period. On the other hand, if L passes through the circle C , there would be two maxima per wobble period. The maxima need not be placed symmetrically within the wobble period unless L passes through the centre of the circle C . The depth of modulation would depend on the relative magnitude of r,C and h . It also depends on whether L passes through the circle C or not. Smaller is r with respect to C , greater is the modulation. And larger the distance of L from the centre of the circle C , greater is the modulation. It may not be meaningful to construct a detailed quantitative picture of the intensity variations, since the basic input, i.e. the structure of the radiating source itself is unknown.

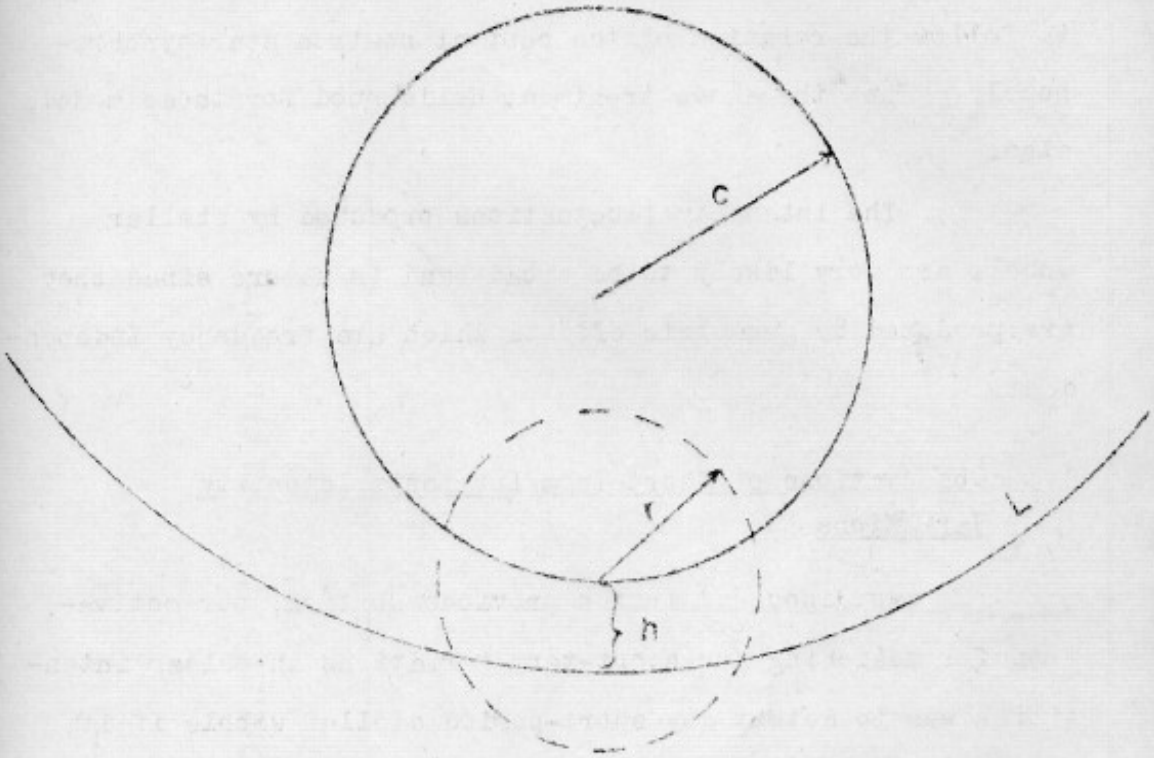

Fig.4.2. The wobble induced circular path C of a radiating source. The radiating source is represented by the dashed circle r. L represents the path of the line of sight.

If the conventional explanation of glitches that they are due to star quakes is to be applicable to the other two models, the emitting region in those models also may have to follow the rotation of the central neutron star synchronously. Then the above treatment holds good for those models also.

The intensity fluctuations produced by stellar wobble are very likely to be broad band in nature since they are produced by geometric effects which are frequency independent.

4.3 Observations of Short-Term Intrinsic Intensity Variations

As discussed in the previous section, our motivation for searching for short-term variations in pulsar intensities was to detect any short-period stellar wobble if it exists. By short period we mean periods of about a few to a few tens of minutes. Interstellar scintillations (ISS) of pulsar radiation which also have similar time scales (Scheuer 1968; Slee et al. 1974; Backer 1975) makes direct observations of such variations very difficult. As all pulsars are in the strong scattering regime at metre wavelengths, modulation indices due to scintillation are close to one. The decorrelation frequencies are much smaller than the observational frequency. The normalised function one would obtain by cross-correlating intensities at adjacent radio frequencies is shown schematically in Fig.4.3 (Lang 1971; Balasubramanian 1979). The initial drop is produced by the

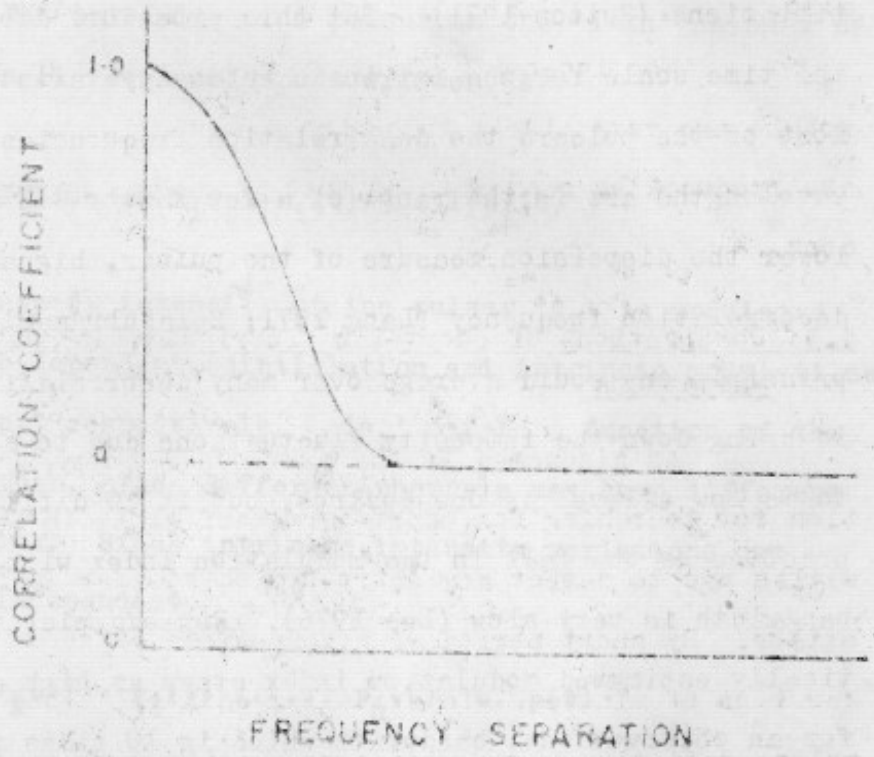

Fig.4.3. A schematic diagram illustrating the decorrelation of intensity variations due to ISS. The constant pedastal d is due to IIV.

decorrelation of the intensity variations caused by scintillations, whereas the constant pedestal d is produced by the intrinsic intensity variations. If the total modulation index is known, it is possible to estimate the modulation index separately for the intrinsic variations and the scintillations (Sutton 1971). But this procedure does not give the time scale for the intrinsic intensity variations. For most of the pulsars the decorrelation frequencies at metre wavelengths are in the range of a few kHz to ~ 1 MHz and lower the dispersion measure of the pulsar, higher is the decorrelation frequency (Lang 1971; Balasubramanian 1979). In principle one could average over many decorrelation bandwidths to bring down the intensity fluctuations due to scintillations to as low a level as one desires, but it is difficult in practice as the fall in the modulation index with increasing bandwidth is very slow (Lee 1976). For example, the theoretically estimated modulation index stays as high as 0.4 even for an observational bandwidth which is 10 times the decorrelation bandwidth. Thus, a method that could separate the IIV from the ISS is required. Such a method is described in the next section.

4.3.1 'HAMSA' - A Method to separate the ACF of IIV from that of ISS

This method is based on the fact that the intensity variations produced by ISS have small correlation frequencies, whereas those produced by the intrinsic reasons have large correlation frequencies compared to the typical observational

bandwidths. For the purpose of this method all intensity variations which are completely correlated over frequency separations larger than the decorrelation frequencies due to ISS are treated as the intrinsic intensity variations.

The intensity of a pulsar in the 'i th' channel of a multichannel receiver can be written as

$$I_i'(t) = a_i\{ 1+s_i(t) \}\{ 1+p_i(t) \}$$

where the steady intensity of the pulsar 'a_i' is modulated by the time dependent scintillation and intrinsic modulations 's_i' and 'p_i' respectively. 'a_i' may be a function of the channel number, since different channels may have different overall gains. Since intrinsic intensity variations are frequency independent,

$$p_1(t) = p_2(t) \ldots\ldots p_n(t) = p(t)$$

where n is the total number of channels. Mean subtracted intensity,

$$I_i(t) = a_i\{ s_i(t)+p(t)+s_i(t)p(t) \}$$

Autocorrelation function (ACF) of the intensity $I_i(t)$,

$$< I_i(t)\, I_i(t+\tau) > = a_i^2\{< s_i(t)s_i(t+\tau)> + < p(t)p(t+\tau)>$$

$$+<s_i(t)s_i(t+\tau)> < p(t)p(t+\tau) > \}$$

where the angular brackets stand for time averaging. Here, we used the fact that $s_i(t)$ and $p(t)$ are statistically independent, and hence (Papoulis 1965),

$$\langle s_i(t)\ p(t+\tau) \rangle = \langle s_i(t) \rangle \langle p(t) \rangle = 0$$

and

$$\langle s_i(t)p(t)s_i(t+\tau)p(t+\tau)\rangle = \langle s_i(t)s_i(t+\tau) \rangle \ \langle p(t)p(t+\tau) \rangle$$

For brevity, from now onwards we would drop out the arguments of $p(t)$ and $s_i(t)$ i.e.

$$\langle p(t)p(t+\tau)\rangle \equiv \langle pp\rangle \quad \text{and so on.}$$

The summed up ACF,

$$\sum_{i=1}^{n} \langle I_i I_i \rangle = \{\langle ss\rangle + \langle pp\rangle + \langle ss\rangle \langle pp\rangle \} \sum_{i=1}^{n} a_i^2$$

In arriving at the above equation, we assumed that,

$$\langle s_i s_i\rangle = \langle s_j s_j\rangle \equiv \langle ss\rangle$$

The above assumption is justified because of the following reason. Though the width (T_s) of the ACF of intensity variations due to ISS depends linearly on the radio frequency(f), the widths of $\langle s_i s_i\rangle$ and $\langle s_j s_j\rangle$ would be practically the same since the difference in the central frequency of different channels is negligible compared to their central frequencies. If by broad band intensity (I_B) we denote,

$$I_B = \sum_{i=1}^{n} I_i(t), \text{ then}$$

$$\langle I_B I_B \rangle = \sum_{i=1}^{n} \sum_{j=1}^{n} \langle I_i I_j \rangle$$

$$= \sum_{i=1}^{n} \sum_{j=1}^{n} a_i a_j \{ \langle s_i s_j \rangle + \langle pp \rangle + \langle s_i s_j \rangle \langle pp \rangle \}$$

To progress further, we make the following two simplifying assumptions:

i) For ISS, the cross-correlation function of intensities at two closeby frequencies and the ACF at one of the frequencies differ only by a constant factor. The error introduced by this assumption is small as can be inferred from the numerically computed curves that were presented in Figs.5,6 and 7 of Lee (1976).

ii) The multiplicative factor depends on only the frequency separation and not on the actual frequencies. This assumption is justified since,

$$BW/f \ll 1$$

where BW is the total bandwidth used for the observations.

Under these assumptions,

$$\langle s_i s_j \rangle = \langle ss \rangle C_{|i-j|}$$

where $C_{|i-j|}$ is the correlation coefficient between the

intensity fluctuations due to ISS observed in the 'i th' and the 'j th' channels for zero time lag. Using the above relation, we get,

$$\langle I_B I_B \rangle = \langle pp \rangle \sum_i \sum_j a_i a_j + \langle ss \rangle (1+\langle pp \rangle) \sum_i \sum_j a_i a_j \, C_{|i-j|}$$

On writing,

$$K1 \equiv \sum_i a_i^2$$

$$K2 \equiv \sum_i \sum_j a_i a_j$$

and $$K3 \equiv \sum_i \sum_j a_i a_j \, C_{|i-j|}$$

we obtain,

$$CN \equiv \sum_i \langle I_i I_i \rangle = K1\langle pp \rangle + K1\langle ss \rangle (1+\langle pp \rangle)$$

and

$$CB \equiv \langle I_B I_B \rangle = K2\langle pp \rangle + K3\langle ss \rangle (1+\langle pp \rangle)$$

where CN stands for the summed up cross-correlation coefficients for the narrow bandwidths and CB stands for the cross-correlation coefficients for the broad bandwidth. From the above two equations we obtain,

$$\langle pp \rangle = \frac{CB/K3 - CN/K1}{K2/K3 - 1}$$

and

$$\langle ss \rangle = \frac{CN/K1 - \langle pp \rangle}{1+\langle pp \rangle}$$

One should remember that CB, CN, <pp> and <ss> are all functions of the lag 'τ' which had been dropped out for notational convenience.

This method gives, in addition to the ACF of the intrinsic intensity variations (<pp>), the ACF of ISS (<ss>) after correcting it for the intrinsic variations which may be present in the data. In fact, the original motivation for developing this method was its possible application to the reduction of the ISS data, as the presence of intrinsic variations causes difficulties in interpreting two station observations of pulsars (Slee et al. 1974) and also in checking the predictions of ISS theories against the observational data (Backer 1975; Balasubramanian 1979).

4.3.2 Analysis procedure

As mentioned in the second chapter, the data were acquired with a sampling period of 2 ms. No information is lost by averaging the pulse intensities in each channel over a few tens of pulse periods, as we are interested in variations having much longer periodicities. The averaging was done in two steps. Firstly, the intensity was averaged separately for each channel over the expected pulse width by using the pulse width and the pulse arrival drift information as obtained by us from the preanalysis of the data. This gives 12 data arrays $I_i^a(K)$, one for each channel i, where I^a is the averaged intensity for the 'K th' pulse. From these values the corresponding base level values $I_i^b(K)$ were

subtracted. The base level values were obtained by averaging the receiver output over a duration comparable to the on-pulse width in the middle of the expected arrival of the adjacent pulses. This has the same effect as Dicke switching the telescope output once per pulse period has on the stability of the receiver output. Though it is a slow switching by conventional standards, it is satisfactory because we are interested in the stability over time scales on the order of a few minutes. Secondly, each array was averaged again to give,

$$I_i'(m) = \sum_{j=1}^{q} I_i''(k')$$

where I'' are the base level subtracted arrays obtained as described above, $k'=q(m-1)+j$ and q is the number of pulses over which the intensity was averaged. q is listed in Table 4.1 for each of the 24 pulsars observed at Ooty. The mean subtracted arrays,

$$I_i(m) = I_i'(m) - a_i$$

are formed, where the mean intensity in each channel

$$a_i = \langle I_i'(m) \rangle$$

In the above equation the angular brackets stand for averaging over m. Another set of arrays $I_i^o(m)$, where the superscript o stands for off-pulse, were formed in a similar fashion from the samples on either side of the pulse in the on-pulse window.

TABLE 4.1. Observational Details and the Results of Application of 'HAMSA' to 24 pulsars

Sr. No.	PSR	Band Width (kHz)	No. of pulses averaged	Signal-to-noise ratio	Data length (hrs)	Modulation index		Time scales (mts)	
						ISS	IIV	ISS	IIV*
(1)	(2)	(3)	(4)	(5)	(6)	(7)	(8)	(9)	(10)
1	0301+19	300	32	1.5	3.0	0.4	0.2	15.5	90.3
2	"	300	32	4.6	6.7	0.5	0.1	12.6	11.8p
3	0611+22	50	32	2.2	1.8	<0.1	0.2	-	15.7p
4	"	300	64	2.7	6.1	<0.1	0.1	-	132
5	0628-28	300	16	6.5	3.6	0.5	0.3	9.6	61
6	0740-28	50	32	1.5	0.9	<0.1	0.1	-	9.6p
7	0818-13	300	16	5.0	1.6	0.1	0.1	2	31
8	"	50	32	3.8	2.1	0.4	0.1	2	17.2p
9	0823+26	300	32	7.3	2.5	0.5	0.2	4.6	17.6p
10	0834+06	300	32	14.4	6.1	0.7	0.3	9.2	27.9
11	1237+25	300	32	12.9	5.8	0.6	0.8	12.5	19.2p
12	1604-00	300	64	7.4	2.1	0.5	0.3	18.9	126
13	1642-03	300	32	23.0	1.8	0.2	<0.05	2.3	-
14	1718-32	50	32	1.4	1.2	<0.2	0.1	-	37.7
15	1818-04	50	32	3.5	2.3	<0.1	0.1	-	11.1p
16	1831-03	50	32	1.2	1.7	<0.1	<0.1	-	-
17	1831-04	50	16	0.7	0.4	<0.2	<0.1	-	-
18	1845-01	50	16	0.65	0.7	<0.2	<0.2	-	-
19	1845-04	50	32	1.2	0.7	<0.1	<0.2	-	-

* Wherever a periodicity is suspected the time scale is followed by the symbol, 'p'.

(1)	(2)	(3)	(4)	(5)	(6)	(7)	(8)	(9)	(10)
20	1857-26	50	64	3.8	3.0	<0.1	<0.1	-	-
21	1900+01	50	16	0.9	0.3	<0.3	<0.2	-	-
22	1907+02	50	32	1.0	2.2	<0.2	<0.05	-	-
23	1917+00	50	32	0.85	3.1	<0.1	<0.2	-	-
24	1919+21	300	64	14.0	5.9	0.5	0.7	11.1	45.6p
25	"	300	32	9.0	3.5	0.6	0.3	9.3	25.7
26	"	300	32	15.5	6.0	0.8	0.4	9.8	14.3p
27	"	300	32	12.9	4.1	0.6	0.3	8.6	10.3
28	2016+28	300	32	14.0	2.0	0.2	0.1	23.8	51
29	2020+28	50	64	3.5	3.1	0.6	0.3	7.6	26p
30	2303+30	50	16	0.8	1.0	0.5	<0.1	4.2	-

The data arrays were subjected to an iterative editing procedure which corrects for occasional interference that may be present in the data. Mean and rms of the raw data were calculated. All data points whose deviation from the mean exceeded seven times the rms were substitued by the mean value of the array. Mean and rms were recalculated for the modified array and the above pruning process was continued until no datum was found to exceed the threshold. In no case it was found necessary to prune more than 2 or 3 data points out of an array of a few thousand points.

The uncorrected zero time lag correlation coefficient between the first and the i th channel is given by,

$$C_{ON}(i\text{-}1) = \frac{1}{\sigma_1 \sigma_i} \langle I_1(m) I_i(m) \rangle$$

where σ_i is the rms of the array $I_i(m)$. Using a similar expression the off-pulse correlation coefficients $C_{OFF}(i\text{-}1)$ are calculated for the arrays $I_i^o(m)$. The presence of the receiver noise reduces the observed correlation coefficients. The noise corrected coefficients are given by,

$$C'(i\text{-}1) = \left[C_{ON}(i\text{-}1) - C_{OFF}(i\text{-}1) \frac{\sigma_1^o \sigma_i^o}{\sigma_1 \sigma_i}\right] \frac{\sigma_1 \sigma_i}{\sigma_{1s} \sigma_{is}}$$

where σ^o is the rms of the arrays, $I_i^o(m)$ and σ_{is} is the noise corrected rms value of the array $I_i(m)$.

As an example, the normalised correlation function obtained after correcting for the receiver noise is shown in

Fig.4.4 for PSR 1919+21 observed during June 1976. The pedastal d is due to intensity fluctuations which are broad band in nature and hence intrinsic according to our convention. The correlation coefficients due only to ISS are given by

$$C_{|i-j|} = \{C'(K-1)-d\}/(1-d)$$

where

$$k-1 = |i-j|$$

Though $C_{|i-j|}$ is free from errors due to the receiver noise and the intrinsic variations, still it carries statistical errors due to the limited duration of the data used in its calculation. The rms error in $C_{|i-j|}$ is given by (Johnson and Kotz 1970),

$$\sigma_{C_{|i-j|}} = \frac{1-\rho^2_{|i-j|}}{\sqrt{N}}$$

where, N is the number of cycles of scintillation in the data and $\rho_{|i-j|}$ is the population correlation coefficient i.e. the ensemble average of $C_{|i-j|}$.

Since C'(k-1) is used for computing the $C_{|i-j|}$ with not only i=k and j=1 , but also for all those $C_{|i-j|}$ for which i-j = k-1 , it is necessary that the correlation coefficients used do not carry an error which depends on the fact that they had been calculated specifically from the first and the 'k th' data array. The following procedure had been adopted for doing the above. For both the filter banks

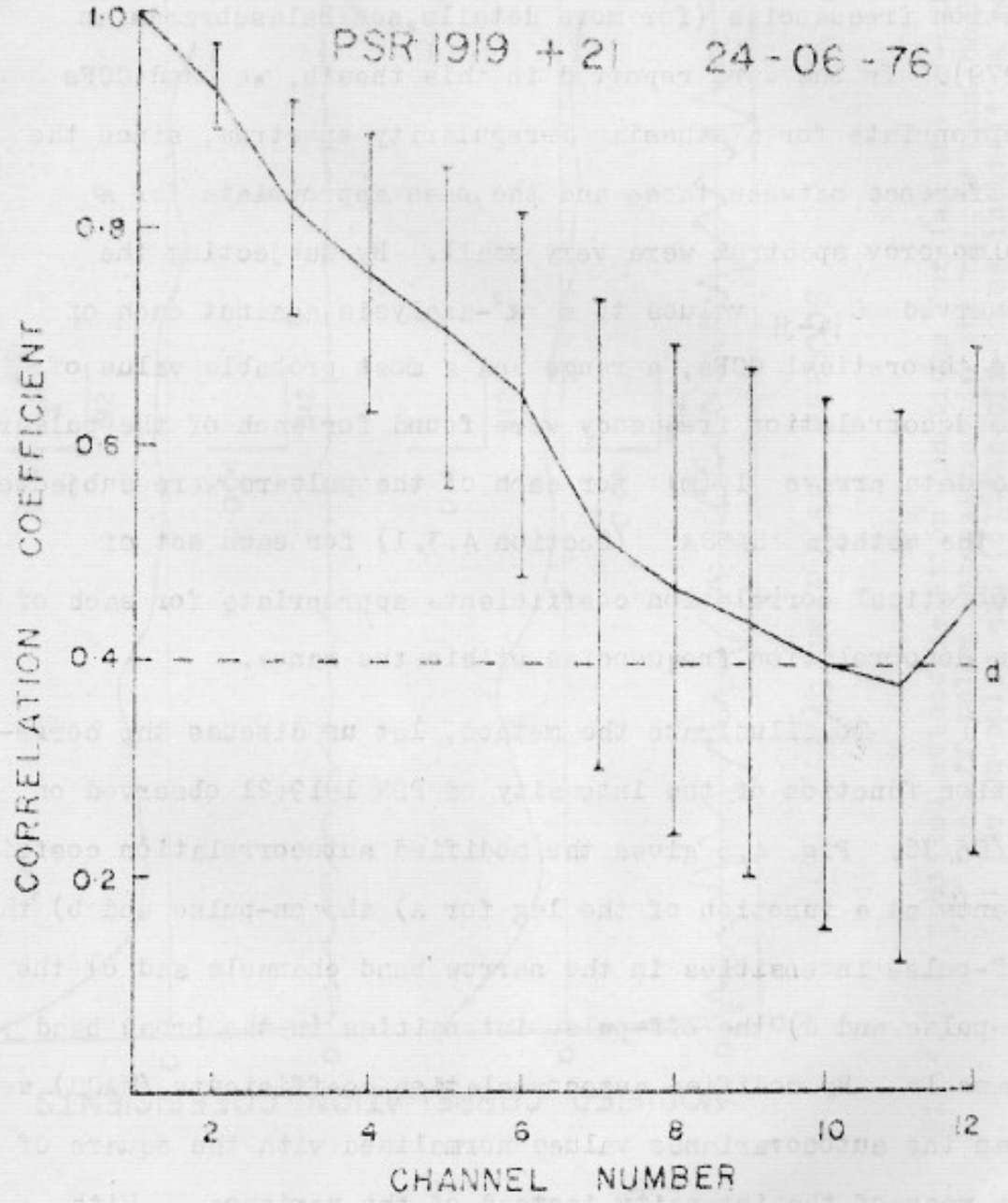

Fig.4.4. A sample cross-correlation function. The function was corrected for the presence of the receiver noise.

used in this work, a set of theoretical cross-correlation functions (CCFs) based on the work of Lee and Jokipii (1975) and Lee (1976) were produced for different assumed decorrelation frequencies (for more details, see Balasubramanian 1979). In the work reported in this thesis, we used CCFs appropriate for a gaussian irregularity spectrum, since the difference between those and the ones appropriate for a Kolmogorov spectrum were very small. By subjecting the observed $C_{|i-j|}$ values to a x^2-analysis against each of the theoretical CCFs, a range and a most probable value of the decorrelation frequency were found for each of the pulsars. The data arrays $I_i(m)$ for each of the pulsars were subjected to the method 'HAMSA' (Section 4.3.1) for each set of theoretical correlation coefficients appropriate for each of the decorrelation frequencies within the range.

To illustrate the method, let us discuss the correlation function of the intensity of PSR 1919+21 observed on 24/06/76. Fig. 4.5 gives the modified autocorrelation coefficients as a function of the lag for a) the on-pulse and b) the off-pulse intensities in the narrow band channels and c) the on-pulse and d) the off-pulse intensities in the broad band channels. By modified autocorrelation coefficients (MACC) we mean the autocovariance values normalised with the square of the mean of the intensity instead of the variance. With this convention the MACC for the zero lag gives directly the square of the modulation index and hence need not be equal to one. For the normalisation of the off-pulse MACCs, we

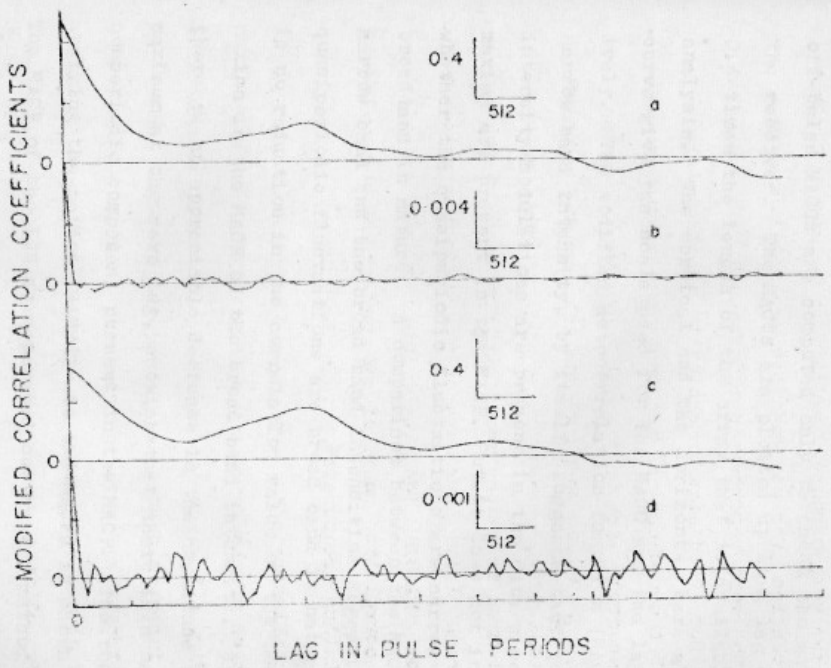

Fig.4.5. Modified autocorrelation functions for (a) the on-pulse, (b) the off-pulse intensities in the narrow band channels, (c) the on-pulse and (d) the off-pulse intensities in the broad band channel. The inserts give the scales of the MACC and the lag in pulse periods.

used the corresponding on-pulse values since the mean values of the off-pulse intensities are equal to zero. The off-pulse MACCs are computed only to check the stability of the receiver. The MACCs are plotted up to a lag which is 0.4 times the length of the array that is available for the analysis. The vertical and the horizontal bars above each curve give the scale used for the MACC and the lag respectively. The modified autocorrelation function (MACF) for the narrow band intensity, by itself, suggests that quasiperiodic intensity modulations are present in the data since secondary maxima are present in the MACF. But it does not indicate whether the quasiperiodic fluctuations are narrow band or broad band in nature. A comparison between the MACFs for the narrow band and the broad band intensities suggest that the quasiperiodic fluctuations are broad band in nature as there is no reduction in the correlation value of the secondary maxima in the MACF of the broad band intensity. In contrast, there is an appreciable decrease in the amplitude of the maximum at the zero lag, showing that there is a narrow band nonperiodic component present in the MACF. The result of applying the method 'HAMSA' to the MACFs is shown in Fig.4.6. The MACF of the IIV as separated out by the method 'HAMSA' gives a clear evidence for the presence of quasiperiodic variations. There is no evidence for such quasiperiodic variations in the MACF of the scintillations. The MACFs for the noise were obtained from the ACFs of the off-pulse intensity shown in Fig.4.5 after subjecting them to the method 'HAMSA'. While

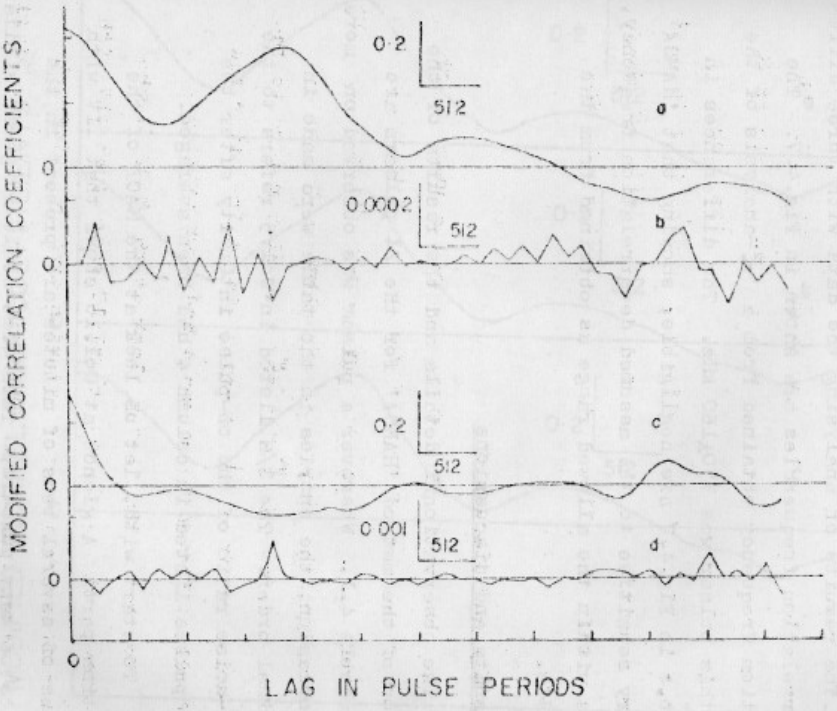

Fig.4.6. Results of applying 'HAMSA' to the correlation functions shown in Fig.4.5. (a) and (b) show the MACF due to the IIV and (c) and (d) show the MACF due to the ISS. (b) and (d) are the results for the noise.

comparing them with those for the on-pulse intensities, one should note that the vertical scale for the off-pulse MACFs are a few hundred times smaller than the scale for the on-pulse MACFs.

The results of analysing the data with three different decorrelation frequencies are shown in Fig.4.7. The decorrelation frequency obtained from a χ^2-analysis of the data for this pulsar was 330±160 kHz. The differences in curves a,b,c in Fig.4.7 are negligible, showing that 'HAMSA' is not very sensitive to the assumed decorrelation frequency, once it is within the allowed range as obtained from the χ^2-analysis.

4.3.3 Results and discussions

The observational details and the results of the application of the method 'HAMSA' for the 24 pulsars are listed in Table 4.1. Wherever a pulsar was observed on more than one occasion, the entries in the table were made in chronological order. The S/N listed in Col.5 refers to the signal-to-noise ratio of the on-pulse intensity after the number of pulses listed in column 4 had been averaged.

To start with, let us look at the MACF of the scintillation part. A glance at Col.10 shows that IIV with time scales of several tens of minutes are present in the intensities of many pulsars. This time scale range is similar to that for scintillations listed in Col.9. A comparison of Col.7 and Col.8 shows that IIV could affect appreciably the

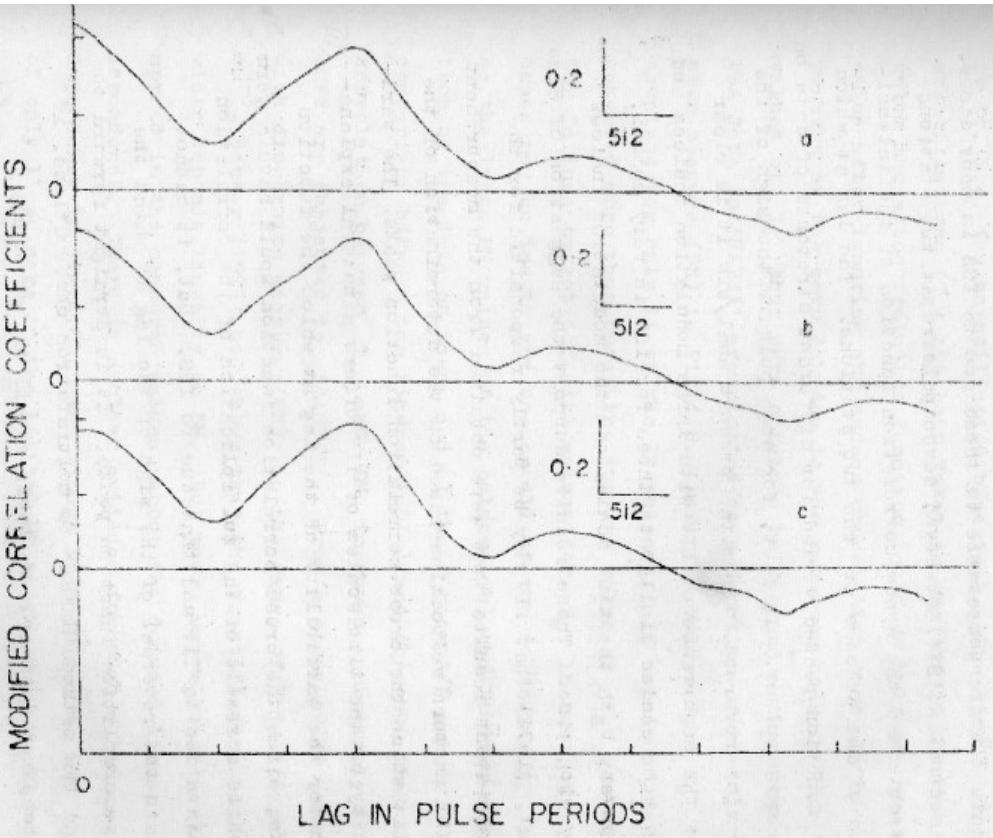

Fig.4.7. Results of analysing the data with three different decorrelation frequencies, (a) 300 kHz , (b) 375 kHz, and (c) 450 kHz.

measurement of ISS parameters since the modulation indices due to IIV are comparable to those due to ISS in many cases. Slee et al. (1974) observed seven pulsars at two stations and obtained the cross-correlation function of the intensities of the pulsars at the two stations. The lag at which the function peaked varied for different stretches of data on the same pulsar. In fact, for some pulsars the sign of the lag also reversed. From the present analysis it is clear that the occurrence of IIV with large modulation indices and with time scales similar to those for ISS is very common. Moreover, both the time scales and the modulation indices vary with time. These results support the suggestion of Slee et al. (1974) that IIV may be partly responsible for the inconsistent results that were obtained from the measurement of ISS pattern velocities based on the determination of the lag at which the cross-correlation function peaks. The variability of the time scales of IIV offers a natural explanation for the variability of the lag at which the function peaks, since the cross correlation function would have a term which is a result of the multiplication of the correlation function due to IIV and that due to ISS. But, it cannot explain the reversal of the sign of the lag at which the cross-correlation function peaks. It is straight forward to extend the method 'HAMSA' to multistation observations, if multichannel data are available at all the stations.

Another parameter whose determination is made difficult by the presence of IIV is the time scale (T_s) for

scintillations, or a quantity which is inversly proportional to it, i.e. the scintillation bandwidth. The time scale for scintillations (T_s) has been taken as the lag in minutes at which the autocorrelation function falls to half the peak value after ignoring any excess correlation that may be present at the zero lag due to the receiver noise. The values of T_s that were obtained before and after subjecting the data to 'HAMSA' are plotted as a function of the dispersion measure (DM) in Fig.4.8. Definite values for T_s were obtained for only 11 of the 24 pulsars. If a pulsar was observed more than once, the average value of T_s was used. Our failure to get definite values for T_s in rest of the cases may be due to any one or all of the following reasons: a) the large DM values of the pulsars, b) the limited duration of the data on them, and c) their poor S/N values. A comparison between the figures 4.8(a) and (b) show that the correlation between T_s and DM improves appreciably if the ACFs are subjected to 'HAMSA'. From a study of 28 pulsars with dispersion measure (DM) in the range of 3 to 160 pc cm^{-3}, Backer (1975) had shown that the scintillation bandwidth depends linearly on DM. But there was a considerable spread in the measured values, about the deduced linear dependence. There is a clear evidence for such a linear dependence in Fig.4.8b, even though it is based on the T_s of only 11 pulsars in the limited DM range of 10 to 50 pc cm^{-3}. Thus, a significant part of the spread in Backer's diagram could be due to the presence of IIV.

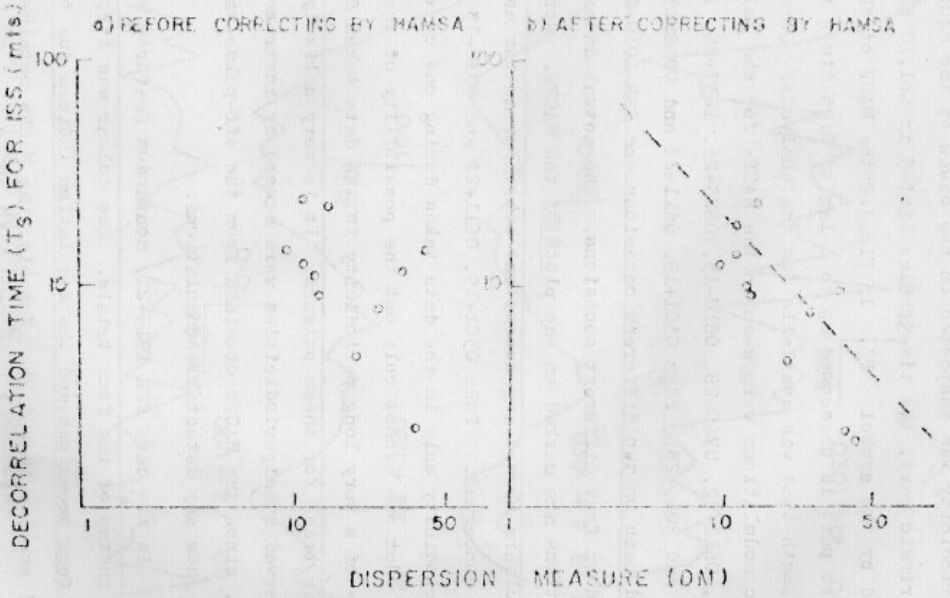

Fig.4.8. A plot of dispersion measure vs decorrelation time.

Now, let us return to the topic of IIV. Wherever a quasiperiodicity was suspected on the basis of the MACF of the intrinsic part, the time scales listed in Col.10 had been followed by the symbol 'P'. In Fig.4.9 the MACF of the intrinsic part is presented up to a lag of 0.25 times the array length that was available for the analysis. Quasi-periodic modulations were seen in the MACFs for the pulsars 0301+19, 0611+22, 0740-28, 0818-13, 0823+26, 1237+25, 1818-04, 1919+21 and 2020+28. PSRs 0301+19, 0611+22 and 0818-13 were observed each on two different occasions and PSR 1919+21 was observed on four different occasions. The actual dates of observations are marked on the plots of the MACFs. None of these pulsars showed any consistent behaviour as far as their IIV are concerned. PSRs 0301+19, 0611+22 and 0818-13 showed quasiperiodicity only in the data taken during one of the trials. But one cannot rule out the possibility of the presence of a very long periodicity in the data taken during the other trial for these pulsars. It is very unlikely that the observed quasiperiodicities were caused by instrumental effects, since the MACFs obtained from the off-pulse values did not show any detectable modulations.

In the case PSR 1919+21, nonrandom features were present in two of the four trials. The pulsar was strong on all the four occasions and the modulation indices due to IIV were all greater than 0.25. Notably, the MACFs obtained from the data acquired on two adjacent days show dissimilar behaviour. For this pulsar the presence of wobble had been

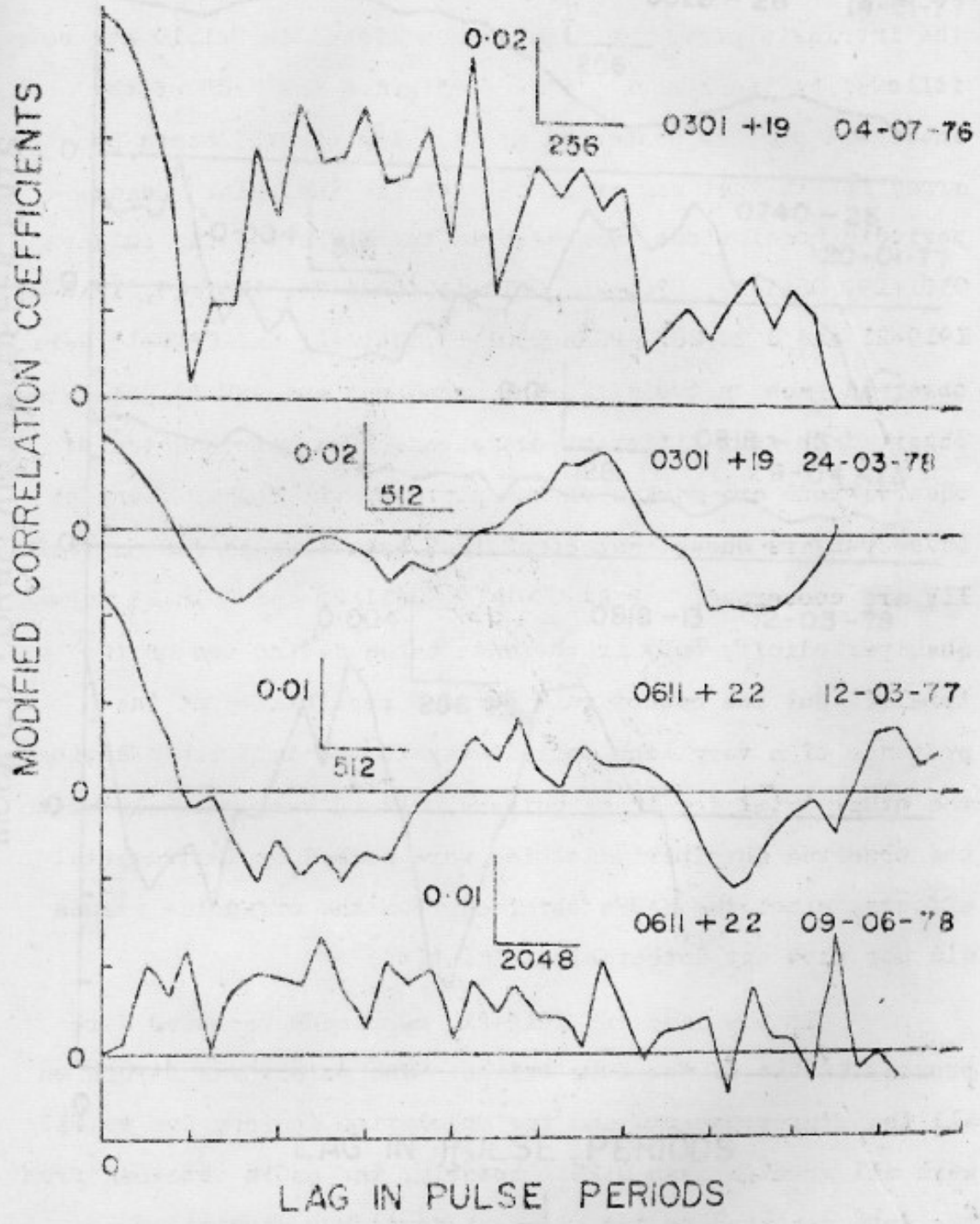

Fig.4.9a Modified correlation functions of the intrinsic intensity variations.

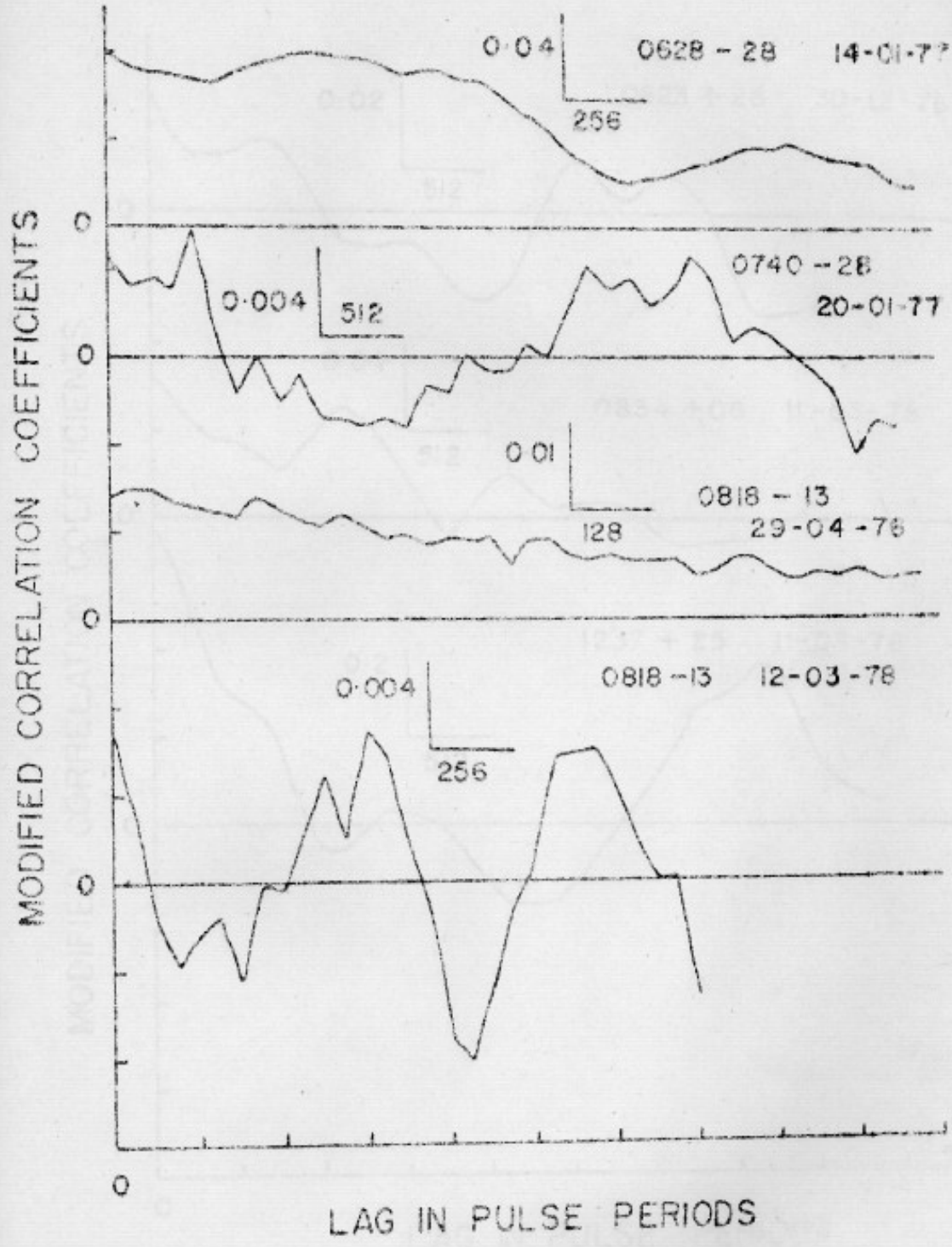
0·04
0628 - 28
14-01-77
256
0
0·004
512
0740 - 28
20-01-77
0
0·01
0818 - 13
128
29-04-78
0
0·004
0818 - 13
12-03-78
256
0
0
MODIFIED CORRELATION COEFFICIENTS
LAG IN PULSE PERIODS

Fig.4.9b

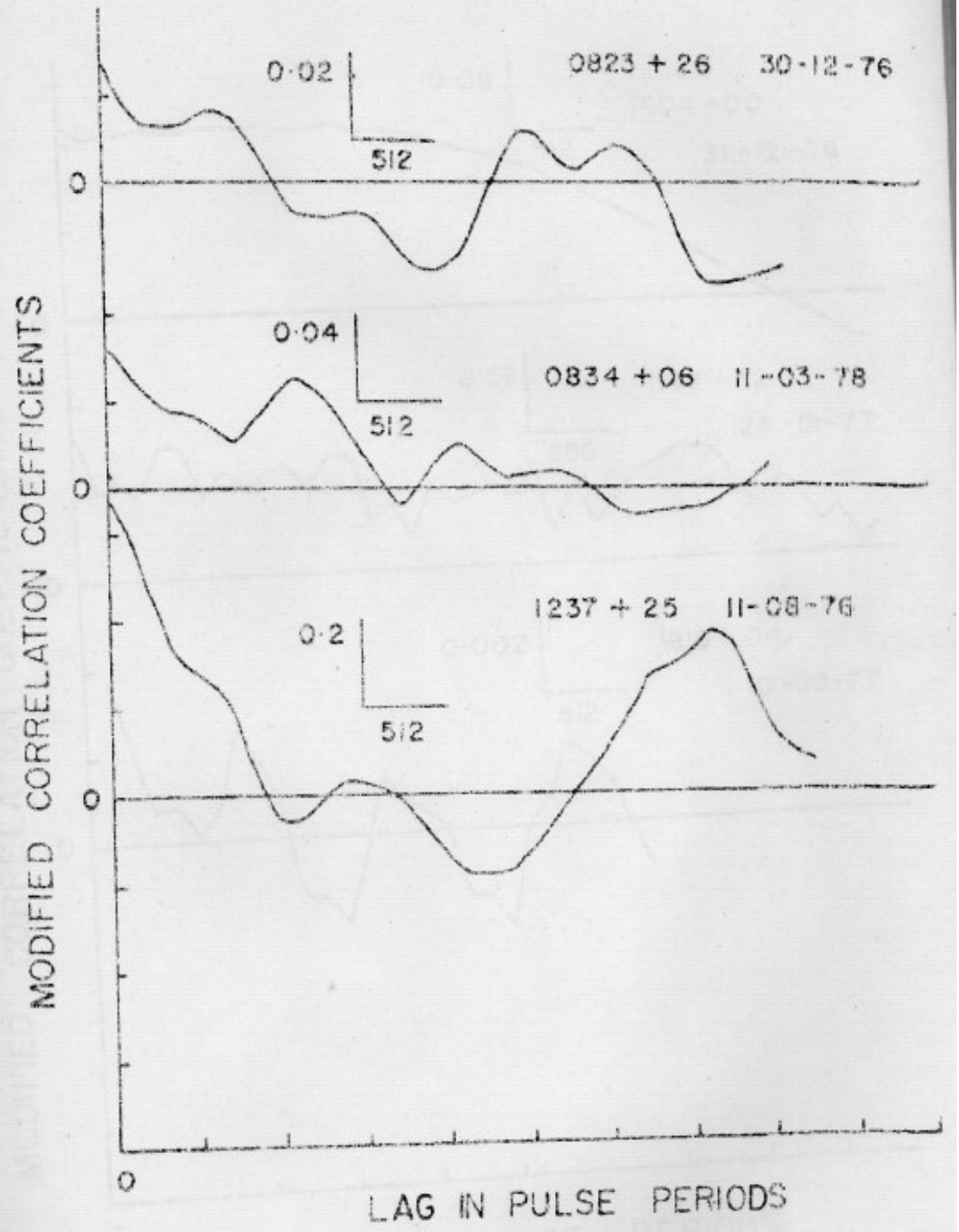
0·02
0823 + 26 30-12-76
512
0
0·04
0834 + 06 11-03-78
512
0
1237 + 25 11-08-76
0·2
512
0
0
MODIFIED CORRELATION COEFFICIENTS
LAG IN PULSE PERIODS

Fig.4.9c

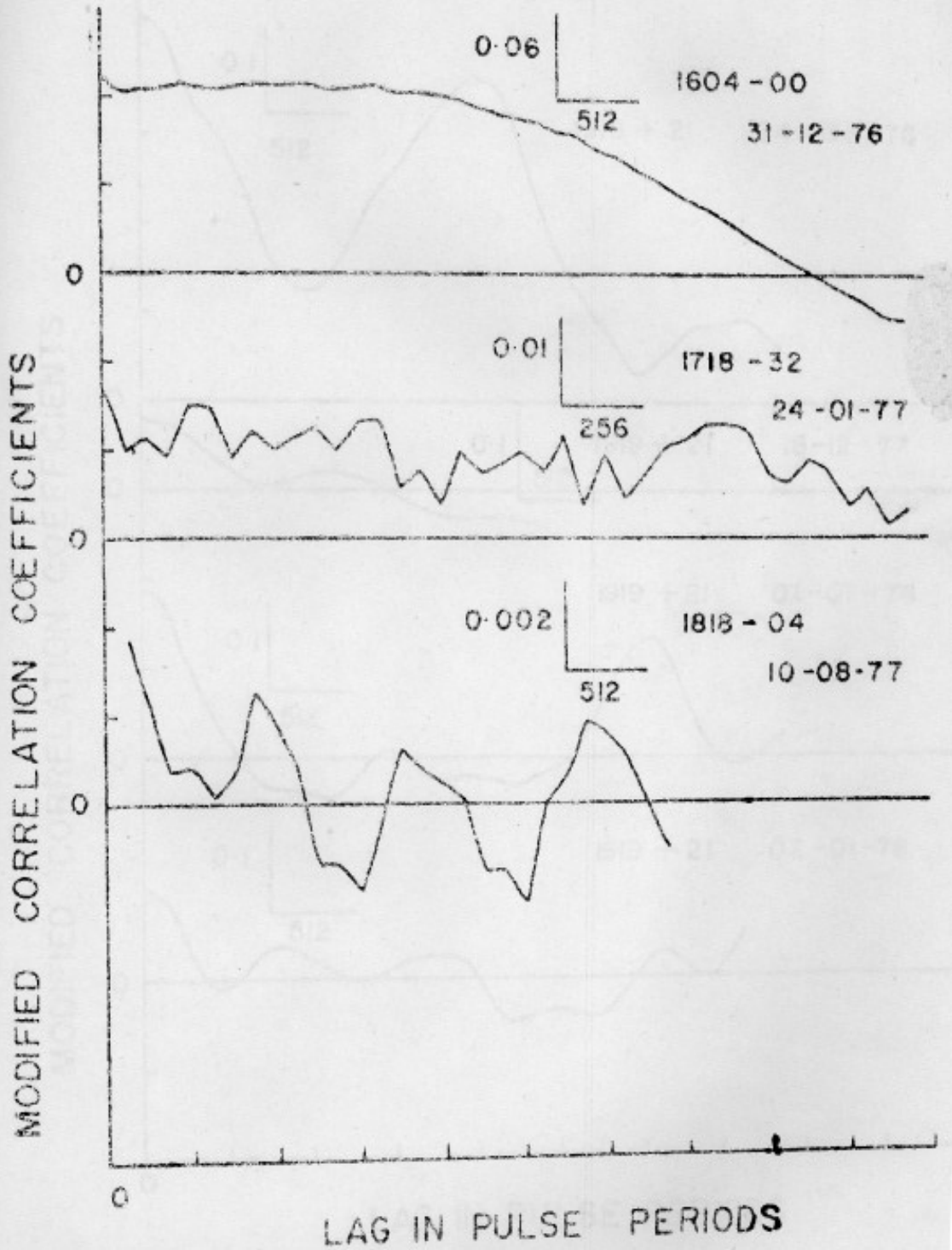
0·06
512
1604 - 00
31 - 12 - 76
0
0·01
256
1718 - 32
24 - 01 - 77
0
0·002
512
1818 - 04
10 - 08 - 77
0
0
MODIFIED CORRELATION COEFFICIENTS
LAG IN PULSE PERIODS

Fig.4.9d

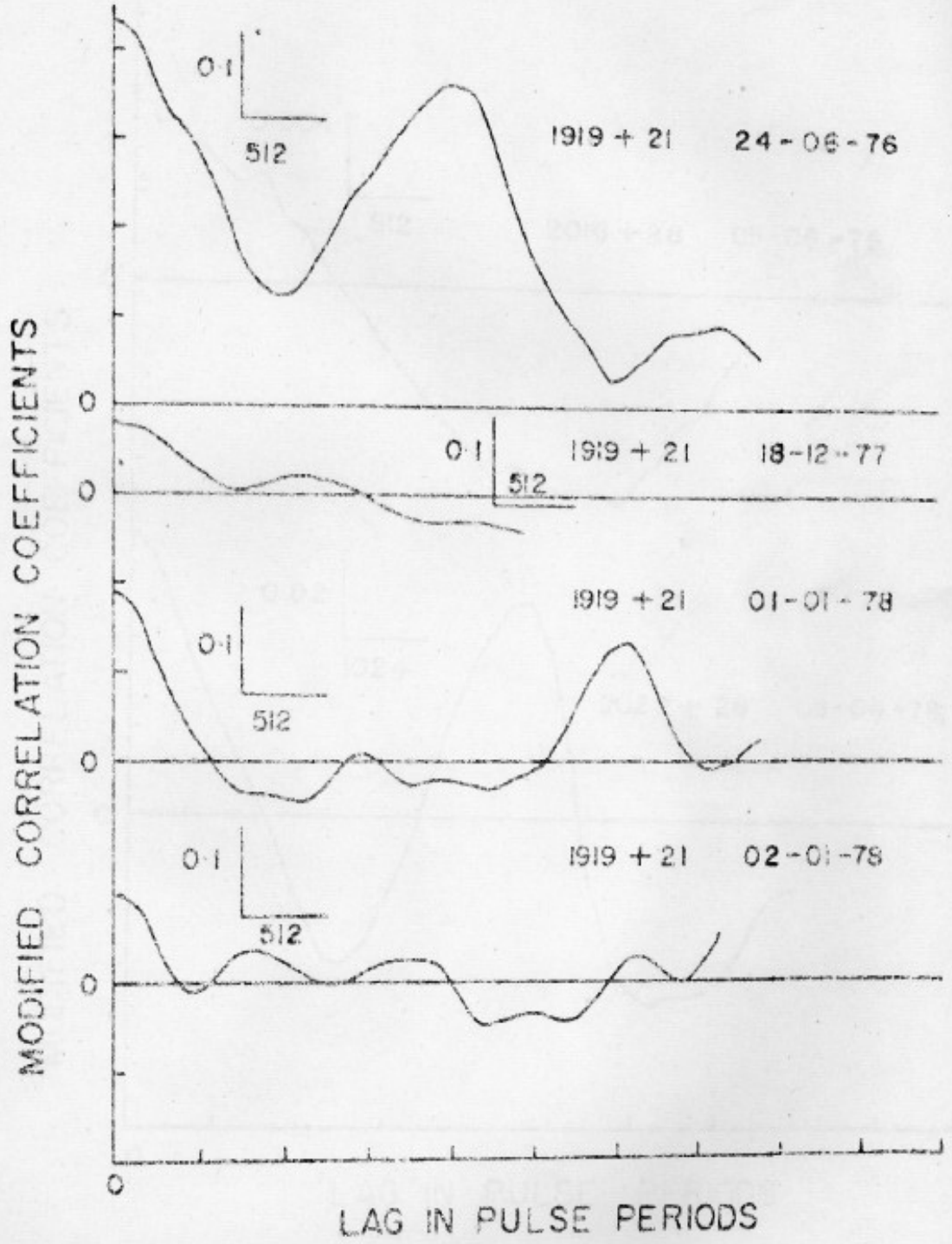
MODIFIED CORRELATION COEFFICIENTS
0·1
512
1919 + 21
24-06-76
0
0·1
1919 + 21
18-12-77
512
0
1919 + 21
01-01-78
0·1
512
0
1919 + 21
02-01-78
0·1
512
0
LAG IN PULSE PERIODS

Fig.4.9e

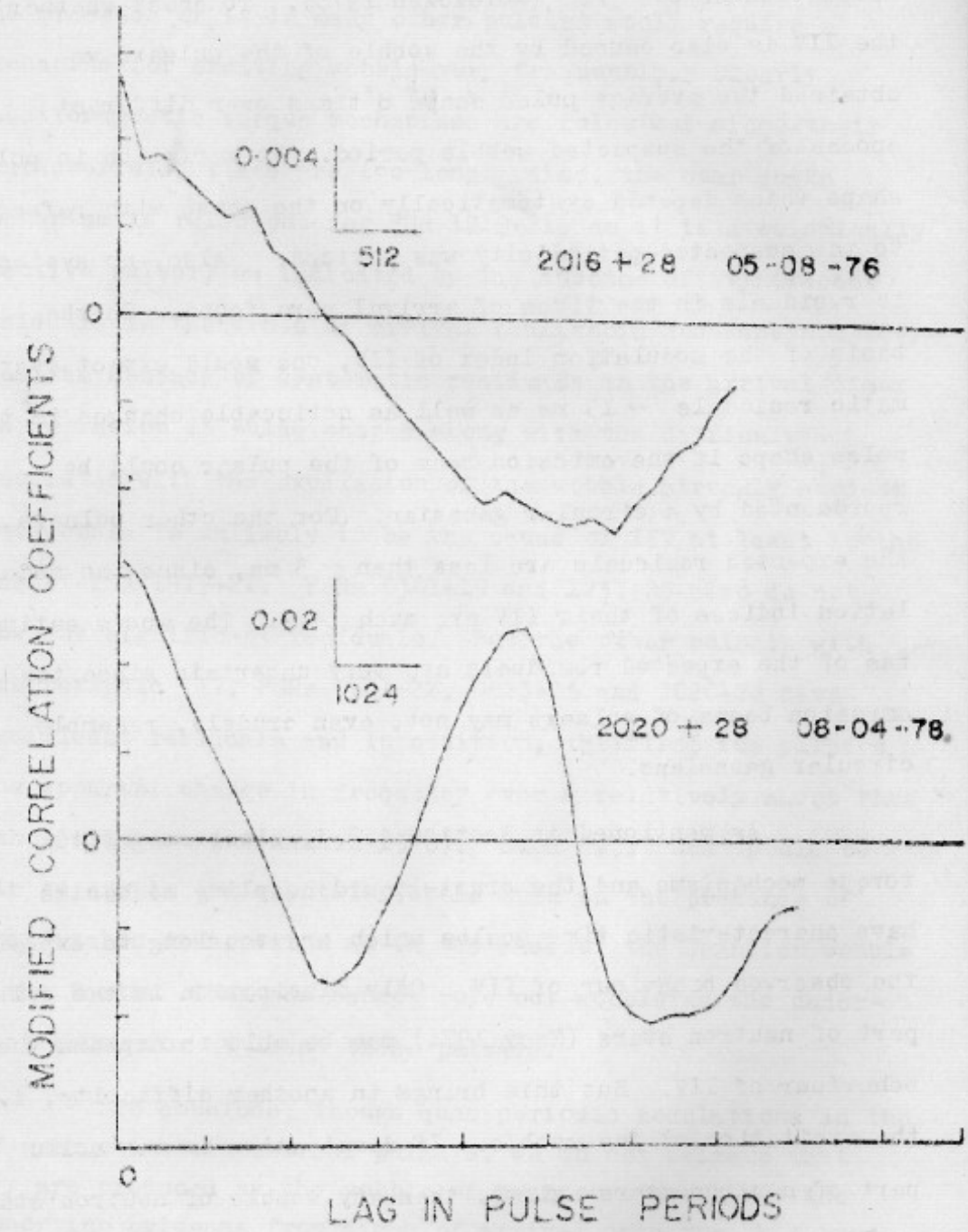
0·004
512
2016 + 28 05-08-76
0
0·02
1024
2020 + 28 08-04-78
0
0
MODIFIED CORRELATION COEFFICIENTS
LAG IN PULSE PERIODS

Fig.4.9f

put forward as a possible explanation for the quasiperiodic modulation of the P_3 (Wolszczan 1978). To check whether the IIV is also caused by the wobble of the pulsar, we obtained the average pulse shape 8 times over different epochs of the suspected wobble period. No variation in pulse shape which depends systematically on the phase with reference to the suspected periodicity was noticed. Also, no systematic residuals in the times of arrival were found. On the basis of the modulation index of IIV, one would expect systematic residuals $\sim$ 15 ms as well as noticeable changes in the pulse shape if the emission beam of the pulsar could be represented by a circular gaussian. For the other pulsars, the expected residuals are less than $\sim$ 3 ms, since the modulation indices of their IIV are much less. The above estimates of the expected residuals are very uncertain since the emission beams of pulsars may not, even crudely, resemble circular gaussians.

As mentioned in Section 4.2.3, electromagnetic torque mechanisms and the crust-liquid coupling mechanims have characteristic time scales which are too long to explain the observed behaviour of IIV. Only dissipation in the solid part of neutron stars (Macy 1974) may be able to explain the behaviour of IIV. But this brings in another difficulty, i.e. the excitation of the wobble. If dissipation in the solid part of neutron stars exists, then any wobble of neutron star would be dissipated during time scales comparable to the wobble period. So, the presence of considerable quasiperiodic

IIV in two out of the four trials on PSR 1919+21 as well as the presence of it in many other pulsars would require a mechanism for exciting wobble very frequently. Clearly electromagnetic torque mechanisms are ruled out since their characteristic times are too long. Also, the star quake mechanism is ruled out for PSR 1919+21, as it is a seismically inactive pulsar, as indicated by the absence of significant residuals in the times of arrival (Gullahorn and Rankin 1978). Thus the absence of systematic residuals in the arrival times and variation in pulse shapes along with the difficulty associated with the excitation of the wobble strongly suggest that wobble is unlikely to be the cause of IIV at least in the case of PSR 1919+21. PSRs 0301+19 and 1237+25 also do not show any significant residuals. But the other pulsars with quasiperiodic IIV, PSRs 0611+22, 0823+26 and 2020+28 have significant residuals and in addition, the first two pulsars show apparent change in frequency over a relatively short time span (Gullahorn and Rankin 1978). Such 'glitches' would be able to excite and maintain wobble even in the presence of considerable dissipation as in the case of the Chandler wobble of the Earth. Thus one cannot rule out wobble as the underlying cause for at least these pulsars.

To conclude, though quasiperiodic modulations in the IIV are noticed in several pulsars, we do not believe that they are produced by the wobble of neutron stars since the supporting evidence from times of arrival data for this hypothesis is lacking. Thus, one may have to examine the possibility of oscillations in the emission mechanism itself for an explanation of the quasiperiodicities.

Chapter 5

EFFECT OF LONG-TERM INTENSITY VARIATIONS ON PULSAR SEARCHES AND LUMINOSITY FUNCTION

5.1 Introduction

Luminosity function (LF) is a very important property of the population of pulsars since it is required for the determination of the birth rate of pulsars. Birth rates derived on the basis of different pulsar searches have been used by several authors to check whether all pulsars are born in supernova events or not (Large 1971; Roberts 1976; Davies, Lyne and Seiradakis 1977; Taylor and Manchester 1977; Manchester 1979). By analysing a sample of 90 pulsars obtained from the Jodrell Bank survey (Davies, Lyne and Seiradakis 1973,1977) and the Arecibo survey (Hulse and Taylor 1974,1975), Taylor and Manchester (1977) showed that the inferred birth rate for pulsars is comparable to or is in excess of the supernova birth rate obtained from the observations of radio remnants (Ilovaisky and Lequeux 1972; Clark and Caswell 1976). They showed that, to be compatible with pulsar birth rates, all stars with a mass greater than about 2.5 $M_{\odot}$ have to end up as neutron stars at the end of their evolution. These conclusions were further strengthened by similar calculations done by Manchester (1979) on a much larger sample of 224 pulsars obtained from the second Molonglo pulsar survey (Manchester et al. 1978).

There are, however, many sources of systematic errors in the derivation of LF. Firstly, the distances

derived on the basis of dispersion measure of pulsars are inaccurate due to the presence of isolated dense ionised regions in the line of sight. For a few of the pulsars, distance estimates based on either neutral hydrogen absorption of pulsar signals (Gómez-González and Guélin 1974; Ables and Manchester 1976) or pulsar supernova associations (Ilovaisky and Lequeux 1972) are available. For pulsars closer than 1 kpc from the Sun one can follow the method of Prentice and ter Haar (1969) and correct the observed dispersion measure for the presence of H_{II} regions surrounding bright O stars. Though, no such correction is possible for pulsars farther away than 1 kpc, the errors are not likely to be large for most of the pulsars. This is because the thickness of the distribution of O stars is only a few tens of pc, whereas that for pulsars is a few hundreds of pc. Thus most of the line of sight may be free from H_{II} regions. Secondly, conversion of the observed flux into a luminosity introduces uncertainties due to the unknown nature of the structure of the radiating beam of the pulsars. Thirdly, pulsar fluxes change from day to day by more than a factor of ten.

In this chapter we deal with the last mentioned source of error, since reasonable amount of data is available on the long-term intensity variations. We show that though the number of new pulsars detected in a repeat survey over a given region is appreciably affected, the LF derived from a single search is insensitive to flux variations.

5.2 Long-term Intensity Variations

Long-term intensity variations, by which we mean the variations with a time scale of a few days or more, are significantly correlated over a wide frequency range. The intensity varies by more than a factor of ten (Hesse 1972; Huguenin, Taylor and Helfand 1973; Helfand, Fowler and Kuhlman 1977). We utilise the long sequence of intensity data spanning over more than one and half years on five pulsars that were published by Huguenin et al.(1973), to obtain the distribution of long-term intensity variations. These observations were not affected significantly by interstellar scintillation, since an observing bandwidth ~ 1 MHz and an integration time ranging from 2 to 4 hours were used in obtaining each intensity point. Histograms of the intensity distributions derived from the above data are shown in Fig.5.1. They are characterised by a fast rise and a slow decay, except for PSR 2217+47. It is notable that the distribution for PSR 2217+47 looks as though it is a mirror reflection of the distribution observed for other pulsars. If the distribution is genuinly different from that for other pulsars, the intensity fluctuations of PSR 2217+47 should be studied carefully in view of the discussion to follow.

Though, there are many known statistical distributions which would fit the histogram reasonably well, we choose the χ^2-distribution for the following reason. High brightness temperatures inferred for pulsar radio emission

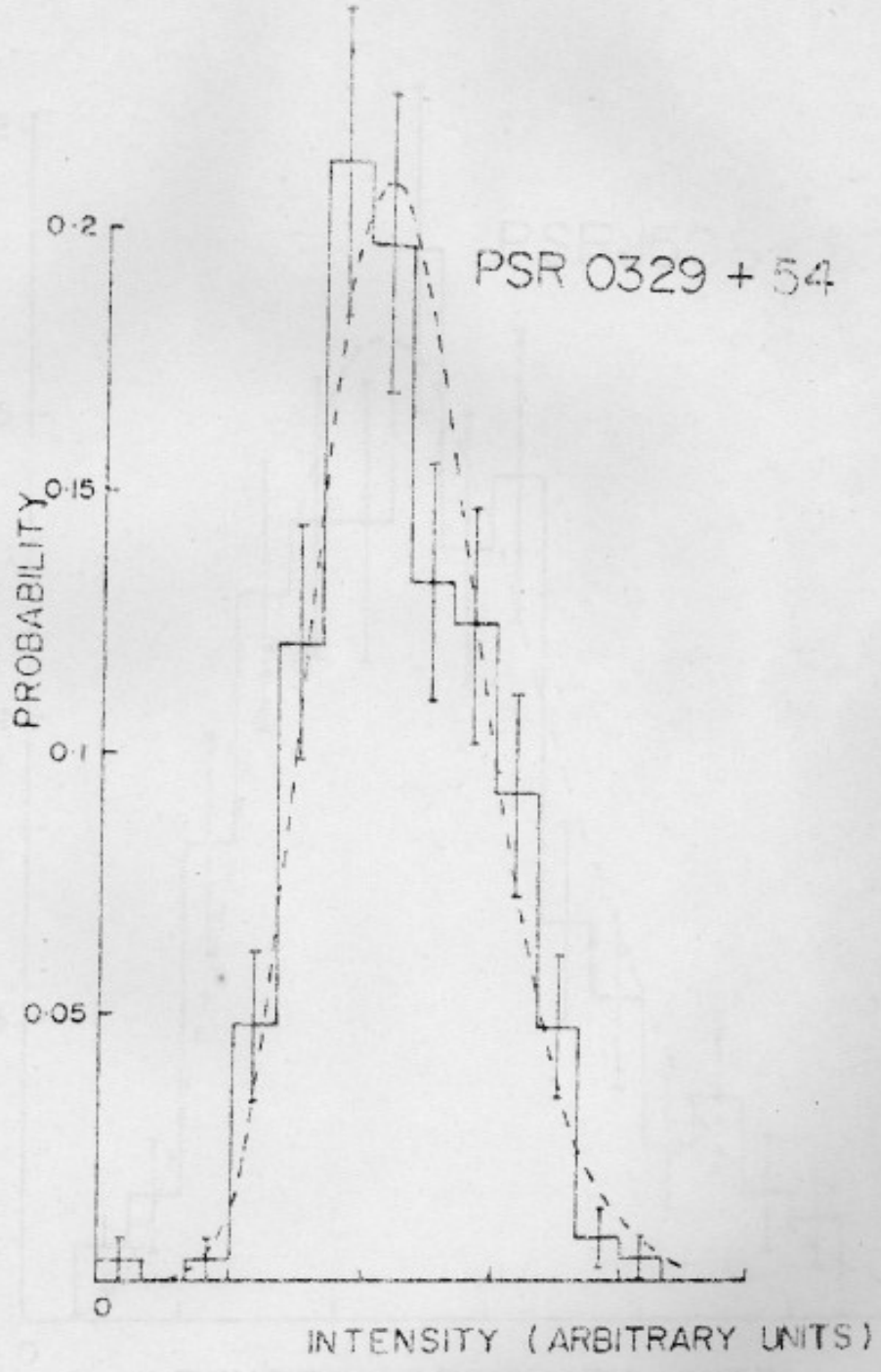

Fig.5.1a. Observed probability density distribution of the long-term intensity variations of pulsars (solid curve). The dashed curve shows the expected χ^2-distribution.

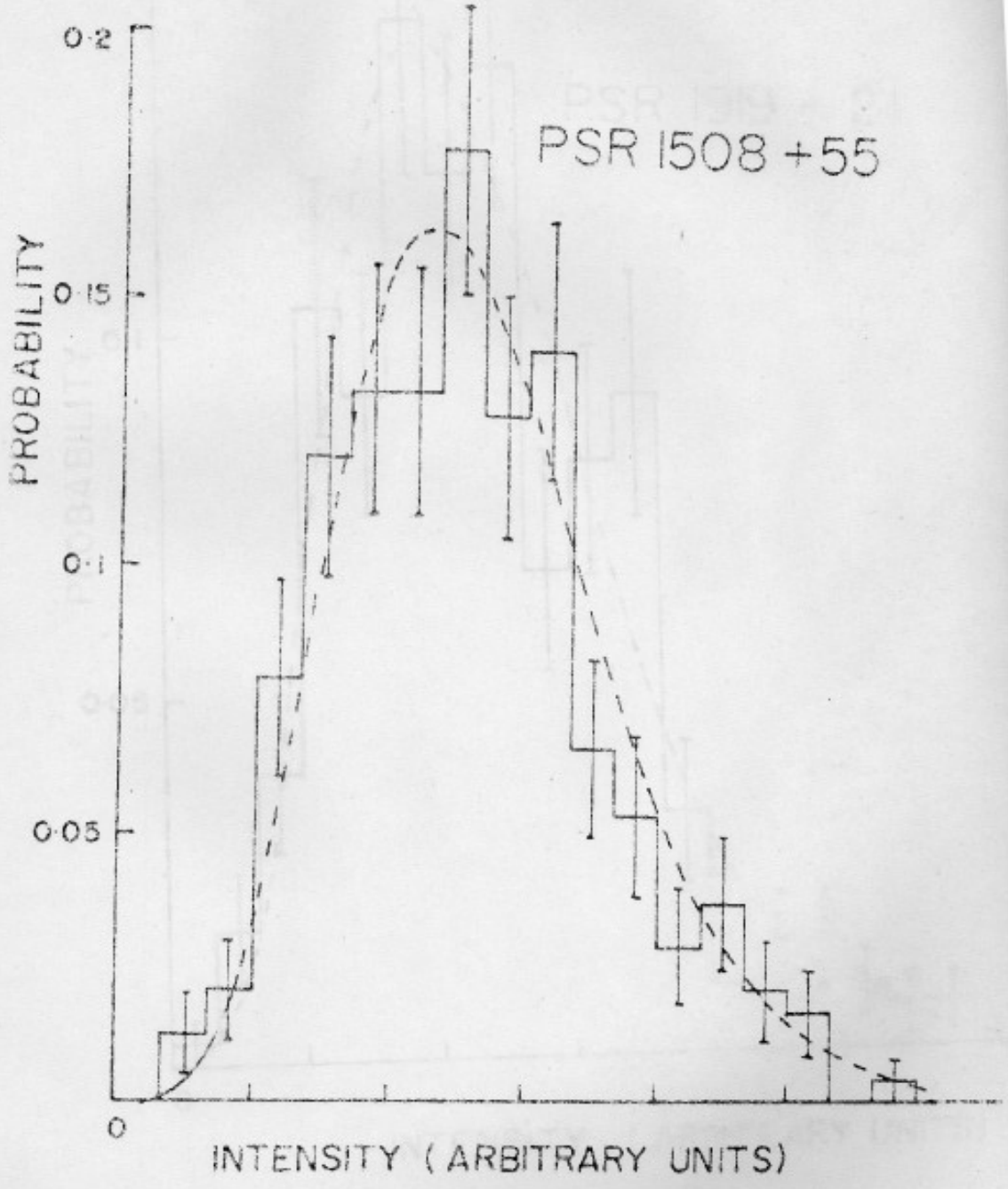
PSR 1508 +55
PROBABILITY
0·2
0·15
0·1
0·05
0
INTENSITY (ARBITRARY UNITS)

Fig.5.1b

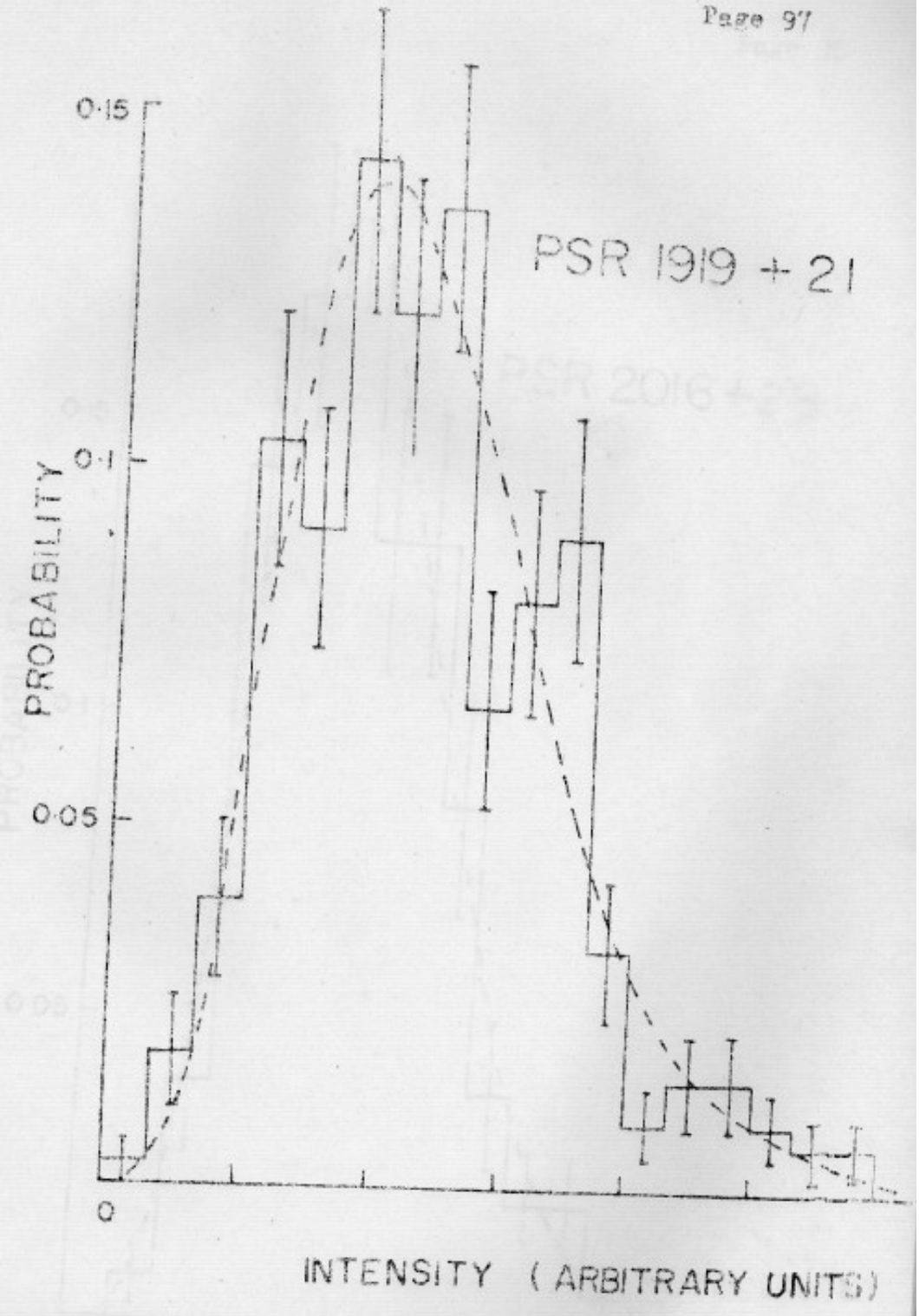
PSR 1919 + 21
0·15
0·1
0·05
0
PROBABILITY
INTENSITY (ARBITRARY UNITS)

Fig.5.1c

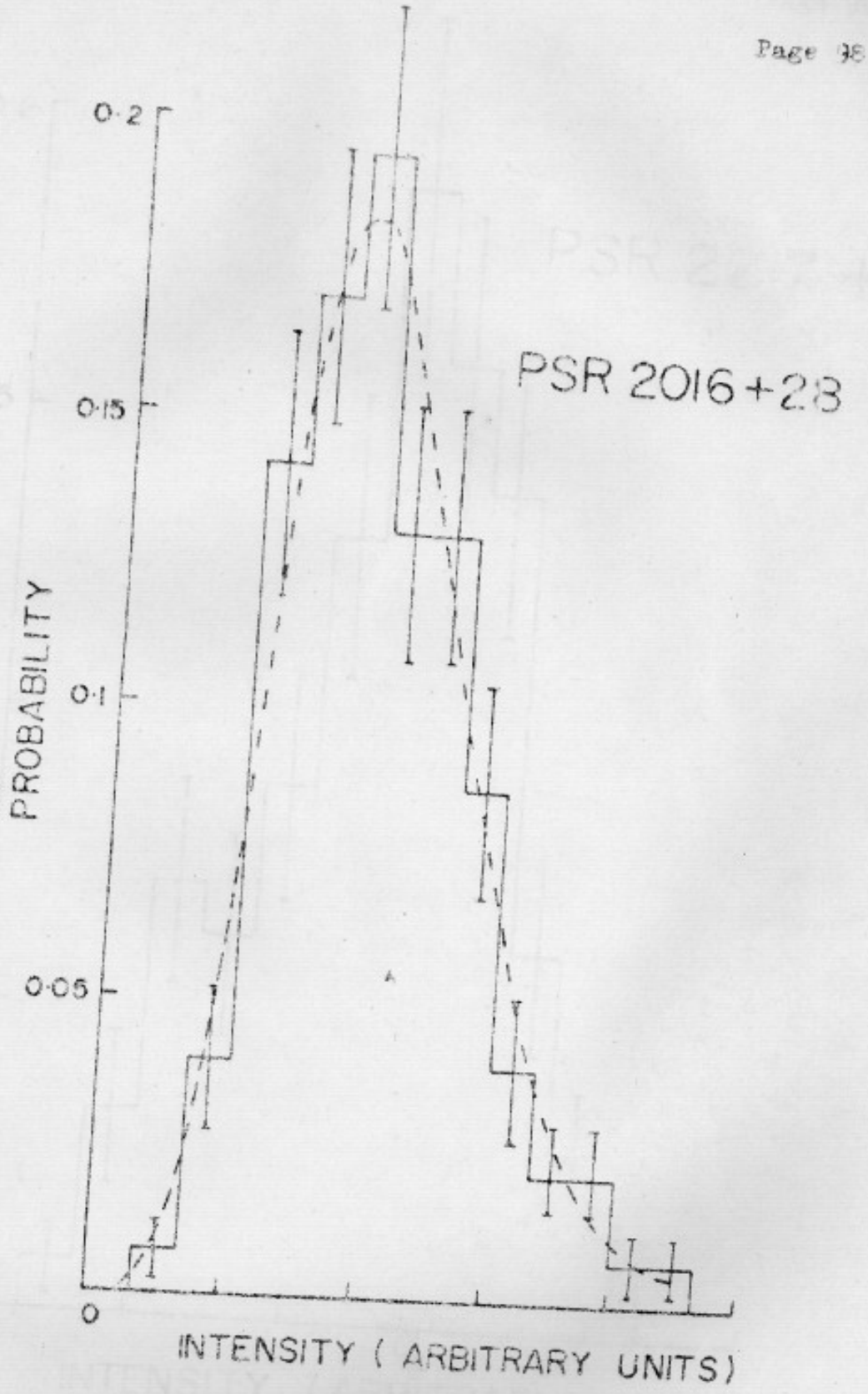
PSR 2016+28
0·2
0·15
0·1
0·05
0
PROBABILITY
INTENSITY (ARBITRARY UNITS)

Fig. 5.1d

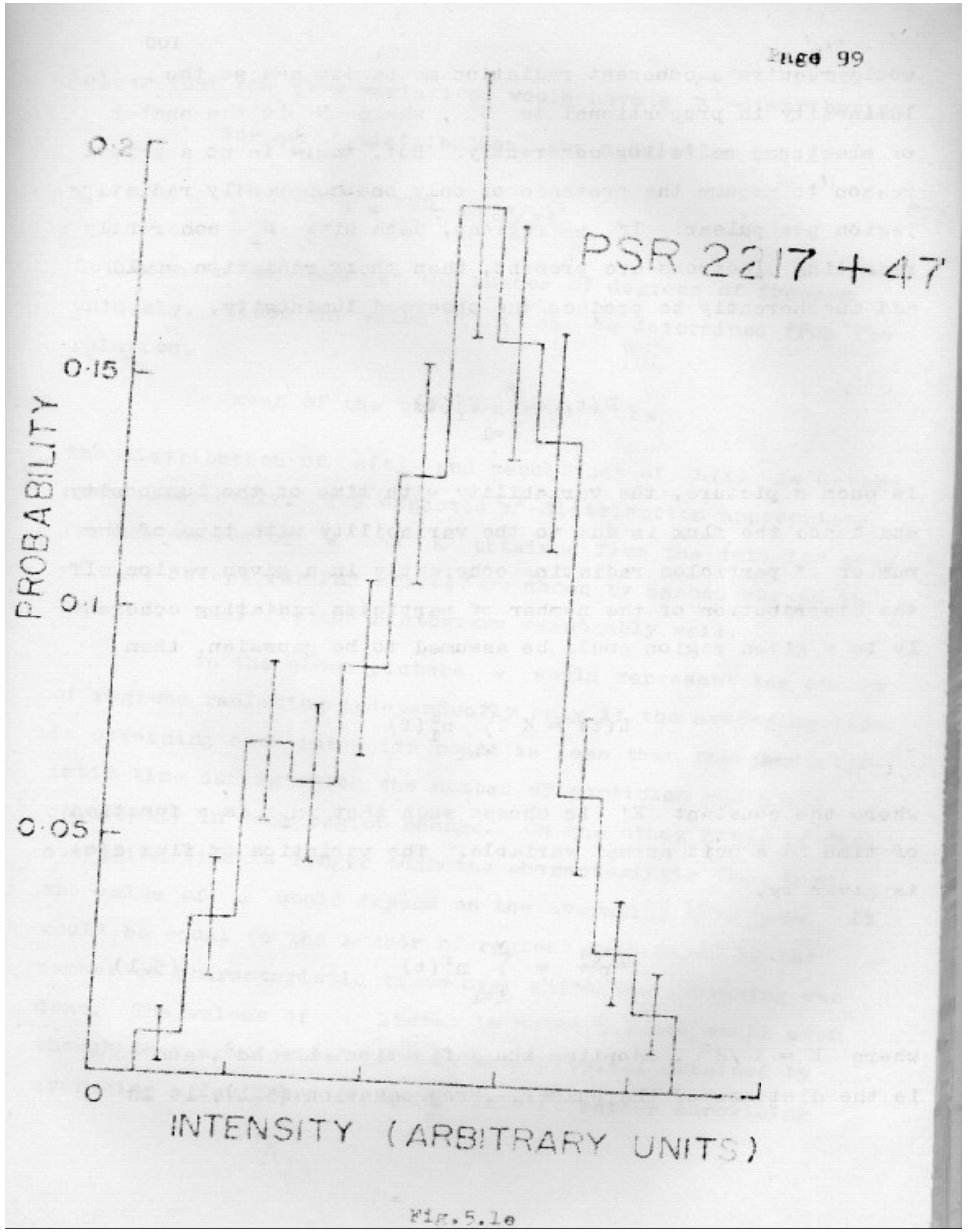
PSR 2217 +47
0·2
0·15
0·1
0·05
0
PROBABILITY
INTENSITY (ARBITRARY UNITS)

Fig. 5.1a

would require a coherent radiation mechanism and so the luminosity is proportional to N^2, where N is the number of electrons radiating coherently. But, there is no a priori reason to assume the presence of only one coherently radiating region per pulsar. If ν regions, each with N_i coherently radiating electrons are present, then their radiation would add incoherently to produce the observed luminosity,

$$L(t) \propto \sum_{i=1}^{\nu} N_i^2(t)$$

In such a picture, the variability with time of the luminosity and hence the flux is due to the variability with time of the number of particles radiating coherently in a given region. If the distribution of the number of particles radiating coherently in a given region could be assumed to be gaussian, then

$$L(t) = K' \sum_{i=1}^{\nu} n_i^2(t)$$

where the constant K' is chosen such that n_i as a function of time is a unit normal variable. The variation of flux $s(t)$ is given by,

$$\frac{s(t)}{K} = \sum_{i=1}^{\nu} n_i^2(t) \qquad (5.1)$$

where $K = K'/d^2$, adopting the definition $L = sd^2$, and d is the distance of the pulsar. From equation (5.1), it is

clear that the flux variations would have a χ^2-distribution.

For a χ^2-distribution, the modulation index,

$$m = \frac{\text{rms}}{\text{mean}} = (2/\nu)^{\frac{1}{2}}$$

So, from m one can get the number of degrees of freedom uniquely. Since the value of K can be determined from the relation,

$$\text{mean of the observed flux} = K\nu$$

the distribution of $s(t)$ and hence that of $L(t)$ is determined completely. The expected χ^2-distribution appropriate for the values of ν and K obtained from the data for each pulsar, except for PSR 2217+47 are shown by dashed curves in Fig.5.1. They fit the histograms reasonably well.

In the above picture ν would represent the number of regions radiating independently only if the averaging time in obtaining each intensity point is less than the characteristic time during which the number of particles radiating coherently in each region change. On the other hand, if the averaging time is longer than the characteristic time then the value of ν would depend on the averaging time also. It would be equal to the number of regions multiplied by the number of characteristic times over which the averaging was done. The values of ν listed in Table 5.1 are small even though they are derived from intensity values obtained by averaging a few hours of data. This is rather surprising

Table 5.1 Modulation index (m) and the derived number of degrees of freedom (ν) for long-term intensity variations

Sr.No.	PSR	m	ν
1	0329+54	0.28	26
2	1508+55	0.38	14
3	1919+21	0.43	11
4	2016+28	0.38	14
5	2217+47	0.33	18

since it would imply characteristic times longer than about ten seconds, whereas intensity fluctuations in pulsars are known to exist down to time scales of the order of a few microseconds. This may imply that the time scales for the fluctuations of N_i span a very wide range, so that when intensities are averaged over a given duration, time scales comparable to it stand out.

5.3 Effect on Searches for New Pulsars

Most of the extensive searches for pulsars are done with computer integration techniques (Davies et al. 1973,1977; Hulse and Taylor 1974,1975; Manchester et al. 1978), so that they have approximately the same sensitivity over a wide range of parameters. Typically, a few minutes of data acquired with a receiver bandwidth of a few MHz are used for searches. Though the variation of flux due to interstellar scintillation is considerably quenched as the bandwidth used is large compared to the scintillation decorrelation bandwidths, intensity variations due to intrinsic causes being wideband in nature are not removed. As we have seen in the previous section, the modulation index can be 0.3 to 0.4 even after a few hours of integration. Such variations affect the completeness of a pulsar search since a pulsar whose mean flux is above the detection limit could be missed if the flux at the time of the search is below the detection limit, and conversly a pulsar whose mean flux is below the detection limit may be detected.

Since pulsars are essentially a disc population (Manchester and Taylor 1977), the number of pulsars whose mean

flux exceed a given mean flux s_m is given by

$$N(>s_m) \alpha\ 1/s_m$$

In arriving at the above relation any galactocentric dependence of the pulsar number density has been ignored. The observed relation between the number density of pulsars and the flux density does not directly give the relation between $N(>s_m)$ vs s_m, since mean fluxes obtained after averaging the flux over a long duration are not available for most of the pulsars. The number of pulsars with a mean flux between s_m and s_m+ds_m is given by

$$n(s_m)ds_m = \frac{C}{s_m^2}\ ds_m$$

In the following discussion we treat the pulsar population as though it has a single ν, since as long as there is no correlation between luminosity and ν, the whole pulsar population could be split into subpopulations with different values of ν, for each of which the following treatment holds good.

At a particular instant of time the probability of finding a pulsar of mean flux s_m between fluxes s and $s+ds$ is given by

$$f(s,s_m)\,ds = \frac{(s/K)^{\nu/2 - 1}\, e^{-s/2K}}{K\, 2^{\nu/2}\, \Gamma(\nu/2)}\, ds$$

where Γ stands for the gamma function.

The probability that a pulsar with a mean flux s_m would be detected in a search with a detection limit s_L is given by,

$$P(s_L,s_m) = \int_{s_L}^{\infty} f(s,s_m)\, ds$$

The probability that a pulsar with a mean flux s_m is not detected in (j-1) previous searches done over the same region of the sky with the same sensitivity, but detected in the 'j th' search is given by

$$P(s_L,s_m)\{\, 1 - P(s_L,s_m)\,\}^{j-1}$$

The assumption of independence of probabilities is justified since the correlation time for long-term variation of pulsar fluxes is only a few tens of days (Huguenin et al. 1973; Helfand et al. 1977). The number of new pulsars contributed by the 'j th' search is given by

$$\int_{s_b}^{\infty} \frac{C}{s_m^{\,2}}\, P(s_L,s_m)\, \{\, 1-P(s_L,s_m)\,\}^{j-1}\, ds_m$$

where $s_b \ll s_L$, but is not equal to zero. In arriving at

the above expression the presence of the receiver noise was ignored, since for a signal-to-noise ratio of 5 to 1 for detection, the effect of receiver noise on detectability of a pulsar is small compared to that due to its flux variations. The ratio of the number of pulsars detected up to the 'j th' search to the number of pulsars detectable in the absence of flux variability is shown in Fig.5.2 for a range of values of ν . The curves do not depend upon the value of s_L . From the plots it is clear that the flux variability, though a nuisance in confirming suspected pulsars, is a blessing in disguise to the pulsar hunters ! They can hope to detect pulsars with mean fluxes below the detection limit of the instrument used, by repeatedly searching the same region !

5.4 Effect on Luminosity Function of Pulsars

Taylor and Manchester (1977) have given a procedure to calculate the luminosity function (LF) of pulsars based on a Monte Carlo approach for the evaluation of selection effects in pulsar searches. In this section we modify their method to include the effect of the variability of pulsar fluxes on LF. Following Taylor and Manchester, the number of pulsars detectable if a volume $V(P,Z,R,L)$ of the galaxy in the galactocentric radii range dR and the perpendicular distance range dZ is searched for pulsars in the period range dP and the luminosity range dL is given by,

$$N'(P,Z,R,L)dP\,dZ\,dR\,dL = V(P,Z,R,L)\,\rho(P,Z,R,L)dP\,dZ\,dR\,dL,$$

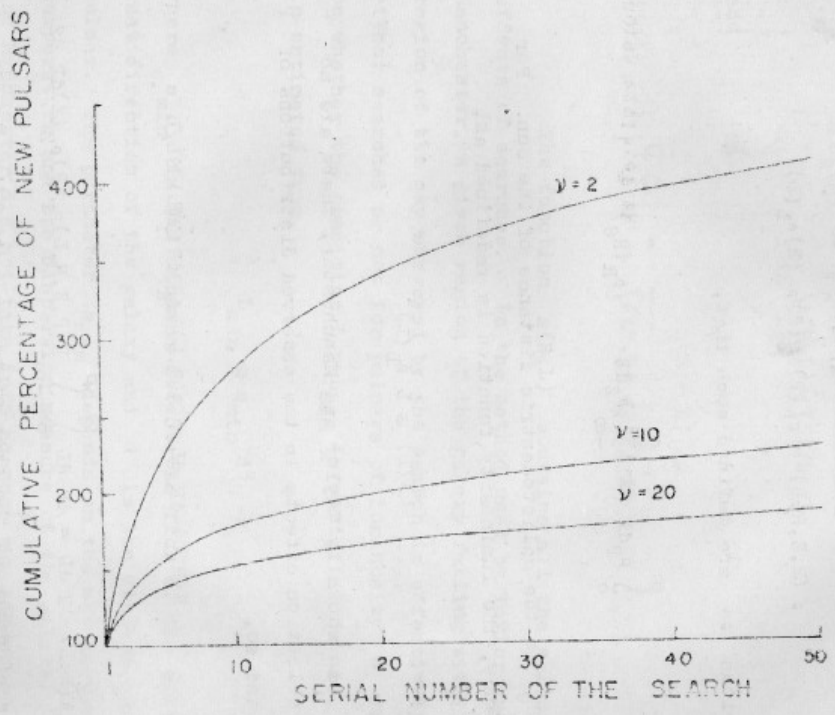

Fig.5.2. Cumulative percentage of new pulsars detectable as a function of the serial number of the search. ν is the number of degrees of freedom of the χ^2-distribution which describes the long-term intensity variations.

where ρ is the number density of pulsars. As indicated by observations, the distribution of pulsars with respect to the parameters P,Z,R and L are either not correlated or only weakly correlated. So, one can write

$$\rho\,(P,Z,R,L) = \rho_P(P)\rho_Z(Z)\rho_R(R)\rho_L(L)$$

The various ρs are defined such that,

$$\int_0^\infty \rho_P dP = \int_{-\infty}^{\infty} \rho_Z dZ = \rho_R(R_\odot) = 1$$

where $R_\odot$ is the galactocentric distance of the Sun. For convenience, the luminosity function is redefined as,

$$\underset{\sim}{\Phi}(L) \equiv L\ \rho_L(L)$$

As shown by Taylor and Manchester, there are no serious selection effects in the observed distributions of P and Z and so,

$$N(R,L)\ dR\ dL = A(R,L)\ \rho_R\ dR\ \underset{\sim}{\Phi}(L)\ dL/L$$

where

$$A(R,L)\ dR\ dL = dR\ dL \int_0^\infty \int_{-\infty}^{\infty} V(P,Z,R,L)\rho_P(P)\rho_Z(Z)dP\ dZ$$

A(R,L) is effectively the area of the galactic disc in the range dR at R which has been searched for pulsars of luminosity L to L+dL . Knowing N(R,L) and A(R,L), one

can obtain $\rho_R(R)$ and $\dot{\Phi}(L)$, iteratively starting from an initial guess from the equations,

$$\rho_R(R) = \frac{\int N(R,L)\, dL}{\int A(R,L)\, \bar{\dot{\Phi}}(L)/L\, dL} \qquad (5.2)$$

and

$$\bar{\dot{\Phi}}(L) = \frac{L \int N(R,L)\, dR}{\int A(R,L)\, \rho_R(R)\, dR} \qquad (5.3)$$

The function $A(R,L)$ contains all the selection effects of searches. In the method used by Taylor and Manchester, a given region of the galaxy falling within the region of the sky surveyed by the search is effectively either searched or not for pulsars of luminosity L depending on whether the condition $L > L_{min}$ is satisfied or not. L_{min} is estimated from,

$$L_{min} \equiv s_{min}\, d^2$$

where s_{min} is the minimum detectable flux of the survey in that direction of the galaxy and d is the distance of the pulsar. The parameter s_{min} depends on the sky background temperature and the dispersion measure of the pulsar. Taylor and Manchester did not take into account the effect of flux variation on $N(R,L)$ and $A(R,L)$. We set up below, a probabilistic approach for the estimation of them in the presence of flux variations. The method is applied to the combined

sample from the Jodrell Bank and the Arecibo searches so that our results can be compared readily with those of Taylor and Manchester (1977).

5.4.1 Corrected luminosity distribution $n(L_m)$

The observed luminosity of a pulsar defined through the relation $L = s\,d^2$ varies with time as the flux s varies with time. The probability distributions of flux and luminosity have the same form since d is a constant for a given pulsar. We are interested in getting the luminosity distribution $n(L_m)$ where, L_m is the mean luminosity of the pulsar defined through

$$L_m = s_m d^2 \qquad (5.4)$$

The number of pulsars of mean flux between s_m and s_m+ds_m which have observed flux s is given by,

$$n(s_m)\, f(s,s_m)\, ds_m \quad ,$$

The probability that a pulsar with an observed flux s has a mean flux in the range s_m to s_m+ds_m is given by,

$$F(s,s_m)\, ds_m = \frac{n(s_m)\, f(s,s_m)\, ds_m}{\int_{s_b}^{\infty} n(s_m)\, f(s,s_m)\, ds_m} \qquad (5.5)$$

where $s_b \ll s_L$, but is not equal to zero. Through equations (5.4) and (5.5), the probability that a given pulsar has come

from a given mean luminosity range can be calculated. By doing this for each of the pulsars in a given sample and summing up the probabilities for each mean luminosity range one can build up the corrected luminosity distribution $n(L_m)$. The result of the application of this method to a sample of 90 pulsars that is obtained from the Jodrell Bank survey and the Arecibo survey is shown in Fig.5.3. The distances used were those given in the compilation by Taylor and Manchester (1975), where the effect of the presence of H_{II} regions on distance estimates were taken care of for pulsars closer than 1 kpc. The fluxes were taken from Davies et al. (1977) for the Jodrell Bank sample and from Hulse and Taylor (1975) for the Arecibo sample, after multiplying by a factor of two for the latter survey to take care of a revision of the flux scale (Taylor and Manchester 1977). Compared to the uncorrected distribution $n(L)$, the corrected distribution $n(L_m)$ is smoother and marginally broader.

5.4.2 Corrected area function $A(R,L_m)$

To calculate $A(R,L_m)$ which contains the selection effects of pulsar searches, a pulsar sample is simulated using a Monte Carlo method. The simulation is such that pulsars are distributed uniformly in the galactic plane over a 40 kpc x 40 kpc area centred on the galactic centre and have an exponential distribution in the perpendicular distance with a scale height of 230 pc so as to closely mimic the actual pulsar population (Taylor and Manchester 1977).

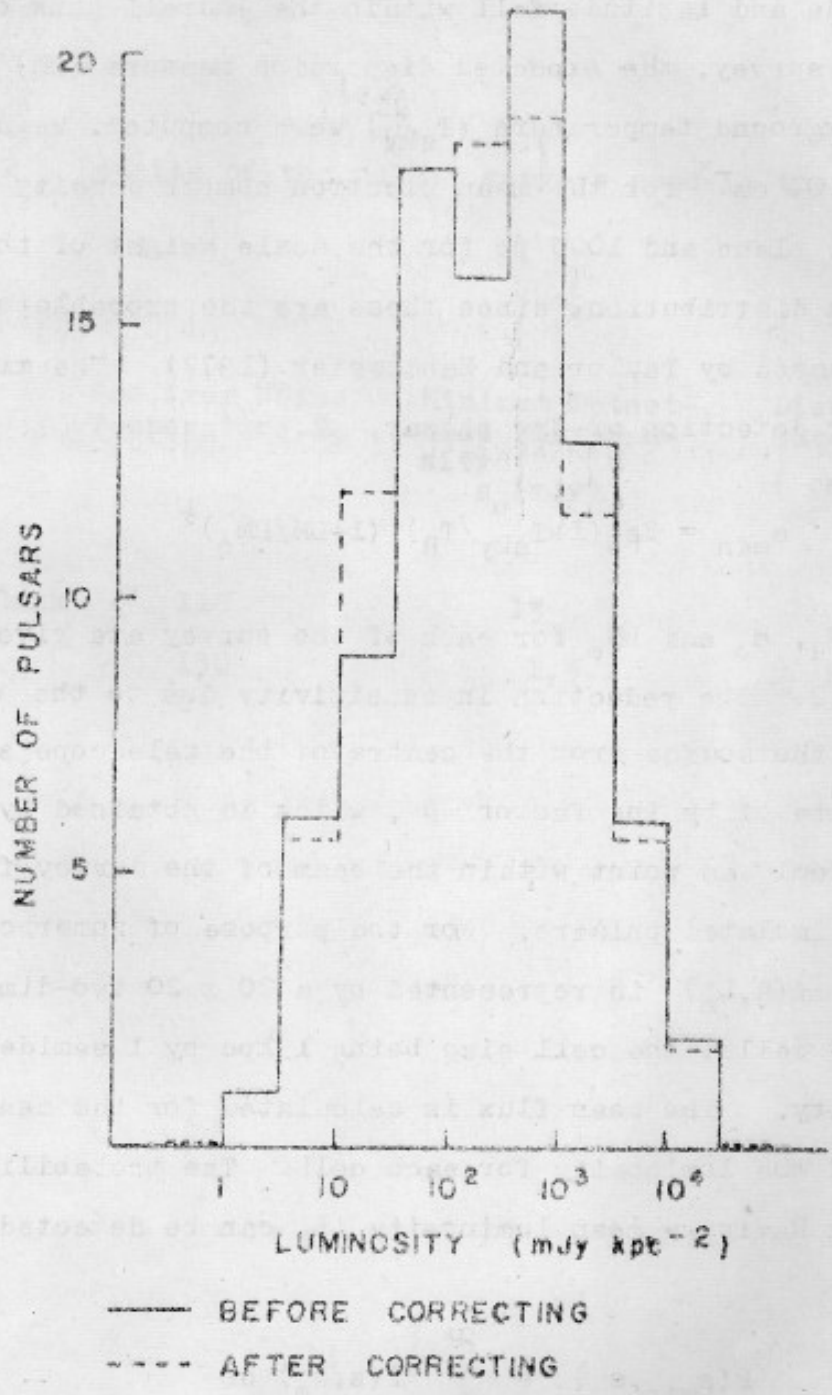

Fig.5.3. Luminosity distribution of pulsars obtained from a combined sample from the Jodrell Bank and the Arecibo surveys.

For each of the simulated pulsars whose galactic longitude and latitude fell within the Jodrell Bank or the Arecibo survey, the expected dispersion measure (DM) and the sky background temperature (T_{sky}) were computed. We used the value 0.03 cm^{-3} for the mean electron number density in the galactic plane and 1000 pc for the scale height of the electron distribution, since these are the probable values as discussed by Taylor and Manchester (1977). The minimum flux for detection of the pulsar,

$$s_{min} = \beta s_o (1+T_{sky}/T_R)\ (1+DM/DM_o)^{\frac{1}{2}}$$

where T_R, s_o and DM_o for each of the survey are given in Table 5.2. The reduction in sensitivity due to the displacement of the source from the centre of the telescope's beam is taken care of by the factor β, which is obtained by simulating randomly as point within the beam of the survey for each of the simulated pulsars. For the purpose of numerical computations $A(R,L_m)$ is represented by a 20 x 20 two-dimensional array of cells, the cell size being 1 kpc by 1 semidecade of luminosity. The mean flux is calculated for the central value of the luminosity for each cell. The probability that a pulsar having a mean luminosity L_m can be detected in the survey,

$$P(s_{min},s_m) = \int_{s_{min}}^{\infty} f(s,s_m)\, ds$$

is calculated for each luminosity interval and the area held

Table 5.2 Details of the pulsar surveys used in the thesis

Survey	Receiver Noise Temperature, T_R	Minimum Detectable Flux Density S_o (mJy)	Dispersion Cutoff, DM_o (cm^{-3} pc)
Jodrell Bank	110	13	250
Arecibo	130	1.5	1200

in the appropriate cell is increased by the above amount. If a particular simulation fell in a region of sky that is covered more than once in the surveys under consideration, then the probabilities P_1, P_2 ..... for detection in trials 1,2, ... respectively are calculated. From these probabilities the probability for detection in at least one of the trials, $P=1-(1-P_1)(1-P_2)$..... is computed. Such a situation arises for a part of the Jodrell Bank survey which was surved twice by that group with offset beam positions, and also in the case of the whole of the Arecibo survey since that survey region was also covered by the Jodrell Bank survey with much less sensitivity. In the later case, the final value of P and the value of P for the Arecibo search alone do not differ appreciably since the s_{min} of the surveys differ by almost an order of magnitude. The above method of calculating the area function has the advantage that it allows two surveys of similar sensitivities done over the same region of the sky to be combined and treated as a single sample. The combined sample could be larger than the individual samples by almost 20 %, as shown in the previous section, and thus has a better statistical stability.

Simulation of pulsar positions and the subsequent calculations were repeated enough number of times to give a statistically stable $A(R,L_m)$ function. The $A(R,L_m)$ function so obtained was normalised so that it represents the effective area in kpc^2 that has been surveyed.

5.4.3 Corrected luminosity function

Once the corrected luminosity distribution $n(L_m)$ and the corrected area function $A(R,L_m)$ are available, ρ_R and $\dot{\Phi}(L)$ can be obtained by solving (5.2) and (5.3) iteratively. The ρ_R so obtained was the same, within the statistical errors, as that obtained by Taylor and Manchester (1977).

We have computed the LF twice - once assuming long-term variability of fluxes and again assuming no variability. The LFs so derived did not differ, outside the error limits, from which we conclude that the variability of fluxes of pulsars does not affect the derived LF. This conclusion is rigidly valid when the sample used to derive the LF is from a single survey since, as shown in Fig.5.2, the total number of pulsars that could be found in a survey are the same, whether there is a variability of flux or not. As this is true irrespective of the detection limit, the number of pulsars detected in a single survey in any flux density range is not affected by the existence of the variability of pulsar flux densities. Also, when the overlapping surveys have very different detection limits, as in the case of the combined Arecibo, Jodrell Bank sample, there is practically no affect on the computed LF. But, if the surveys have similar detection limits, then one may over estimate the total number of pulsars unless proper procedure, as outlined in this chapter, is followed in computing the LF.

Chapter 6

SUMMARY AND COMMENTS

In this chapter we summarise the principal results from our analysis of three different types of intrinsic intensity variations of pulsars as to what they imply about the models of pulsars, the wobble of neutron stars and the birth rate of pulsars. These intensity variations pertain to the drifting subpulses, and the short-term and the long-term intensity variations.

(1) The expected dependence of the slope of the subpulse bands on the subpulse longitude for the polar cap (P.C.) model as developed by Ruderman and Sutherland (1975) and for the relativistic beaming (R.B.) model as developed by Zheleznyakov (1971) have been worked out. The results show that the slope is a very useful parameter since the expected dependences differ for the two models. For the P.C. model the modulus of the slope decreases as we go from the edges to the centre of the average pulse shape whereas for the R.B. model it increases as we approach the mid pulse region.

We measured the slope for the subpulses of PSR 0031-07 observed on two different days by analysing the data using the longitude-resolved Fourier transform method (Backer 1970a). This pulsar has three distinctly different values for the P_3 of its drifting subpulses, the predominant value being $P_3 \sim 7$ pulse periods. As the presence of

different values for P_3 may complicate the interpretation of the observed slope, we verified that the contamination by modulations having a value for P_3 other than 7 pulse periods is indeed negligible by subjecting the data to a two-dimensional correlation analysis. The observed longitudinal dependence of the slope of subpulse bands agrees better with the predictions of the relativistic beaming model than that of the polar cap model. We also show that the known subpulse behaviour of a few other pulsars also agrees with what is expected from the relativistic beaming model. The predictions of the polar cap model can be made compatible with the observations only if a clear physical basis is found for the speeds of the subpulse-producing sparks to depend on their position on the polar cap.

(2) Currently available models of neutron stars do not exclude the possibility of the existence of solid central cores. If solid cores do exist, the neutron stars may wobble with periodicities of a few minutes to roughly an hour. Wobble, if present, would produce variations of pulsar intensities due to geometric effects. But the study of intrinsic intensity variations (IIV) with such time scales has been difficult due to the presence of interstellar scintillations (ISS), which also have similar time scales. The IIV are expected to be fully correlated across the bandwidths that are used in typical observations; but, the ISS are correlated over only a few kHz to $\sim$ 1 MHz at metre wavelengths, depending on the dispersion measure of the

pulsar. As such, the relative strength of their fluctuating power depends on the actual bandwidth used. We have developed a method to separate out the autocorrelation function (ACF) due to IIV from that due to ISS by using multichannel data of the intensity of pulsars. The method has been applied successfully to the data from 24 pulsars observed with 12 channel filter banks available with the Ooty radio telescope.

The results show that the presence of IIV with large modulation indices and time scales similar to those for ISS is very common in pulsars. Both the modulation indices and the time scales change with time. This supports the suggestion of Slee et al. (1974) that IIV may be partially responsible for the inconsistent behaviour of the ISS pattern velocities deduced from multistation observations. The time scales for IIS, uncontaminated by IIV, have been obtained for 11 of the 24 pulsars. We have shown that the results support the conclusion of Backer (1975) that the scintillation bandwidth depends linearly on DM instead of DM^2 as predicted by ISS theories. Our results suggest that a significant part of the spread around the inferred relationship in the diagram presented by Backer may be due to the presence of IIV.

Significant quasiperiodic modulations were seen in the IIV of 9 pulsars. Three of them were observed on two different days and one of them, PSR 1919+21 which has a large

modulation index for IIV was observed on four different days. The time scales and the modulation indices obtained on different days for the same pulsar were different from one another. In particular, PSR 1919+21 had shown different behaviour even on two consecutive days. Wobble of the pulsar had been suggested earlier (Wolszczan 1978) as a possible explanation of the observed quasiperiodic variations of the P_3 of this pulsar. If the observed quasiperiodicities in the IIV are also attributed to wobble one would expect residuals of $\sim$ 15 ms in the time of arrival and significant variations in the pulse shape. Although, these calculations are very crude, as we assumed a circular gaussian for the shape of the emission beam, still measurable periodic residuals should have been present in the data. But we have not found any significant residuals which depend systematically on the phase of the suspected wobble period, of a magnitude greater than a fraction of a millisecond. Based on the absence of significant seismic activity in PSRs 0301+19, 1237+25 and 1919+21 as indicated by the absence of significant residuals in their times of arrival data (Gullahorn and Rankin 1978), we conclude that wobble is a very unlikely explanation for the quasiperiodicities in the IIV. One has to examine the possibility of variations in the emission mechanism itself for an explanation of the observed quasiperiodicities.

(3) We have shown that the probability distribution of long-term intensity fluctuations derived from the data of

Huguenin, Taylor and Helfand (1973) can be described by χ^2-distributions. We have shown also that the χ^2-distributions are logically to be expected because of the coherent nature of the radiation from pulsars.

Using these distributions we have shown that sizable number of new pulsars could be detected on repeatedly searching a given region of the sky with the same sensitivity. For example, on the first repeat search one can detect 20 % more new pulsars compared to the first search. Plots of the cumulative number of new pulsars detectable as a function of the number of the search are presented. In the above calculations we have assumed that the number of pulsars above a flux level s_m is proportional to $1/s_m$. It should be noted that this assumption ignores any dependence of the number density of pulsars on the galactocentric distance.

Luminosity function (LF) is a very important property of pulsars since it is required for calculating the birth rate of pulsars. Observationally derived birth rates were used by several investigators to check whether all pulsars are born in supernova events or not. But there are several effects which make the calculated LF inaccurate. Long term intensity variations were suspected to be one of the important effects (Manchester 1979). To examine this, we adopted a probabilistic approach to the detectability of a pulsar while determining the selection effects of pulsar searches. The derived χ^2-distributions were used in calculating the probability of detection. By applying this

procedure to the combined sample of the Jodrell Bank and the Arecibo searches whose selection effects are well documented, we have shown that the calculated LF is unaffected by the presence of intensity fluctuations. However, the two searches had detection limits which differ by an order of magnitude. But, when different surveys over the same region of the sky with similar detection limits are combined to derive the LF and hence the birth rates, the latter could be overestimated by more than 20 %, unless the probabilistic approach outlined in the thesis is adopted in calculating the LF.

(4) To summarise, we have made an attempt to use intensity variations of pulsars to investigate about the models of pulsars and neutron stars. Our results show that as far as drifting subpulses are concerned the relativistic beaming model is to be preferred over the polar cap model. Quasiperiodic IIV with large modulation indices have been observed in several pulsars. But, they could not be ascribed to the wobble of neutron stars, since other evidence to support the hypothesis is lacking. Observations of more pulsars with better time resolution and good signal-to-noise ratio are likely to clarify whether low amplitude wobbles exist in neutron stars or not.

REFERENCES

Ables,J.G., and Manchester,R.N., 1976. Astron. Astrophys., 50, 177.

Anderson,P.W., and Palmer,R.G., 1971, Nature Phys. Sci., 231, 145.

Anderson,B., Lyne,A.G., and Peckham,R.J., 1975. Nature, 258, 215.

Argyle,E., and Gower,J.F.R., 1972. Astrophys.J., 175, L89.

Baade,W., and Zwicky,F., 1934. Proc. Nat. Acad. Sci., 20,255.

Backer,D.C., 1970a. Nature, 227, 692.

Backer,D.C., 1970b. Nature, 228, 42.

Backer,D.C., 1970c. Nature, 228, 1297.

Backer,D.C., 1973. Astrophys.J., 182, 245.

Backer,D.C., 1975. Astron. Astrophys., 43, 395.

Backer,D.C., Rankin,J.M., and Campbell,D.B., 1975. Astrophys. J., 197, 481.

Backer,D.C., and Sramek,R.A., 1976. Astron. J., 81, 1430.

Balasubramanian,V., 1979. Ph.D. Thesis submitted to the University of Bombay

Baym,G., Pethic,C., Pines,D., and Ruderman,M., 1969. Nature, 224, 872.

Baym,G., and Pines,D., 1971. Ann. Phys., 66, 816.

Baym,G., and Pethic,C., 1975. Ann. Rev. Nucl. Sci., 25, 27.

Baym,G., Lamb,D.Q., and Lamb,F.K., 1976. Astrophys.J., 208, 829.

Brecher,K., 1972. Nature, 239, 325.

Burns,J.A., 1970. Nature, 228, 986.

Cameron,A.G.W., and Canuto,V., 1974. Proc. 16th Solvay Conf. on Physics, P.221, Editions de l' Universite' Bruxells.

Chau,W.Y., Henriksen,R.N., and Rayburn,D.R., 1971. Astrophys. J., 168, L79.

Cheng,A.F., and Ruderman,M.A., 1977. Astrophys. J., 212, 800.

Chiuderi,C., and Occhionero,F., 1970. Nature, 226, 337.

Clark,D.H., and Caswell,J.L., 1976. Mon. Not. Roy. astr. Soc., 174, 267.

Cole,T.W., 1970. Nature, 227, 788.

Davies,J.G., Lyne,A.G., and Seiradakis,J.H., 1973. Nature Phys. Sci., 244, 84.

Davies,J.G., Lyne,A.G., and Seiradakis,J.H., 1977. Mon. Not. Roy. astr. Soc., 179, 635.

Drake,F.D., and Craft,jun,H.D. , 1968. Nature, 220, 231.

Ginzburg,V.L., and Zaitzev,V.V., 1969. Nature, 222, 230.

Ginzburg,V.L., and Zheleznyakov,V.V., 1975. Ann. Rev. Astron. Astrophys., 13, 511.

Gold,T., 1968. Nature, 218, 731.

Goldreich,P., and Julian,W.H., 1969. Astrophys.J., 157, 869.

Goldreich,P., 1970. Astrophys.J., 160, L11.

Goldstein,H., 1950. Classical Mechanics, Addison-Wesley Publishing Company.

Gómez-Gonáles,J., Guélin,M., 1974. Astron.Astrophys., 32, 441.

Gullahorn,G.E., and Rankin,J.M., 1978. Astron. J., 83, 1219.

Hankins,T.H., 1971. Astrophys.J., 169, 487.

Hegyi,D., Novick,R., and Thaddeus,P.,1971. The Crab Nebula, IAU Symp.46, p.129, ed. Davies,R.D., and Smith,F.G., Dordrecht Reidel.

Heiles,C., Campbell,D.B., and Rankin,J.M., 1970. Nature, 226, 529.

Heintzmann,H., Kundt,W., and Schrüfer,E., 1973. Astron. Astrophys., 27, 45.

Helfand,D.J., Manchester,R.N., and Taylor,J.H., 1975. Astrophys.J., 198, 661.

Helfand,D.J., Fowler,L.A. and Kuhlman,J.V., 1977. Astron. J., 82, 701.

Henrikson,R.N., Feldman,P.A., and Chau,W.Y., 1971. Nature, 234, 450.

Hesse,K.H., 1972. Nature Phys. Sci., 235, 27.

Hesse,K.H., Sieber,W., and Wielebinski,R., 1973. Nature Phys. Sci., 245, 57.

Hewish,A., Bell,S.J., Pilkington,J.D.H., Scott,P.F., and Collins,R.A., 1968. Nature, 217, 709.

Huguenin,G.R., Taylor,J.H., and Troland,T.H., 1970. Astrophys. J., 162, 727.

Huguenin,G.R., Taylor,J.H., and Helfand,D.J., 1973. Astrophys. J., 181, 139.

Hulse,R.A., and Taylor,J.H., 1974. Astrophys.J., 191, L59.

Hulse,R.A., and Taylor,J.H., 1975. Astrophys.J., 201, L55.

Ilovaisky,S.A., and Lequeux,J., 1972. Astron. Astrophys., 20, 347.

Johnson,N.L., and Kotz,S., 1970. Continuous Univariate Distributions-2, P.225, Houghton Mifflin Co., Boston.

Krishnamohan,S., and Balasubramanian,V., 1976. Bull. Astr. Soc. India, 4, 84.

Lang,K.R., 1971. Astrophys. J., 164, 249. MNRAS, 191, 237 (1980)

Large,M.I., 1971. The Crab Nebula, I.A.U.,Symp. 46, P.165, ed. Davies,R.D., and Smith,F.G., Dordrecht Reidel.

Lee,L.C., and Jokipii,J.R., 1975. Astrophys. J., 201, 532.

Lee,L.C., 1976. Astrophys.J., 206, 744.

Lovelace,R.V.E., and Craft,jun,H.D., 1968. Nature, 220, 875.

Lyne,A.G., 1971. Mon. Not. Roy. astr. Soc., 153, 27P

Macy,W.W., 1974. Astrophys.J., 190, 153.

Manchester,R.N., Taylor,J.H., and Van,Y.Y., 1974. Astrophys. J., 189, L119.

Manchester,R.N., Taylor,J.H., and Huguenin,G.R., 1975. Astrophys.J., 196, 83.

Manchester,R.N., and Taylor,J.H., 1977. Pulsars, Freeman, San Francisco.

Manchester,R.N., Lyne,A.G., Taylor,J.H., Durdin,J.M., Large,M.I., and Little,A.G., 1978. Mon. Not. Roy. astr. Soc., 185, 409.

Manchester,R.N., 1979. Aust. J. Phys., 32, 1.

Mansinha,L., and Smylie,D.E., 1968. Science, 161, 1127.

Maraschi,L., and Treves,A., 1977. Astron. Astrophys., 61,L11.

Mc Lean,A.I.O., 1973. Mon. Not. Roy. astr. Soc., 165, 133.

Oster,L., and Sieber,W., 1976. Astrophys.J., 210, 220.

Otnes,R.K., and Enochson,L., 1972. Digital Time Series Analysis, P.284, John Wiley and Sons.

Page,C.G., 1973. Mon. Not. Roy. astr. Soc., 163, 29.

Pandharipande,V.R., Pines,D., and Smith,R.A., 1976. Astrophys. J., 208, 550.

Papoulis,A., 1965. Probability, Random Variables and Stochastic Processes, P.337, Mc Graw-Hill.

Pines,D., and Shaham,J., 1972a. Phys. of the Earth and Planet Interiors, 6, 103.

Pines,D., and Shaham,J., 1972b, Nature Phys. Sci., 235, 43.

Pines,D., Shaham,J., and Ruderman,M., 1972. Nature Phys. Sci., 237, 83.

Pines,D., Pethic,C.J., and Lamb,F.K., 1973. Ann. N.Y. Acad. Sci., 224, 237.

Pines,D., and Shaham,J., 1974. Nature, 248, 483.

Prentice,A.J.R., and ter Haar,D., 1969. Mon. Not. Roy. astr. Soc., 146, 423.

Radhakrishnan,V., and Cooke,D.J., 1969. Astrophys. Lett.,3, 225.

Rickett,B.J., 1977. Ann. Rev. Astron. Astrophys., 15, 479.

Ritchings,R.T., and Lyne,A.G., 1975. Nature, 257, 293.

Ritchings,R.T., 1976. Mon. Not. Roy. astr. Soc., 176, 249.

Roberts,D.H., 1976. Astrophys.J., 205, L29.

Ruderman,M., 1970. Nature, 225, 838.

Ruderman,M., 1972. Ann. Rev. Astron. Astrophys., 10, 427.

Ruderman,M.A., and Sutherland,P.G., 1975. Astrophys.J., 196,51.

Scheuer,P.A.G., 1968. Nature, 218, 920.

Slee,O.B., Ables,J.G., Batchelor,R.A., Krishna-Mohan,S., Venugopal,V.R., and Swarup,G., 1974. Mon. Not. Roy. astr. Soc., 167, 31.

Smart,W.M., 1965. Text-Book on Spherical Astronomy 5th edn., Cambridge University Press.

Smith,F.G., 1969. Nature, 223. 934.

Smith,F.G., 1970. Mon. Not. Roy. astr. Soc., 149, 1.

Sturrock,P.A., 1971. Astrophys. J., 164, 529.

Sutton,J.M., 1971. Mon. Not. Roy. astr. Soc., 155, 51.

Swarup,G., Sarma,N.V.G., Joshi,M.N., Kapahi,V.K., Bagri,D.S., Damle,S.H., Ananthakrishnan,S., Balasubramanian,V., Bhave,S.S., and Sinha,R.P., 1971. Nature Phys. Sci., 230, 185.

Taylor,J.H., Jura,M., and Huguenin,G.R., 1969. Nature,223,797.

Taylor,J.H., and Huguenin,G.R., 1971. Astrophys.J., 167, 273.

Taylor,J.H., Huguenin,G.R., Hirsch,R.M., and Manchester,R.N., 1971. Astrophys. Lett., 9, 205.

Taylor,J.H., and Manchester,R.N., 1975. Astron.J., 80, 794.

Taylor,J.H., Manchester,R.N., and Huguenin,G.R., 1975. Astrophys. J., 195, 513.

Taylor,J.H., and Manchester,R.N., 1977. Astrophys.J., 215,885.

Taylor,J.H., Fowler,L.A., and Mc Culloch,P.M., 1979. Nature, 277, 437.

Unwin,S.C., Readhead,A.C.S., Wilkinson,P.N., and Ewing,M.S., 1978. Mon. Not. Roy. astr. Soc., 182, 711.

Vila,S.C., 1969. Nature, 224, 157.

Wolszczan,A., 1978. Astron. Astrophys., 63, 425.

Zheleznyakov,V.V., 1971. Astrophys. Sp. Sci., 13, 74.

Zheleznyakov,V.V., and Shaposhnikov,V.E., 1975. Astrophys. Sp. Sci., 33, 141.